

**INVESTIGATION ON THE MECHANICAL PROPERTIES
AND MICROSTRUCTURE ANALYSIS OF MICRO-
RESISTANCE SPOT WELDING BETWEEN STAINLESS
STEEL 316L AND TI-6AL-4V**

MUHAMMAD SAFWAN MOHD MANSOR

**FACULTY OF ENGINEERING
UNIVERSITY OF MALAYA
KUALA LUMPUR**

2020

**INVESTIGATION ON THE MECHANICAL
PROPERTIES AND MICROSTRUCTURE ANALYSIS OF
MICRO-RESISTANCE SPOT WELDING BETWEEN
STAINLESS STEEL 316L AND TI-6AL-4V**

MUHAMMAD SAFWAN MOHD MANSOR

**DISSERTATION SUBMITTED IN FULFILMENT OF
THE REQUIREMENTS FOR THE DEGREE OF MASTER
OF ENGINEERING SCIENCE**

**DEPARTMENT OF MECHANICAL ENGINEERING
FACULTY OF ENGINEERING
UNIVERSITY OF MALAYA
KUALA LUMPUR**

2020

UNIVERSITY OF MALAYA
ORIGINAL LITERARY WORK DECLARATION

Name of Candidate: Muhammad Safwan bin Mohd Mansor

Matric No: KGA150081

Name of Degree: Master of Engineering Science

Title of Project Paper/Research Report/Dissertation/Thesis (“this Work”):

Investigation on the Mechanical Properties and Microstructure analysis of
micro-resistance spot welding between stainless steel 316L and Ti-6Al-4V

Field of Study: Advance Manufacturing Technology

I do solemnly and sincerely declare that:

- (1) I am the sole author/writer of this Work;
- (2) This Work is original;
- (3) Any use of any work in which copyright exists was done by way of fair dealing and for permitted purposes and any excerpt or extract from, or reference to or reproduction of any copyright work has been disclosed expressly and sufficiently and the title of the Work and its authorship have been acknowledged in this Work;
- (4) I do not have any actual knowledge nor do I ought reasonably to know that the making of this work constitutes an infringement of any copyright work;
- (5) I hereby assign all and every rights in the copyright to this Work to the University of Malaya (“UM”), who henceforth shall be owner of the copyright in this Work and that any reproduction or use in any form or by any means whatsoever is prohibited without the written consent of UM having been first had and obtained;
- (6) I am fully aware that if in the course of making this Work I have infringed any copyright whether intentionally or otherwise, I may be subject to legal action or any other action as may be determined by UM.

Candidate’s Signature

Date:

Subscribed and solemnly declared before,

Witness’s Signature

Date:

Name:

Designation:

ABSTRACT

In this study, ASS 316L and Ti-6Al-4V were welded together by micro-resistance spot welding (μ RSW) at different combinations of welding parameters using specifically design electrode geometry in order to acquire the optimal combination of welding parameters. The welded joint were subjected to tensile shear strength test to determine the influence of welding current, welding time, welding force and different design of electrode tip on the mechanical properties and the strength of the welded joint. The experiment was conducted by using full factorial design of experiment (DoE) with L_{27} orthogonal array and utilizing the analysis of variance (ANOVA) to obtain the most significant welding parameter which affect the strength of the welded joint. In addition, micro hardness and microstructural examinations of the fracture mode (failure analysis) were carried out. The results revealed that by using combination of 2.0 kA welding current, 100 ms welding time and 241 N welding force yield the highest load value, 378.25 N. Welding current found to be the most significant welding parameter. Vickers microhardness test reveal an average hardness value of 963 HV at the fusion zone (FZ). After the optimal parameters have been obtained, an investigation has been carried out to obtain the suitable design of electrode geometries by implementing three different design of electrode tip, triangle, square and hexagon shape through comparison study. The comparison study involves the joint strength and microhardness evaluation. Based on the SEM observations, dendritic grain structures can be seen at the FZ. In addition, EDS mapping analysis revealed the formation of Ti-Fe and Ti-Fe₂ intermetallic compound at the FZ. This is further supported by results obtained by vickers microhardness test as hardness value (HV) at the FZ is significantly higher than the base metals. Lastly, the overall results reveal that pimped tipped (PT) electrode with triangle shape electrode tip shows superior welded joint strength.

ABSTRAK

Dalam kajian ini, austenitik keluli tahan karat 316L dan aloi titanium (ASTM gred 5) dikimpal bersama oleh kimpalan rintangan bintik mikro pada kombinasi parameter kimpalan yang berbeza dan dengan menggunakan reka bentuk geometri elektrod yang khusus. Bahagian cantuman yang dikimpal dikenakan ujian kekuatan ricih tegangan untuk mengenal pasti kekuatan bahagian cantuman tersebut. Pengaruh daripada arus elektrik, masa kimpalan, tekanan kimpalan dan rekabentuk elektrod ke atas sifat mekanik bahagian cantuman telah diselidiki. Eksperimen ini dijalankan dengan menggunakan reka bentuk eksperimen faktorial penuh dengan susunan orthogonal L_{27} untuk memperoleh kombinasi parameter kimpalan yang paling optimum dan analisis varians (ANOVA) digunakan untuk mendapatkan parameter kimpalan yang paling penting yang mempengaruhi kekuatan cantuman yang dikimpal. Di samping itu, kekerasan mikro dan pemeriksaan mikrostruktur mod patah (analisis kegagalan) telah dijalankan untuk mengkaji pengaruh parameter kimpalan pada bahagian cantuman yang dikimpal. Keputusan menunjukkan bahawa dengan menggunakan gabungan parameter kimpalan arus elektrik 2.0 kN, masa kimpalan 100 ms dan tekanan kimpalan 241 N dapat menghasilkan nilai beban tertinggi, 378.25 N. Arus elektrik adalah parameter kimpalan paling bermakna yang diperolehi melalui Analisis Varians (ANOVA). Ujian kekerasan mikro Vickers menunjukkan nilai kekuatan sebanyak 963 HV dalam zon fusi. Selepas parameter optimum diperolehi, ujian telah dijalankan untuk mendapatkan reka bentuk elektrod yang sesuai dengan menggunakan tiga bentuk penghujung elektrod yang berbeza melalui kajian perbandingan iaitu bentuk segi tiga, segi empat sama, dan heksagon. Kajian perbandingan yang dinyatakan melibatkan penilaian ke atas kekuatan cantuman dan kekerasan mikro. Berdasarkan pemerhatian SEM, struktur dendritik kolumnar dapat dilihat dengan jelas pada zon fusi (FZ) nugget bahagian cantuman yang telah dikimpal. Di samping itu, analisis pemetaan EDS mendedahkan pembentukan sebatian intermetalik

Ti-Fe dan Ti-Fe₂ di FZ. Keputusan ini disokong dengan hasil yang diperolehi oleh ujian kekerasan mikro Vickers kerana nilai kekerasan (HV) pada FZ jauh lebih tinggi daripada logam asas. Akhir sekali, hasil menunjukkan bahawa reka bentuk elektrod dengan penghujung berbentuk segi tiga mendedahkan kekuatan yang lebih tinggi.

University of Malaya

ACKNOWLEDGEMENTS

In the name of Allah, my sincerest gratitude to my supervisor, Assoc. Prof. Dr. Farazila binti Yusof for her continuous, whole-hearted support and knowledge provided to me during my graduate studies. She continually and persuasively conveyed a spirit of adventure regarding my research studies and the excitement in teaching new things to expand my thinking skills. Without her constant supervision and help with this research, it would not have been possible. It has been a pleasure and a great experience working alongside her. Furthermore, I would like to acknowledge all my friends who always encourage me and stretched their helping hand whenever necessary during the entire study period. Besides, a special thank goes to Mr. Mohd Fauzi bin Bakri who helped me a lot during my workpiece preparation with the CNC Milling machine. I also deeply thankful to everyone who assisted me to completes this research project especially to all staff of Center of Advanced Manufacturing and Material Processing (AMMP) and laboratories of faculty of engineering for their assistance and support.

Finally, I would like to share this moment of contentment and express the appreciations to my parents, Prof. Dr. Mohd Mansor bin Ismail and Shahrum binti Ismail for providing financial support for this thesis work and encouraged me at every step in my life. I would never be this far without their supports and encouragements.

TABLE OF CONTENTS

Abstract	i
Abstrak	ii
ACKNOWLEDGEMENTS	iv
Table of Contents	v
List of Figures	viii
List of Tables.....	xii
List of Symbols and Abbreviations.....	xiii
CHAPTER 1: INTRODUCTION.....	1
1.1 GENERAL BACKGROUND	1
1.2 MATERIALS AND APPLICATION.....	3
1.3 PROBLEM STATEMENT.....	6
1.4 OBJECTIVES.....	9
1.5 SCOPE OF THE STUDY.....	9
1.6 ORGANIZATION OF THE THESIS	10
CHAPTER 2: LITERATURE REVIEW.....	12
2.1 INTRODUCTION	12
2.2 ADVANTAGES AND DISADVANTAGES.....	15
2.3 WELDING PROCESS PARAMETERS	16
2.3.1 Welding current	16
2.3.2 Welding time	18
2.3.3 Welding force	19
2.3.4 Tool geometry	20
2.4 RESISTANCE SPOT WELDING OF DISSIMILAR MATERIAL	23

2.5	METHOD OF INVESTIGATION	29
2.5.1	Design of experiment	29
2.5.2	Analysis of Variance (ANOVA)	31
2.6	MECHANICAL PROPERTIES AND MICROSTRUCTURE ANALYSIS	33
2.6.1	MICROHARDNESS TESTING	42
2.6.1.1	Vickers hardness test	42
2.7	EFFECT OF PROCESS PARAMETERS ON THE FAILURE MODES	46
2.8	RESEARCH GAP	53
2.9	SUMMARY.....	54
CHAPTER 3: RESEARCH METHODOLOGY		55
3.1	OVERVIEW OF METHODOLOGY.....	55
3.2	PREPARATION OF MATERIALS AND ELECTRODE.....	58
3.3	EXPERIMENTAL DESIGN AND PROCEDURE	65
3.4	TENSILE SHEAR TEST MEASUREMENT	71
3.5	MICROSTRUCTURAL CHARACTERIZATION ANALYSIS.....	72
3.6	MICROHARDNESS TEST	73
3.7	SUMMARY.....	73
CHAPTER 4: RESULTS AND DISCUSSION		74
PHASE 1: THE INVESTIGATION OF OPTIMIZATION PROCESS PARAMETERS		
	OF μ RSW	74
4.1	INTRODUCTION	74
4.2	MECHANICAL PROPERTY ANALYSIS	74
4.2.1	Tensile Shear Strength Analysis.....	74
4.2.2	Regression analysis	82
4.2.3	Failure modes	83

4.2.4	Vickers Micro Hardness Test	87
4.3	CHARACTERIZATION OF MICROSTRUCTURE	91
4.4	CHARACTERIZATION ANALYSIS OF INTERMETALLIC COMPOUNDS (IMC) OF THE WELDED JOINT	95
	PHASE 2: THE OPTIMAL DESIGN OF ELECTRODE GEOMETRY	97
4.5	INTRODUCTION	97
4.6	MECHANICAL PROPERTY ANALYSIS	97
4.6.1	Tensile Shear Strength Analysis.....	97
4.6.2	Vickers Micro Hardness Test	101
4.7	CHARACTERIZATION OF MICROSTRUCTURE	108
4.8	CHARACTERIZATION ANALYSIS OF INTERMETALLIC COMPOUNDS (IMC) OF THE WELDED JOINT	114
4.9	SUMMARY	120
	 CHAPTER 5: CONCLUSION.....	 123
5.1	Conclusion	123
5.2	Recommendation for Future Work.....	125
	 REFERENCES 126	
	 LIST OF PUBLICATIONS.....	 133

LIST OF FIGURES

Figure 1.1: Basic illustration of eyeglass frame with numbered parts (Chino et al., 1994)	3
Figure 2.1: chronological order of a simple RSW process (Resistance Spot Welding (RSW) Working Principle and Advantages-disadvantages, 2014)	14
Figure 2.2: Illustration of various electrode geometry (TUFFALOY Company).....	20
Figure 2.3: Schematic diagram of resistance spot welding arrangement (W. Zhang et al., 2015)	22
Figure 2.4: Simple models describing stress distribution at the.....	34
Figure 2.5: Typical load–displacement curve during the TS test along with the extracted parameters: P_{max} : peak load; W_{max} : energy absorption; L_{max} : elongation at peak load. (Pouranvari & Marashi, 2013)	35
Figure 2.6: Cross-section images of the joint welded by (a) 4 kA, (b) 5 kA, (c) 6 kA, (d) 7 kA, (e) 8 kA, and (f) 9 kA welding currents at constant 4 cycles welding time (Kianersi et al., 2014).....	36
Figure 2.7: SEM images taken from weld nugget area (a and b) welded by using 4 kA welding current and (c and d) welded by using 8 kA welding current. EDS elemental analysis were carried out at the determined points (Kianersi et al., 2014)	38
Figure 2.8: Optical microscope images of the weld nugget of resistance spot welded joints joined at: (a) 2000 N, 15 cycle, (b) 2000 N, 15 cycle-Argon, (c) 4000 N, 15 cycle, (d) 4000 N, 15 cycle-Argon, (e) 6000 N, 15-cycle and (f) 6000 N, 15 cycle-Argon. (Kahraman, 2007)	40
Figure 2.9: Micro X-ray diffraction profile of interfacial region in the welded joint (W. Zhang et al., 2015)	41
Figure 2.10: Schematic of the microhardness measurements taken from cross section of the samples (Kianersi et al., 2014).....	43
Figure 2.11: Microhardness profiles of welds manufacture by using various welding current (Kianersi et al., 2014)	43
Figure 2.12: Hardness variation in the welded specimens obtained at 3 kN electrode force and at (a) 3 kA,(b) 5 kA and (c) 7 kA welding currents (Kaya & Kahraman, 2012)	45

Figure 2.13: Schematic representation of various failure modes which can occur during mechanical testing of resistance spot welds, (a) IF; (b) PF; (c) partial interfacial failure (PIF); (d) PT-PP (Pouranvari & Marashi, 2013).....	47
Figure 2.14: Various types of failure modes obtained from tensile shear test samples (Kianersi et al., 2014).....	48
Figure 2.15: Failure modes: (a) IF mode. (b) Magnification view of IF mode (1 and 2 are point of EDS analysis). (c) PIF mode. (d) Magnification of PIF mode (Ertek Emre & Kaçar, 2016).....	49
Figure 2.16: Effect of welding parameters on the tensile shear strength and failure types: (a) uncoated; (b) galvanized (Ertek Emre & Kaçar, 2016).....	49
Figure 2.17: Interfacial fracture with dendrite and ductile characteristics. (a) A view of low magnification, (b and c) magnified views of the weld nugget with dendrite and ductile fracture characteristics, (d) characteristic dendrite, (e) dimple-like ductile fracture characteristics, (f) dendrite and ductile shear combination area, where the locations of micrographs (b-f) are indicated by B-F, respectively, for the sample welded with 8.35 kA (Ma et al., 2008).....	52
Figure 3.1 Flow chart of research methodology.	55
Figure 3.2 Schematic diagram of tool.....	61
Figure 3.3 Electrodes used during the experiment.....	62
Figure 3.4 Schematic illustration of micro resistance spot welding.....	62
Figure 3.5: Schematic diagram of the different design of electrodes used, (a) triangle shape, (b) square shape, and (c) hexagon shape electrode tip.....	64
Figure 3.6: Micro-resistance spot welding machine.	65
Figure 3.7: Schematic illustration of tensile shear test specimen.....	72
Figure 4.1: Effects of different control factors on Load (N).....	78
Figure 4.2: Mean of maximum load for each level of the welding parameters: (a) welding current [kA]; (b) welding time [ms]; (c) welding force [N].....	80
Figure 4.3: Interaction plot for maximum load.....	81
Figure 4.4: Fracture surface of ASS 316L side of the μ RSW joint.....	85
Figure 4.5: Fracture surface of Ti-6Al-4V side of the μ RSW joint.....	85
Figure 4.6: Vickers micro-hardness profile of μ RSW joint.....	87

Figure 4.7: Effects of welding parameters on the average microhardness values at the FZ	88
Figure 4.8: Typical macrostructure and microstructures of RSW joint: (a) Macrostructure; and microstructure of (b) region B in (a); (c) region C in (a); (d) region D in (a); (e) Schematic diagram for the Fusion Zone (FZ)	91
Figure 4.9: Microstructure image of the FZ of various samples: (a) FZ for sample 2; (b) FZ for sample 6; (c) FZ for sample 16; (d) FZ for sample 17; (e) FZ for sample 20; (f) FZ for sample 25	94
Figure 4.10: SEM micrographs of TiFe intermetallic compound formed (a) at the PMZ on Ti-6Al-4V side, (b) at the PMZ on ASS 316L side, and (c) at the FZ.....	96
Figure 4.11: Maximum load achievable obtained from four different shape of electrode tip	100
Figure 4.12: Vickers micro-hardness profile of μ RSW joint.....	102
Figure 4.13: Effects of different design of electrodes on the average microhardness values at the FZ	103
Figure 4.14: Effects of different design of electrodes on the micro-hardness values (HV) at the PMZ.....	107
Figure 4.15: Macrostructure and microstructure of welded joint by using triangle shape electrode tip: (a) Macrostructure; and microstructure of (b) PMZ on the ASS 316L side; (c) the FZ; (d) PMZ on the Ti-6Al-4V	108
Figure 4.16: Macrostructure and microstructure of welded joint by using square shape electrode tip: (a) Macrostructure; and microstructure of (b) PMZ on the ASS 316L side; (c) the FZ; (d) PMZ on the Ti-6Al-4V	111
Figure 4.17: Macrostructure and microstructure of welded joint by using hexagon shape electrode tip: (a) Macrostructure; and microstructure of (b) PMZ on the ASS 316L side; (c) the FZ; (d) PMZ on the Ti-6Al-4V	112
Figure 4.18: SEM micrographs of (a) the PMZ on Ti-6Al-4V side, (b) the PMZ on ASS 316L side, and (c) TiFe intermetallic compound formed at the FZ for specimen using triangle shape electrode tip.....	115
Figure 4.19: Ti-Fe binary phase diagram.....	117
Figure 4.20: SEM micrographs of (a) the PMZ on Ti-6Al-4V side, (b) the PMZ on ASS 316L side, and (c) TiFe and TiFe ₂ intermetallic compound formed at the FZ for specimen using square shape electrode tip.....	117

Figure 4.21: SEM micrographs of (a) the PMZ on Ti-6Al-4V side, (b) the PMZ on ASS 316L side, and (c) TiFe and TiFe₂ intermetallic compound formed at the FZ for specimen using hexagon shape electrode tip..... 119

University of Malaya

LIST OF TABLES

Table 2.1: Experimental data collected as per full-factorial design of experiments. (Pashazadeh et al., 2016).....	32
Table 2.2: Analysis of variance: (a) nugget diameter (b) nugget height. (Pashazadeh et al., 2014).....	33
Table 2.3: EDS elemental analysis of the welded samples with 4 kA and 8kA welding current (Kianersi et al., 2014)	37
Table 3.1: Chemical composition of ASS 316L and Ti6Al4V	59
Table 3.2: Physical properties of base material	59
Table 3.3: Welding parameters used in the study	67
Table 3.4: Number of experiments during welding and joining process	67
Table 4.1: Experimental data collected as per full-factorial design of experiments	75
Table 4.2: Analysis of variance (ANOVA), $S=0.0752264$, $R^2=0.9363$, adj. $R^2=0.9172$, pred. $R^2=0.8840$	77
Table 4.3: Predicted and experimental values	83
Table 4.4: The element atomic percentage in sample specimen with 1.8 kA welding current, 150 ms welding time, 362 N welding force.....	96
Table 4.5: Experimental results of tensile shear strength test obtained in Phase 1 and Phase 2.....	98
Table 4.6: The element atomic percentage in sample specimen using triangle shape electrode tip.....	115
Table 4.7: The element atomic percentage in sample specimen using square shape electrode tip.....	118
Table 4.8: The element atomic percentage in sample specimen using hexagon shape electrode tip.....	120

LIST OF SYMBOLS AND ABBREVIATIONS

RSW	:	Resistance Spot Welding
μ RSW	:	Micro-resistance Spot Welding
BM	:	Base Metals
HAZ	:	Heat Affected Zone
PMZ	:	Partially Melted Zone
FZ	:	Fusion Zone
CDZ	:	Columnar Dendritic Zone
IMC	:	Intermetallic Compound
DOE	:	Design of Experiment
ANOVA	:	Analysis of Variance
WME	:	Weld Metal Expulsion
EDS	:	Energy Dispersive X-ray Spectroscopy
XRD	:	X-ray Diffraction
TC	:	Truncated Cone
PT	:	Pimple-tipped
LSRSW	:	Large scale resistance spot welding
SSRSW	:	Small scale resistance spot welding
ASS 316L	:	Austenitic stainless steel 316L
Ti-6Al-4V	:	Titanium alloy (ASTM grade 5)

University of Malaya

CHAPTER 1: INTRODUCTION

1.1 GENERAL BACKGROUND

Nowadays there have been an extensive usage in welding and joining process that have been employed for joining either similar or dissimilar metal parts in various fields of different manufacturing industries. These welding and joining processes include soldering, brazing, welding, rivet, and mechanical fasteners. Depending on the types and or combination of energy, the welding processes are classified into two major groups, which are fusion welding and solid-state welding. The fusion welding process utilizes an intense localized heat source to melt the base metal, while solid-state welding is performed under pressure, or a combination of heat and pressure. If heat is used as the main source to melt the base metal, the temperature for solid-state welding process to take place is below the melting point of the materials used.

Resistance spot welding (RSW) is one of the oldest of the electric welding processes in use by industry today. The weld is made by a combination of heat, pressure and time. As the name implies, it is the resistance of the material to be welded to current flow that causes a localized heating in the part. The pressure is exerted by the tongs and tips. The time is the period of current flows in the joint, which is determined by the material thickness and type, amount of the current, and cross-sectional area of the welding tips and contact surfaces. In a typical resistance spot welding (RSW) process, two or three overlapped or stacked stamped components are welded together as a result of the heat created by electrical resistance. This is provided by the work pieces as they are held together under pressure between two electrodes. The welding current is then switched off and the weld nugget will begin to solidify, while at the same time maintaining the electrode pressure.

Spot welding may be performed manually, robotically or by a dedicated spot-welding machine. The heat generation is based on Joules law, which can be expressed as follows, $Q = I^2Rt$ where Q is the heat input in joules, I stand for current in amperes, R stand for the resistance in ohms whereas t stands for the time in seconds. Therefore, the amount of heat generated depends on three factors: the current, the resistance, and the duration of the welding current.

There are three different category of resistance spot welding, large scale, small scale, and micro scale. The thickness range for large scale RSW are 1.5 to 3.2 mm. The thickness range for small scale RSW are 0.6 to 1.5 mm. The thickness range for micro-scale RSW are 12.5 μm to 0.6 mm.

Micro-scale resistance spot welding (μRSW) is a group of micro-joining process (such as resistance spot, parallel gap, series, cross-wire and seam welding), in which micro-joint (sheet metal less than 0.5 mm) are formed between two sheets by resistance heating caused by the passage of electric current. These processes are commonly used in electronic or medical devices, however, despite the ever-increasing application, there is limited research work done. In comparison, extensive studies have been carried out on 'large-scale' resistance spot welding (LSRSW) and 'small-scale' resistance spot welding (SSRSW) of sheet metal thicker than 0.5 mm.

The main consideration in achieving high quality welding solution are the properties of the materials to be joined and the quality requirements of the desired welded joint. There are four main types of structural materials: metals, ceramics, plastics/polymers and semiconductor. Of these, only metals can be resistance welded because they are electrically conductive, soften on heating and can be forged together without breaking. Alloys are formed as the results of the resistance spot welding. Alloys are a mixture of two or more metals. An alloy is normally harder, less conductive, and more brittle than

the parent metal which has bearing on the type of joint one can expect when resistance welding a combination of dissimilar metals.

1.2 MATERIALS AND APPLICATION

μ RSW has evolved as a better joining technology of choice in welding between dissimilar metals with different mechanical properties such as austenitic stainless steel 316L and ASTM titanium alloy grade 5 (Ti-6Al-4V). This is further supported by AMADA CO. LTD where it is stated in the RSW material weldability tool matrix that a good weldability can be obtained when joining between these two dissimilar metals. Throughout history, consumer goods are steadily expanding in the market and now comprises a wide variety of products. Consumer goods are manufactured in small lots and diverse product types. While titanium is used mainly in industries, its application to consumer goods is expected to stimulate repetitive demand for it as consumers become familiar with it. Consumer goods made of titanium alloy or stainless steel using similar RSW process run a wide spectrum of products from conventional accessories like eyeglass frames to sporting goods and household utensils.

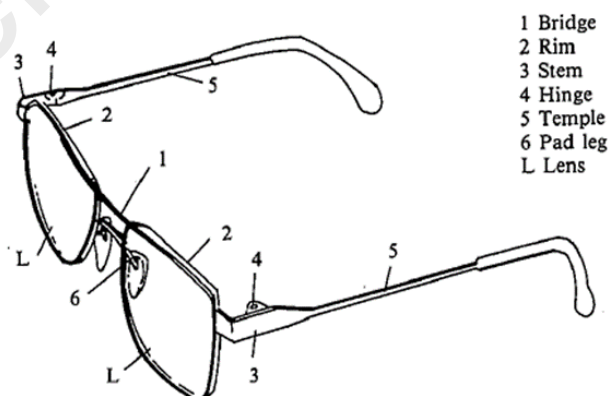


Figure 1.1: Basic illustration of eyeglass frame with numbered parts (Chino et al., 1994)

Nowadays, material properties and consumer needs are the major concerns for the eyeglass frame (ophthalmic frame) industry. The ophthalmic frame is the part of a pair of glasses which is specifically designed to hold the lenses in proper position. The eyeglass frame consists of temples, a bridge, rims, stems, hinges and pad legs, as shown in Figure 1.1, and has at least 14 joining point (Chino et al., 1994). The frames come in a variety of styles, sizes, materials, shapes and colors. In the eyeglass frame industry, manufacturers and engineers are constantly researching ways to reduce the weight of the material used while continuously improving the other aspects of the eyeglass frame properties. There are several important material properties to be considered in order to obtain the highest quality eyeglass frame. One of the most cost-effective ways to improve these material properties is by combining different material together. These could lead to a fabrication of an eyeglass frame with different material properties combined to give the best performance for the consumer. There are five different frame materials which have been used by manufacturer's worldwide, plastic, metal, nylon, natural materials and stone.

RSW has also been successfully implemented in various other applications. This RSW technology application range from large scale to micro scale level. Some of these are involved in the manufacturing of several parts either complex or simple in shipbuilding and marine industries, aerospace, railway, and automotive industries.

Recently there has been an interesting research area for demands on combining the properties of lightweight and corrosion resistance for materials used in the manufacturing of the eyeglass frame. Researchers have focused their efforts to develop an enhanced eyeglass frames with stronger durability and with better properties throughout history. Eyeglass frame materials must be able to overcome many property constraints which include light weight, strength, corrosion resistance, and formability, hypo-allergenic and surface treatability. Eyeglass frames have been historically made of iron, copper, nickel,

and titanium in that order. Initially, commercially pure titanium was used for the eyeglass frames, and commercially pure high-strength titanium (TiX-80) was then investigated for its high strength and 950°C transformation temperature. More recently, commercially pure titanium is giving place to the half alloy (Ti-3Al-2.5V) and titanium alloy grade 5 (Ti-6Al-4V). These type titanium alloys are used due to good drawability, and with the existence of alpha and beta phase inside the composition of the alloys, it has good cold workability and no phase transformation. These types of titanium alloys were comparatively investigated for rim wire formability, number of cycles to rim failure, platability and brazed joint strength.

The major problems for the manufacturing of eyeglass frame is the total cost which includes the materials and the manufacturing process used. The production cost of using titanium alloy grade 5 for eyeglass frames is too expensive. In order to reduce the total cost, austenitic stainless steel 316L is introduced to replace some parts. These types of stainless steel are used due to lower cost than titanium alloys, high flexibility rate, springy properties, stainless technology, and low toxicity. Furthermore, ASS 316L is used because its nickel composition is low, but nickel is necessary to resist carburization and thermal shock. The carbon content is also low as desired to prevent carbide precipitate formation during welding process which makes ASS 316L a suitable choice for μ RSW. The eyeglass frame consists of temples, a bridge, rims, stems, hinges and pad legs and has at least 14 joining point. This calls for the development of a reliable brazing method that solves the problem of dissimilar metal joining. Therefore, μ RSW is used to weld and join these two materials. Other than that, by implementing μ RSW between ASS 316L and Ti-6Al-4V, the total cost can be further reduce as there are no filler metals or flux needed. Thus, reducing the total weight of the eyeglass.

1.3 PROBLEM STATEMENT

Nowadays, research and study are still in progress on μ RSW of dissimilar metals particularly in between austenitic stainless steel 316L and ASTM titanium alloy grade 5 (Ti-6Al-4V). There are many problems and welding defects that possibly could formed during the welding process due to the different element composition and mechanical properties of each material. For example, the difference in the melting point temperature of each material causing an uneven heat distribution during welding thus affecting the localization of the heat to form the weld nugget. Due to these irregularities, the strength of the welded joint might be compromised.

Problems also arises due to fact on finding which combination of welding parameters is the most suitable to be used for this dissimilar μ RSW. In order to achieve better quality in terms of the weld nugget formation and the strength of the welded joint, an optimized process conditions should be achievable by changing the combination between welding current, welding time, and welding force. Different combination of welding process parameters affects the strength differently and a slight change in each welding parameters used will cause significance results change either the formation of the weld nugget and the welded joint strength. Therefore, a systematic statistical analysis is needed to resolve this problem with precise and accurate calculations.

In order to solve the problems with regard of the indifferece materials used, a linear model from statistical analysis is designed to analyze the effects and interactions of the welding parameters with each other by employing full factorial design of experiment (DoE) with L_{27} orthogonal array. In addition, analysis of variance (ANOVA) is used to determine the most influence welding parameter on the strength of the welded joint. This is a very crucial steps because the linear model created must be effective and robust in terms of replicability.

Other than that, current design of electrode tip geometry is not proper to be utilized for this dissimilar μ RSW. Therefore, a new design is introduced in order to reduce the welding defects that may formed. Truncated cone (TC) and pimple tipped (PT) style electrode tip are employed instead of flat nose electrode tip to provide better heat distribution and allowing uniform welding current pass through the electrode tip/ surface of workpiece interface.

Furthermore, limited amount of existing research work and restricted data access increased the needs for performing this research in order to gain benefits for the feasibility study purposes in the future. For micro-scale or small-scale RSW process between similar metals, there have been only two material that have been used such as austenitic stainless steel by (Fukumoto et al., 2008) and TC2 titanium alloy by (Zhao et al., 2013). For dissimilar metals, several researches have been done. For example (Saeed et al., 2014) has performed micro resistance spot welding between titanium and nickel with an addition of alloy filler metal. Another research which have been done by (Xu et al., 2007) which involve studies of small-scale resistance spot welding (SSRSW) of a refractory alloy 50Mo-50Re thin sheet with 0.127 mm thickness. In addition, (Ely & Zhou, 2001) performed micro-resistance spot welding on 0.2-0.5 mm thickness Kovar, steel, and nickel by using different types of power supply.

There are several challenges and difficulty faced by researchers in μ RSW between ASS 316L and Ti-6Al-4V specifically for sheet metal that have thickness less than 0.5 mm. Firstly, excessive indentation would prone to happen without proper knowledge with regard the right used of electrode tip geometry and electrode force (welding force). This could lead to the formation of micro-cracks and holes within the weld nugget. With these weld defects, it'll compromise the strength of the welded joint thus lead to failure in terms

of dissimilar welding. Furthermore, excessive indentation could also lead to weld metal expulsion (WME).

Secondly, without the right welding current and welding time, the electrode tip may adhere or stick to the contact surface area of the workpiece. Without the right design of electrode tip geometry, it could also lead to electrode sticking. This pose a problem towards long term usage as the tip needs to undergoes proper electrode dressing thus leading to material wear and tear. Next, burn-thru may also occur if the welding current used is too high. This is because since the weld metal sheet is less than 0.5 mm, the correct size of weld nugget must be within it limits. If the current supplied is way more than the limit, the excessive heat distribution will cause burn-thru. Lastly, during experimental investigation where trial and error method is employed, non-round weld nugget may form which greatly influence the overall strength of the welded joint.

The aim of this research study is to investigate a proper evaluation on the influence of the welding parameters such as welding current, welding time, welding force (pressure exerted by the electrodes), and the design of the electrode geometry on the formation of the weld nugget and the mechanical properties such as the allowable shear stress load on the welded joint of micro-resistance spot welding (μ RSW) between austenitic stainless steel 316L and ASTM titanium alloy grade 5 (Ti-6Al-4V). The subsequent effect on their microstructural and the mechanical properties is also investigated.

1.4 OBJECTIVES

There are three main objectives to be achieved throughout this research:

1. To determine the optimum combination and the most significant micro-resistance spot welding (μ RSW) parameters between ASS 316L and Ti-6Al-4V by using Design of Experiment (full-factorial) and ANOVA technique.
2. To investigate the performance of μ RS welded part by performing mechanical engineering tests and microstructure characterization on the fusion zone (FZ).
3. To determine the suitable tool design based on the optimum parameters by performing proper investigation through various experiment analysis.

1.5 SCOPE OF THE STUDY

Because of the μ RSW machine capabilities and some constraint factors, only three parameters were considered as the manipulate variable while others process parameters were kept constant. The welded joint between dissimilar metals were evaluated in terms of appearance, metallographic microstructure and mechanical properties. There are two separate sets of experiment performed in this research study known as Phase 1 which refer to the study of optimization on the welding process and Phase 2 which refer to the optimal design of electrode geometry for efficiency purposes. Phase 1 will cover the first and second objective whereas the third objective will be achieved in Phase 2.

In Phase 1, the process parameter which is considered as the manipulate variables throughout the experiment run is the welding current (kA), welding time (ms), and welding force (N). The process parameters which are kept constant at all the time are

electrode geometries, squeeze time, hold time and the welding environment where all the experiment is conducted at room temperature.

In Phase 2, the process parameters which is considered as the manipulate variables is the design of the electrode geometry. There are three different design used in the experiment which are triangle, square and hexagon. The process parameters which are kept constant are welding current (kA), welding time (ms), welding force (N), squeeze time, hold time and the welding environment.

The testing for mechanical properties included tensile shear stress test, coach peel test, Vickers micro-hardness test meanwhile the metallographic analysis and microstructure study comprises of optical microscope, scanning electron microscope (SEM), energy-dispersive X-ray spectrometer (EDS), and X-ray diffraction (XRD) analysis. The optimization of the process parameters is obtained by using full factorial design of experiment (DOE) and the data obtained are further analyzed by using statistical analysis tool, ANOVA in order to determine the most significant parameters that affect the welding process.

1.6 ORGANIZATION OF THE THESIS

This dissertation consists of five chapter. The chapters included are as follows:

Chapter one provides and explain the general background on the micro-resistance spot welding and problem statement that need to be solved and investigated in this study. It also includes the scope and limitation of research and objectives that need to be achieved in this study.

Chapter two introduces the literature review, which summarizes the whole literature and sources like journal papers, reference books and article papers. The related theory of the study and the previous work and available outcomes are presented in this

chapter. Furthermore, research gap is discussed, and the findings are concluded in a summary.

In chapter three, the material selection and preparation process used during experiment and testing in this research study will be discuss thoroughly. The design and fabrication of the welding electrodes are briefly explained. Also, the design of experiment (DOE) and statistical analysis tool used to conduct this experiment will be listed down for future reference. Furthermore, this chapter includes a detailed description and information of the methodology used in this research which also includes the range of parameters used and the optimum set up condition to conduct the mechanical testing for accurate measurement.

Chapter four presents the results and discussion of this research. The results will be displayed in the form of table and figures for quick and easy access before performing analysis and data tabulation. Then the collected data will be analyzed by using MINITAB software and explained in graphical form. The SEM image are studied and further investigated by employing EDX point analysis.

In chapter five, the major findings have been agreed or disagreed to the objectives are concluded. Finally, the recommendations are suggested for future improvement.

CHAPTER 2: LITERATURE REVIEW

2.1 INTRODUCTION

μ RSW has gained a lot of attention among researchers and industries because of its benefits and advantages. Welding and joining between dissimilar materials to form a strong and durable welded metal joint has been recognized as an interesting research area, with large scale research conducted within the last decade especially with respect to different types of stainless steel and different grades of Ti alloy. In μ RSW, the material thickness usually used as the workpiece is no more than 0.5 mm. This is because low voltage is used by the μ RSW machine during the welding process. Other than that, small size design of electrode geometry is used to grip the workpiece together firmly to avoid the presence of air in between of the workpiece. Consistent electrode tip contact is compulsory during welding. The electrode design and material are important as it supplied the welding current.

There are many differences between micro-scale RSW and large-scale RSW. Simply downsizing from large-scale to micro-scale may lead to the formation of welding defects at the welded joint such as weld metal expulsion (WME), micro-cracks, voids, embrittlement of the weld, and formations of non-round weld. In order to avoid such mishap, a detailed investigation and proper selection must be made to determine the optimum welding parameters for obtaining the ideal weld nugget shape and strength.

Main welding parameters used in this research study is welding current, welding time and welding force. So, a statistical tool will further help to perform specific analysis to obtain the most optimum welding parameters. Furthermore, material selection for μ RSW also an extremely important aspect that should be prioritized by researchers and manufacturers such as the material compatibility, mechanical properties, weldability with each other metals and etc. This will help to avoid problems in the future. Experiments by

using trial and error are an important method besides using another existing knowledge. This will help to improve and gaining a reliable data throughout the research process.

μ RSW is performed in a few simple steps:

1. First, the welding parameters was selected, and the values are inserted in a system controller. The welding electrode material and the design geometry is chosen properly to match the respective material of the weldment.
2. The upper welding electrode is plunged into the lap joint of the sheet metals. After the electrode tips come in contact with the surface of the sheet metals the squeeze time will start. During this period of time, the upper and lower electrode will squeeze both of the sheet metals so that there will be no air gap during the welding process in order to prevent some of the welding defects.
3. After the squeeze time ended, the process will enter the welding time phase. Throughout this period, the current is supplied from the upper part of the electrodes towards the lower part. The heat from the current will cause both of the sheet metals to melt and formed a weld nugget at the faying surfaces between the sheet metals. As the heat is supplied, the electrode maintains it pressure until the welding process ended.

Once the welding time ended, it will proceed to hold time phase. During this phase the pressure exerted by the welding electrodes is maintained while the weld nugget is allowed to cool as the welding current cease away from the process. After the hold time ended, the welding electrode is retracted. Figure 2.1 shows the schematic illustration of the basic steps in μ RSW process.

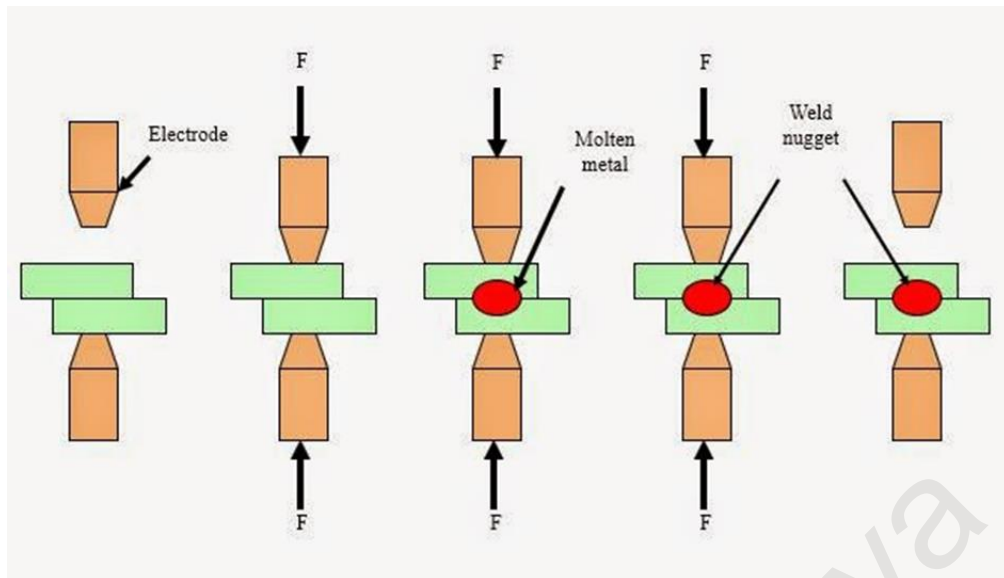


Figure 2.1: chronological order of a simple RSW process (Resistance Spot Welding (RSW) Working Principle and Advantages-disadvantages, 2014)

There are several different zones exist in the study of μ RSW. First and foremost, the heat affected zone (HAZ) where the peak temperatures are too low to undergo melting, but the temperature is high enough to barely cause the microstructure and materials properties to change drastically. Next, the fusion zone (FZ) where both of the base metals reached liquidus temperature and melt. Subsequently both of the base metals elements mix together to form an alloy after solidification take place. Lastly, the partially melted zone (PMZ). It is an area immediately outside the weld metal where liquation can occur during welding. The base metal is heated up to between eutectic temperature T_E and the liquidus temperature T_L during welding. Therefore, the fused materials become a solid-plus-liquid mixture, which is partially melted (Kou, 2003).

2.2 ADVANTAGES AND DISADVANTAGES

The μ RSW joining technology has some distinctive advantages over the large scale RSW and other conventional welding processes which include very little operator skill are needed to operate the μ RSW machine. Furthermore, the operator safety is ensured as very low current is used throughout the welding process. Moreover, μ RSW produces a reliable electro-mechanical joint at micro level that have good quality and high strength properties which also inexpensive as the material size/thickness is smaller.

Besides, μ RSW requires a very short amount of process time to complete one welded joint. These features are extremely important in industry as high production rate in a short amount of time is prioritize and well suited for mass production as in return a huge profit is achievable. Due to the heating of the work-piece confined to a very small area, less heat distortion formed throughout the welding process and conveniently if defects exist, it can be easily detected and troubleshoot as early possible. Additionally, by utilizing this technique, no filler rod or flux is needed for the formation of the welded joint. It is also possible to weld dissimilar metals which have different mechanical properties as well as metal plates with different sheet metal thickness. Another advantage of μ RSW is that the process is clean and environmentally friendly. Furthermore, there are no consumables used in this process except for the electrical power as the welding current and a relatively small electrode wear which can be overcome by electrode tip dressing process.

Although the μ RSW technology has many distinctive advantages either for industry or research purposes, it is not bereft of disadvantages or weaknesses. One of the main disadvantages is that the workpiece material requires firm clamping in between the surfaces of the upper and lower electrode tip with the sheet metals and the faying surface between each base metal in order to prevent the existence of an air gap which will lead to formations of certain welding defects such as voids, porosity and shrinkage cavity. Thus,

suitable jigs and fixture are necessary to reduce the degrees of freedom. Other than that, some μ RSW operations are only limited to lap joints. Therefore, a lot of complex geometry are nearly impossible to be welded by using this technology. Due to the complex nature of the μ RSW machine, a skilled person is needed for the maintenance process. Lastly, bigger metal sheet thicknesses cannot be welded and joined together by using this process.

2.3 WELDING PROCESS PARAMETERS

Achieving good weld quality starts with a good process design that minimizes the variables encountered in welding. Electrode force, welding current density and welding time are the most important welding parameters in electrical resistance spot welding. An electronic control unit is employed in welding machines to pursuit the welding variables. The desired weld nugget diameter can only be obtained by adjusting welding current density versus welding time properly. When time is held short, the weld nugget diameter decreases. On the contrary, when it is held long the amount of molten metal increases and fused metal spurts out and as a result the strength of welding joint decreases.

2.3.1 Welding current

The amount of weld current is controlled by two things: first, the setting of the transformer tap switch determines the maximum amount of weld current available; second, the percent of current control determines the percent of the available current to be used for making the weld. Low percent current settings are not normally recommended as this may impair the quality of the weld. The weld current should be kept as low as possible. Hence, high welding current reduces the possibility of forming a good round weld nugget. This is because the weld nugget has a high liquation cracking susceptibility. The cracks appear at the fusion zone (FZ) of the weld nugget when the welding current used is higher from the limit value. The usage of higher welding current will increases

the cracking tendency because of increased pressure around the weld nugget and the tensile stress in heat affected zone (HAZ) during cooling time (Saha et al., 2012). When determining the current to be used, the current is gradually increased until weld spatter occurs between the metal sheets. This indicates that the correct weld current has been reached (Aslanlar, 2006).

Among several factors which influence physical and mechanical properties of a welded joint, the most important parameter affecting tensile-shear load bearing capacity is the weld nugget diameter size. Base on the research reported by Kianarsi et al. (2014), the weld nuggets diameter will increase if the welding current increased. Other than that, the amount of energy absorption also increases within an increase in the welding current. However, the welding current also should be controlled properly for every level of RSW process. This is because as it is expected that within increasing the welding current, the failure mode and fracture characteristics can be characterized from solely interfacial failure mode (IF) to a complete tear around the weld nugget area or HAZ. Other than that, similar observations have been reported by Kocabekir et al. (2008). It was found out that the increasing of the welding current related with welding time will increase the dimension of the weld nugget thus increasing the tensile shear strength of the welded joint. Furthermore, there exist several cavities at the center of the weld nugget that can be observed through optical examination process in some of the welded sample. These internal defects are generally caused by high usage of welding current which produce excessive weld heat input.

Emre & Kacar (2016) performed resistance spot welding of zinc galvanized-coated with uncoated TRIP800 steel sheets 1.5 mm in thickness and the details are investigated. It was found that the nugget diameter increased with increasing welding currents greater than 6 kA for all welding times (15, 20 and 25 cycles). By using a welding current greater

than 6 kA causes more forging of soft zones and decrease the nugget height. Furthermore, the tensile shear strength of both weldments improves by increasing the heat input associated with the welding time and the welding current, except 9 kA. The coating prevents negative effect on the strength of the joint and the failure mode (Ertek Emre & Kaçar, 2016).

2.3.2 Welding time

The time used in RSW process can be divided into three different time phase, squeeze time, welding time, and hold time. Squeeze time is the time interval between the initial application of the electrode force on the work and the first application of current. It is necessary to delay the weld current until the electrode force has attained the desired level. After that, the weld time is measured and adjusted in cycles of line voltage as are all timing functions. When it is held long, the amount of molten metal increases and fused metal spurts out and a series of peaks and valleys occur on a microscopic scale on the surfaces of metal components and crystal structure of material changes. When the electrodes are removed immediately, the heat will dissipate, and contact surface area becomes dark. After the welding operation, the electrodes should be applied to the sheet to chill the weld. Hold time is necessary to allow the weld nugget to solidify before releasing the welded parts, but it must not be too long as this may cause the heat in the weld spot to spread to the electrode and heat it. When welding galvanized carbon steel, a longer hold time is recommended (Aslanlar, 2006).

By increasing both, the welding current and welding time, it will lead to a relatively large formation of weld nugget diameters when compared if only increasing the welding current, but the welding time are kept constant. There is not an obvious interaction between the welding time and the nugget height, however by increasing the welding current causes the decrease in the weld nugget height. The welding current are the most

important parameter affecting the formation of the nugget (Pashazadeh et al., 2016). By increasing the electrode force, welding current and welding time will increase the tensile-shearing strength of the commercially pure (CP) titanium sheets 1.5 mm in thickness that were welded by using RSW process (Kaya & Kahraman, 2012). From the observation made, it is found out that the optimum results obtained in tensile shearing tests were achieved at 6 kN electrode force, 7 kA weld current and 30 cycles welding time.

2.3.3 Welding force

A key parameter of all three types of resistance welding are the weld pressure or force. The proper and consistent application of force improves the mating of the materials increasing the current paths, reducing the interface resistance, and ensuring that any oxide barriers between the work pieces are broken through. The purpose of the electrode force is to squeeze the metal sheets to be joined together. This requires a large electrode force because else the weld quality will not be good enough. However, when the electrode force is increased the heat energy will decrease. This means that the higher electrode force requires a higher weld current. When weld current becomes too high, spatter will occur between electrodes and sheets. This will cause the electrodes to get stuck the sheet. An adequate target value for the electrode force is 700 kg/cm². One problem, though, is that the size of the contact surface will increase during welding. To keep the same conditions, the electrode force needs to be gradually increased. As it is rather difficult to change the electrode force in the same rate as the electrodes are “mushroomed”, usually an average value is chosen (Aslanlar, 2006).

Excessive used of welding force also proven to compromise the overall strength of the welded joint. There are two main factors which are responsible for the reduction in the welded joint strength as the welding force is increased; (1) higher welding force will reduce the heat input thus reducing the weld nugget size; (2) the indentation caused from

the electrode tips on the sheet surfaces induces high stress concentration in the regions around the weld nugget (Russo Spena et al., 2016).

2.3.4 Tool geometry

Welding electrodes are installed in the weld head to hold and maintain contact with the work pieces through the full weld schedule. The welding electrodes play three different roles in resistance welding: maintaining uniform current density, concentrating current at welding points, and maintaining thermal balance during welding. Electrodes are available in many shapes. Electrode material and shape are determined by considering the force necessary for welding and the thermal conductivity of the workpieces. In conventional macro-welding, the electrodes are made of copper alloys and usually water-cooled. However, in micro-welding, the electrodes are made of a wide variety of conductive and refractory materials depending on the parts to be joined, and air-cooled. Several designs of electrodes geometry can be observed in Figure 2.2.



Figure 2.2: Illustration of various electrode geometry (TUFFALOY Company)

In resistance spot welding, the electrode tip is utilized to create the spots at the desired location between the metal sheets to be joined. The tip of the electrode has its own unique geometrical configurations, which can be designed to fulfill various jobs of specific

welding process (Saeed et al., 2014). Furthermore, the design of electrode tip shape contribute significant effects on stresses, welding current flow, and heat distribution (Zhou et al., 2000). Furthermore, the effect of electrode tip geometry on welding current distribution has been investigated by (Bowers et al., 1990). A mathematical model was introduced to determine welding current distribution in both truncated cone (TC) and pimped tipped (PT) electrodes. They discovered that electrode tip and metal sheet interface contact angles approaching 90° provide the most uniform heat distribution supplied from the electrode tip. It was concluded that an efficient design of electrode tip geometry must be well balanced in terms of mechanical and thermal properties as well as able to maintain the welding current uniformity and heat distribution. Similar research have been performed by (Y. Li et al., 2013). Base on the research done, a multi-physics finite element model was used to investigate the effect of the cone angle variation on resistance spot welding. The results showed that the cone angle variation affects not only weld quality but also electrode life.

The size of the weld will not be larger than the electrode face. Therefore, it is important to utilize electrodes of the same tip diameter as the desired weld nugget. The current density at the workpiece interfaces varies as the square of the diameter of the electrode face. Electrode positioning is critical: electrodes should be positioned where the weld is desired, should generally not overhang the edges of the part (except in wire and small terminal welding), should not bend, should be perpendicular to the plane of the workpieces, should maintain constant diameter (constant area) as they wear, and should be cleaned and dressed regularly. Electrodes should be dressed by using 600 grit silicon carbide paper or polishing disk pulled with light force in one direction only. Furthermore, electrodes should be replaced when the tip is damaged or blows out. It is best to have all electrode tips reground regularly by a qualified machine shop.

In every μ RSW process run, if the dimension of the electrode tip morphology is too small, it may result in the formation of weak spot weld with the existence of welding defects. Smaller dimension of electrode tip also may cause severe heat concentration and surface burnt-thru or excessive indentation on the surface of the workpiece (Saeed et al., 2014). Electrode tip with larger surface contact area led to lower heat distributed towards the workpiece which are the results in decreasing of welding current density. This is an important factor that should not be overlooked by researchers because by increasing the heat input, it will significantly affect the grain growth and forming higher concentration of intermetallic compound (IMC) such as TiFe and TiFe₂ particles inside the fusion zone. These IMC formations lead to poor joint with inferior tensile strength due to its brittle behaviour. Furthermore, Saeed et al. (2014) found that the geometry of the electrode influence formation and final shape of the weld nugget at the welded joint.

Zhang et al. (2015) found out that the morphology of electrodes used in RSW of 6008-T66 aluminium alloy and H220YD galvanised high strength steel was optimised, which were a planar circular tip electrode with tip diameter of 10 mm on steel side and a spherical tip electrode with spherical diameter of 70 mm on aluminium alloy side. The schematic diagram of RSW arrangement are shown in figure 2.3.

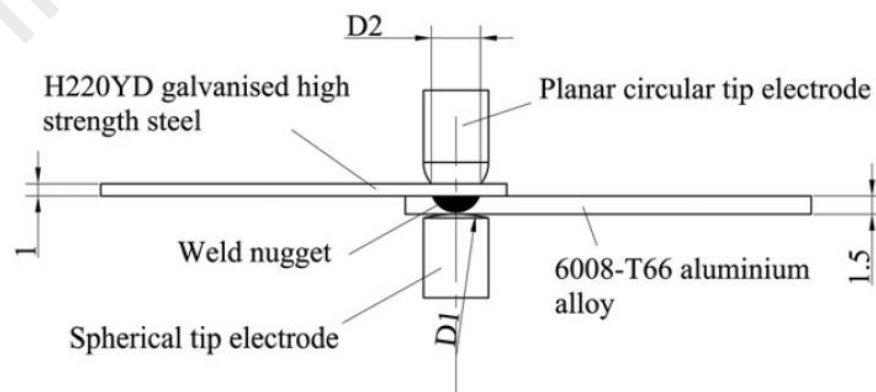


Figure 2.3: Schematic diagram of resistance spot welding arrangement (W. Zhang et al., 2015)

Furthermore, the welded joint obtained with optimized electrodes could be regarded as special welded-brazed joint with a straight interface between aluminum nugget and steel, which was formed by means of wetting and spreading of molten aluminum nugget on solid steel. Moreover, tensile shear loads up to 5.4 kN was achieved and the welded joint exhibited nugget pull-out failure mode during tensile shear testing (W. Zhang et al., 2015).

2.4 RESISTANCE SPOT WELDING OF DISSIMILAR MATERIAL

Resistance spot welding process between dissimilar materials are considered one of the most challenging part in the material engineering history. In order to obtain a welded joint which, inherit multiple properties from the base material, metals are welded by RSW and the welded joint are thoroughly studied. There are several methods used to determine the strength of the welded joint, mechanically or numerical analysis. Microstructure analysis are used to study the metallographic condition of the weld nugget in order to investigate whether its exhibit brittle or ductile properties. Due to the difference in thermal cycle experienced with each metal causes the dissimilar resistance spot welding to be more complex than similar welding. Despite of various application of dissimilar RSW, reports in the literature dealing with mechanical behaviors of them are limited.

There are two major problem exist in RSW of dissimilar metals. First and foremost, the uneven heat distribution throughout the weld nugget formed due to the difference of materials properties and the possibilities of facing difficulties in observing and analyzing the metallography of the alloy produced when joining dissimilar materials. Heat distribution in the weld nugget largely depends on the difference in thermo-physical properties of the materials involved. There exists a risk where the fusion zone of the weld nugget will form inside the sheet of the material used and not at the interface if one of the materials have significantly larger electrical resistivity. Furthermore, in order to maintain

the heat balance throughout the entire welding process, dissimilar electrode is used for the upper and lower part. For example, larger diameter electrode can be used at the less conductive material side to dissipate the excess current.

Similar findings were discovered by W. Zhang et. al. (2015) in dissimilar RSW of aluminum alloy and galvanized high strength steel. They found that the optimal design of electrode geometry was a planar circular tip electrode with tip diameter of 10 mm on the steel side and a spherical tip electrode with spherical diameter of 70 mm on the aluminum alloy side. Next, problems will arise for the metallography due to difficulties in identifying the grain structure or boundaries of the mixture formed at the weld nugget through either optical microscope or scanning electron microscope (SEM). Moreover, sometimes the zone formed at the weld nugget does not follow the regular formation as there may be no phase transformation upon the mixture of two different materials.

Second major problem faced in RSW of dissimilar metals are the formation of hard and brittle intermetallic compound (IMC) and how its mechanical properties affecting the strength of the welded joint. Usually this problem is difficult to overcome since there are no general rule to follow and each materials combination need to be considered individually. The formation of the intermetallic compound and/or solid solutions are an important aspect that need to be predicted at an early stage. The heat generation and distribution can be adjusted by using the welding parameters in order to achieve more desirable phases. Furthermore, interlayers and filler materials also commonly used since the addition of third materials can improve and modify the properties of the phase produced at the weld nugget. (W. Zhang et al., 2015) concluded that due to the difference in elemental composition of each materials, hard and brittle intermetallic compound (IMC) layer composed of Fe_2Al_5 and $\text{Fe}_4\text{Al}_{13}$ with an overall thickness of about $4.0 \mu\text{m}$

was formed at the aluminum/steel interface. This is a big hurdle towards the researchers as IMC formed may compromised the overall strength of the welded joint.

A few studies have been undertaken in order to study the resistance spot welding between different metals. Ignasiak et al. (2012) present their findings which shows the results of metallographic investigations on spot welds made of high-strength steel HSLA340 and dual phase DP600 steel. In the weld nugget of HSLA steel, low-carbon martensite microstructure was found meanwhile the DP600 steel exhibit martensite and bainite microstructure. Moreover, in both steels, there are no trans crystallization were formed which indicate a good fusion of the metals within the welded joint (Ignasiak et al., 2012). Arghavani et al., (2016) explored and investigate the effects of zinc layer on microstructure and mechanical behavior of resistance spot weld between aluminum to galvanized (GS-Al joint) and low carbon steel (PS-Al joint). The obtained results showed that the nugget 'diameters' of PS-Al and GS-Al joints are almost the same in size since the melted zinc layer was pushed toward the outer regions of the weld nugget even though the weld nugget 'volume' in PS-Al joint was larger. The melting and evaporation of zinc coat induce the reduction of Al-Fe intermetallic layer thickness. The fixture-induced tensile stress has been reduced by the presence of zinc element inside the welded joint (Arghavani et al., 2016).

Verma et al. (2014) investigated that a good resistance spot welding process require the most optimum condition that can afford allowance in the parametric values for a high-quality weld nugget formation. In their research, austenitic stainless steel 304 and 316 are used for the RSW process and the tensile strength and hardness are investigated by utilizing the Taguchi method for the design of experiment (DOE) and the analysis of variance (ANOVA) while the microstructure analysis are done by using the Schaeffler diagram. They have summarized the investigation of the research. The tensile shear

strength for different grade of austenitic stainless steels (ASS 304 to ASS 316) was found to be comparatively higher when compared with tensile shear strength for similar sheets (ASS 304 to ASS 304 and ASS 316 to ASS 316). An asymmetric fusion zone was obtained for the dissimilar RSW between the austenitic stainless steels due to the material properties difference in electrical resistivity and the coefficient of thermal expansion. From the ANOVA, they have found out that current is the most influencing factor on the dissimilar welding process (Verma et al., 2014).

Vural et al. (2006) presents an experimental investigation on the fatigue strength of resistance spot welded galvanized steel sheets and austenitic stainless steel (AISI 304) sheets. Lap joint are used for the joining purpose of the sheet materials. The nugget diameter and material combination were used as the experimental welding parameters. For each specimen, the high cycle fatigue tests were performed and $S-N$ curves are obtained. The highest fatigue limit is shown by the combination of the galvanized steel sheet. The minimum fatigue limit is obtained from the galvanized-AISI 304 sheet combination (Vural et al., 2006).

Liu et al. (2010) developed a new technique by employing different electrode geometry for the resistance spot welding (RSW) of magnesium to steel which producing a welded joint strength as high as 95% of that of Mg to Mg joint. They have investigated the dissimilar joining by performing mechanical testing and metallurgical examination. In this research, they have been using different electrode geometry for the upper and lower part. This is crucial and important in order to keep the temperature of steel below its melting point during the welding process. The results show that the mechanisms of joining during RSW of a magnesium alloy to Zn-coated steel involve braze welding, solid-state bonding, and soldering. The joint formation in comparison of RSW of Zn-coated steel with steel, Au-plated Ni, and bare Ni sheets is discussed. A possible

expansion of this technology also is revealed through the findings in their research (Liu et al., 2010).

Resistance spot welding of 1.5 mm thickness sheets of 6008-T66 aluminum alloy and 1.0 mm thickness sheets of H220YD galvanized high strength steel sheets were used by W. Zhang et al. (2015) through lap joint. The morphology of the welding electrodes was design optimally. The optimized electrodes were a planar circular tip electrode with tip diameter of 10 mm on the steel side and a spherical tip electrode with spherical diameter of 70 mm on the aluminum alloy side. Based on their study, the obtained welded joint with optimized electrodes could be regarded as a special welded-brazed joint because of the formation of a straight interface between aluminum nugget and steel due to wetting and spreading of molten aluminum nugget on solid steel. Moreover, an intermetallic compound layer with maximum thickness of about 4.0 μm was formed at the aluminum/steel interface in the welded joint. Furthermore, it is found that the current density distribution during welding with optimized electrodes was more homogeneous than that with F type electrodes.

A study was reported by Marashi et al. (2008) where resistance spot welding was used to join 1.1 mm thick galvanized low carbon steel and 1.2 mm thick austenitic stainless steel. The main objective of their research is to analyze and study the failure behavior of dissimilar resistance spot welds. Based on their study, the relationship between weld fusion zone characteristics (size and microstructure) and failure mode are investigated. It was found that the strength of the spot welded joint in the pullout failure mode are controlled by the strength and the fusion zone size from the galvanized carbon steel side. Moreover, in order to determine the failure mode, the hardness of the fusion zone which is determined by the dilution level between two base metals, and the fusion zone size on galvanized carbon steel side are investigated (Marashi et al., 2008).

Similar study was reported which also used carbon steel as the base metals. The main objective of the research is to study the corrosion fatigue behavior of RSW for dissimilar metals with significant difference in thickness of the sheet metals. The material used for the resistance spot welding are 1.0 mm thick-austenitic stainless steel SUS304 and carbon steel SS400 with thickness of 3.0 mm. The welding parameters that have been employed throughout the research are welding current, welding time and electrode force (Ilman & Soekrisno, 2011).

In 2015, RSW of aluminum-steel was found with respect to the usage of comparative study between experimental and simulation analysis. It was reported by (Wang et al., 2015) who developed a simulation model for Al-steel resistance spot welding process, which directly couples the thermal, electrical and mechanical fields and thereby solved the equations simultaneously. The newly developed model provides valuable information on dynamic current flow, heat generation and transfer, nugget growth and mechanical deformation during the process.

A two-dimensional axisymmetric model is employed to model the Al-steel RSW process in ANSYS v15. Throughout the welding process, 2.0-mm thick Al alloy AA6022-T4 sheet and a 2.0-mm thick zinc-coated low carbon steel sheet were used. Electrodes made from ZrCu (C15000) were employed with a face diameter of 10 mm and weld face radius of curvature of 25 mm.

Thermo-compensated resistance spot welding (RSW) with a Zn interlayer was designed by Y. Zhang et al. (2015) in order to join AA5052-H12 (Al) aluminum alloy to AZ31B (Mg) magnesium alloy. Zn interlayer is introduced in between both base metals in order to restrict the formation of Mg-Al brittle intermetallic compound thus improving the tensile-shear properties of the welded joint significantly. In this study, the applied welding current have been reduced compared with traditional RSWs. The welded joints

were characterized by their microstructure analysis and mechanical properties. Moreover, there are two types of failure modes that were observed and critically analyzed in the Mg/Al with Zn interlayer thermo-compensated RSW joints.

Since titanium metal is quite expensive to acquire, the research regarding titanium was rather limited. The dissimilar Al/Ti resistance spot weld has been studied by Y. Li et al. (2015). The main objective of the study is to investigate the impact of electromagnetic stirring (EMS) upon the microstructure and mechanical properties of the Al/Ti welded joint. They also have study the effects of the welding current, welding time, and electrode force upon the tensile shear properties and the microstructures in the Al/Ti resistance spot weld joint were characterized by comparing them to those in an Al/Al resistance spot weld joint. Based on the method that have been used, they found that the electromagnetic stirring caused by an external magnetic field promotes the rotation of the molten metal, which results in the enlargement of the bonding diameter of the Al/Ti joint.

2.5 METHOD OF INVESTIGATION

2.5.1 Design of experiment

In order to critically analyze the quality and performance of the resistance spot welding, several tests and examination methods are used. Statistical modelling and experimental investigation are an important method to be utilized to select the most optimal combination of welding process parameters for obtaining the highest weld strength. Design of experiments (DOE) such as Taguchi method, full factorial methodology, response surface methodology (RSM), artificial neural network (ANN), and multi-objective genetic algorithm are used to screen and select the welding parameters.

To investigate the possible interactions between each given parameter, a proper DOE need to be implemented. Design of experiment (DOE) is a structured and organized method that is used to determine the possible interactions between different factors affecting a process and the results of the process (Phadke, 1995). It is considered as one powerful technique for improving the quality of a process and enhancing the productivity rate to an optimum level. Through experimentation, changes are introduced into a process or a system to observe any significant effect on the performance. It is by far the most efficient statistical method used for optimizing changes. DOE methods can also be useful in establishing statistical control of a process. If a set of control charts have shown an out-of-control process, where there are several or many controllable input variables, DOE methods help to identify the most influential process variables. Furthermore, DOE is not just only an important engineering tool for improving an existing process, it also has extensive applications in the development of producing an efficient and effective new process.

In statistical analysis, a full factorial design of experiment is an experiment which the analysis consists of two or more factors, each with a distinctive level where the experimental unit consist of all the possible interaction of combination of each level across all factors. In a simple explanation, the experiments will be conducted under all combinations of factor levels. For example, an experiment is conducted with two levels for each factor. So, for K factors, the number of experiments will be 2^K . The experimenter can observe the main effects (effects of each factor separately) and interaction (a result that generates when two or more factors are set together) effects. Therefore, in cases of full factorial DOE for two factors and two levels, there are four (2^2) possible outcomes. (Patel, 2013) used 3^3 full factorial DOE to determine efficiently the effect of several parameters on the welded joint of the RSW experiment.

The key steps in designing an experiment include:

1. Identify factors of interest and a response variable.
2. Determine the appropriate levels for each explanatory variable.
3. Determine a design structure.
4. Randomize the order in which each set of conditions is run and collect the data.
5. Organize the results in order to draw an appropriate conclusion.

2.5.2 Analysis of Variance (ANOVA)

After the results are obtained and tabulated by using DOE, the next step is to identify which welding parameters have the most significant effect which influence most of the outcomes/results of the welding process. These investigations are identified by using multi-way analysis of variance (ANOVA). This analysis consists of simultaneous hypothesis tests to determine if any of the effects are significant. It involves two or more independent factors, and if there is replication at each combination of levels in a multi-way ANOVA, a factorial design will be created. A factorial design using ANOVA has at least two independent variable which the interaction with each other are calculated (Navidi, 2008).

Pashazadeh, (2016) successfully identify three welding parameters, the welding time, the welding current, and the welding pressure/force as the main effective welding parameters on the weld nugget dimensions including the weld nugget diameter and height using full factorial design of experiments. This show the effectiveness of statistical analysis tool to investigate the interaction of each parameters and determine the most significant parameters affecting the weld nugget dimensions. The experimental data collected are shown in Table 2.1. Table 2.2 shows the analysis of variance which were derived from the full factorial DOE. The regression equation is used to establish an input-output relationship throughout the welding process. This equation is derived from the

regression analysis, as only the effective terms are considered in the equation. The following regression equation is obtained for the weld nugget diameter:

$$\text{Nugget diameter} = 3.586 + 0.2725 (\text{current}) + 0.210 (\text{time}) - 0.2125 (\text{pressure} * \text{current}) - 0.0525 (\text{pressure} * \text{time}) - 0.0988 (\text{current} * \text{time}) + 0.0863 (\text{pressure} * \text{current} * \text{time})$$

Table 2.1: Experimental data collected as per full-factorial design of experiments. (Pashazadeh et al., 2016)

Run order	Welding pressure (kgf/cm ²)	Welding current (kA)	Welding time (cycles)	Nugget diameter (mm)	Nugget height (mm)
1	3	5	6	2.68	0.44
2	3	5	6	2.53	0.47
3	4.4	5	12	3.79	0.51
4	4.4	6.5	6	3.53	0.38
5	4.4	6.5	12	3.89	0.33
6	3	6.5	12	4.2	0.37
7	4.4	5	6	3.45	0.7
8	3	5	12	3.57	0.5
9	4.4	5	12	3.7	0.51
10	3	6.5	6	3.91	0.35
11	3	5	12	3.43	0.52
12	4.4	6.5	12	3.79	0.36
13	3	6.5	6	3.98	0.37
14	3	6.5	12	4	0.39
15	4.4	5	6	3.36	0.66
16	4.4	6.5	6	3.57	0.37

Table 2.2: Analysis of variance: (a) nugget diameter (b) nugget height. (Pashazadeh et al., 2014)

Source	DF	SS	MS	F	P
(a) Analysis of variance for nugget diameter					
Pressure	1	0.0380	0.0380	5.30	0.050
Current	1	1.1881	1.1881	165.59	0.000
Time	1	0.7056	0.7056	98.34	0.000
Pressure*current	1	0.7225	0.7225	100.70	0.000
Pressure*time	1	0.0441	0.0441	6.15	0.038
Current*time	1	0.1560	0.1560	21.75	0.002
Pressure*current*time	1	0.1190	0.1190	16.59	0.004
error	8	0.0574	0.0071		
total	15	3.0307			
(b) analysis of variance for nugget height					
Pressure	1	0.1050	0.1050	35.77	0.000
Current	1	0.1207	0.1207	411.09	0.000
Time	1	0.0039	0.0039	13.30	0.007
Pressure*current	11	0.0150	0.0150	51.09	0.000
Pressure*time	1	0.0189	0.0189	64.36	0.000
Current*time	1	0.0027	0.0027	9.38	0.016
Source	DF	SS	MS	F	P
Pressure*current*time	1	0.0076	0.0076	26.06	0.001
error	8	0.0023	0.0002		
total	15	0.1818			
S = 0.0847054, R-Sq = 98.11 %, R-Sq(adj) = 96.45 %					
S = 0.0171391, R-Sq = 98.71 %, R-Sq(adj) = 97.58 %					

2.6 MECHANICAL PROPERTIES AND MICROSTRUCTURE ANALYSIS

Nowadays, μ RSW is the most dominant process in small scale sheet metal joining. From consumer goods such as the eyeglass frames and wristwatch to medical equipment such as surgery instrument and dental equipment. To ensure and maintain the structural integrity of the welded joint under service condition such as a crash situation, the remotest possibility of creating even one or two defective welds in a critical component need to be prevented. Therefore, the evaluation of the welded joint quality is a vital issue which requires the investigation of welding process variables and the weld mechanical performance.

Spot weld mechanical performance is generally considered under static/quasi-static, fatigue and impact loading conditions (Marashi Pournvari & Marashi, 2013). In majority industry and research field, the most widely used tests for evaluating the spot weld mechanical behaviors are the tensile–shear (TS), cross tension (CT) and coach peel (CP) tests (H. Zhang & Senkara, 2011). The TS, CT and CP tests are representing predominantly shear loading (i.e. shear force to the weld interface), tensile loading (i.e. normal force to the sheet/sheet interface) and tensile loading induced by bending momentum conditions respectively. The schematic representation of the sample geometry and stress state for these loading conditions are shown in Figure 2.4.

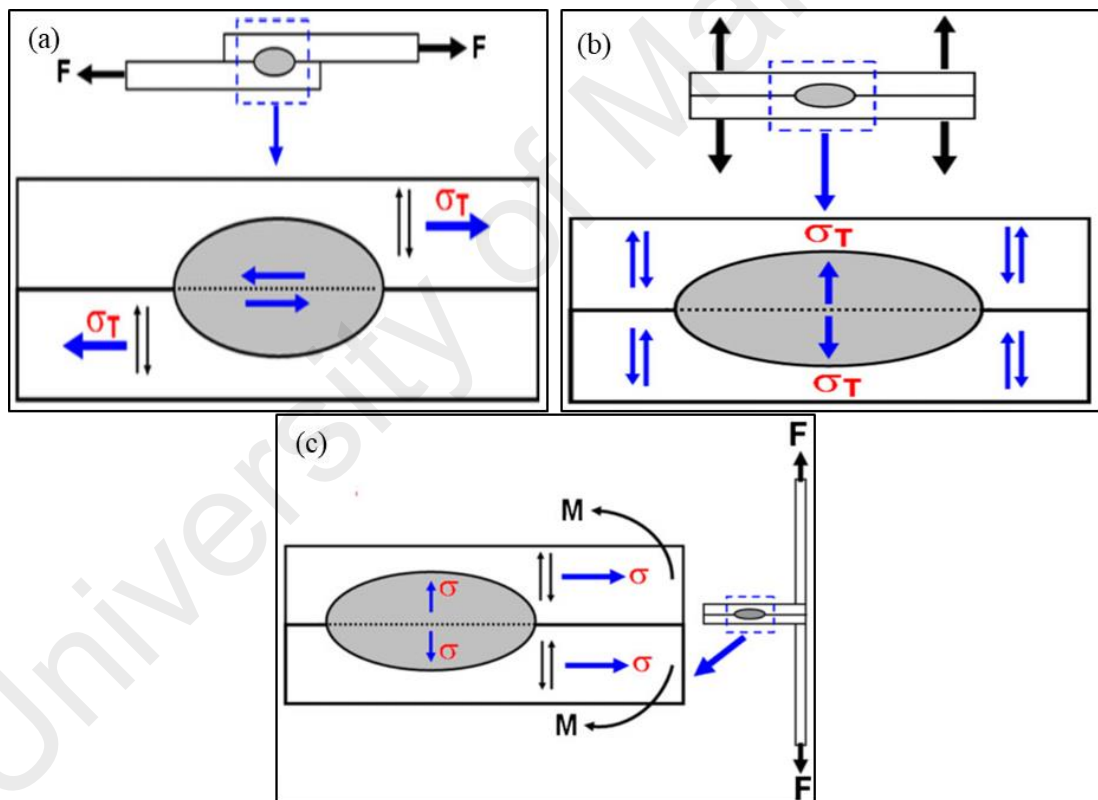


Figure 2.4: Simple models describing stress distribution at the interface and circumference of a weld nugget during (a) TS, (b) CT and (c) CP tests. (Pournvari & Marashi, 2013)

Figure 2.5 shows a typical load–displacement of a spot weld during the tensile-shear (TS) loading condition. To completely describe the mechanical behavior of a spot weld, the following parameters can be extracted from load–displacement curve:

- (i) Peak load, P_{max}
- (ii) Elongation at the peak load, L_{max}
- (iii) Failure energy, W_{max} at peak load.

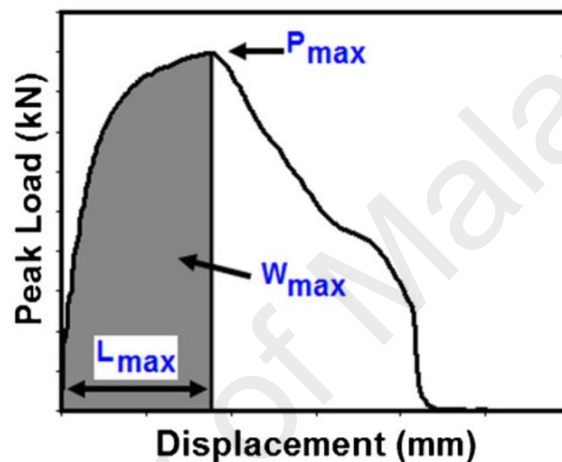


Figure 2.5: Typical load–displacement curve during the TS test along with the extracted parameters: P_{max} : peak load; W_{max} : energy absorption; L_{max} : elongation at peak load. (Pouranvari & Marashi, 2013)

During microscopic examination or microstructure analysis, the structure of material is studied under magnification. The properties of materials determine how it'll perform under a given application, and these properties are dependent on the material's structure. Scanning electron microscopy is used to determine abnormalities such as inclusions, segregation, and surface layers, as well as fracture features. When used in combination with energy dispersive X-ray spectroscopy (EDS), the microstructure analysis can identify inclusion type and corrodents on the fracture face.

A carefully prepared specimen and magnification are needed for microscopic examination. Proper preparation of the specimen and the material's surface requires that

a rigid step-by-step process be followed. The first step is carefully selecting a small sample of the material to undergo microstructure analysis with consideration given to location and orientation. This step is followed by sectioning, mounting, grinding, polishing and etching to reveal accurate microstructure and content. Detailed viewing of samples is done with a metallurgical microscope that has a system of lenses (objectives and eyepiece) so that different magnifications (typically 50X to 1000X) can be achieved. Scanning Electron Microscopes (SEMs) are capable of much higher magnifications and are utilized for highly detailed microstructural study.

Cross-section macroscopic images of the welded AISI 316L austenitic stainless-steel specimens joined at various welding current from 4 kA to 9 kA at the constant welding time (4 cycles) are shown in Fig. 2.6. It can be easily observed that weld nugget size increases within increasing welding current (Kianersi et al., 2014).

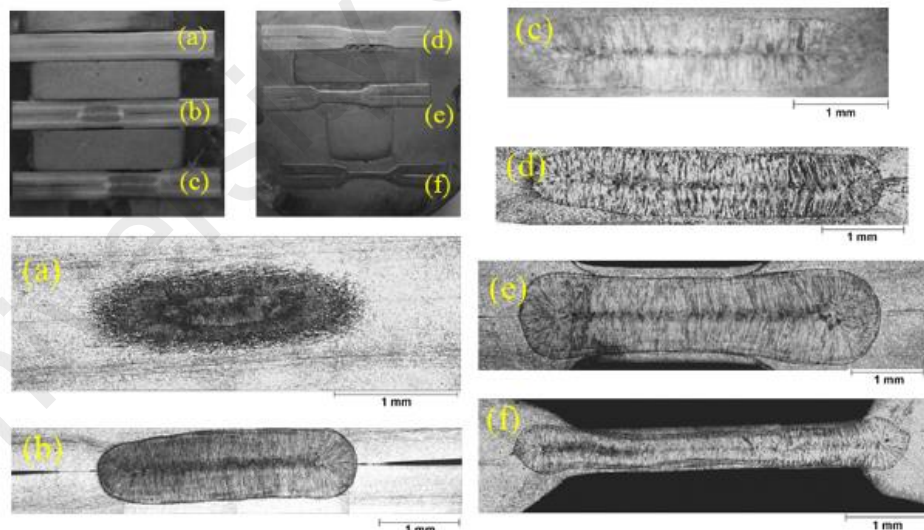


Figure 2.6: Cross-section images of the joint welded by (a) 4 kA, (b) 5 kA, (c) 6 kA, (d) 7 kA, (e) 8 kA, and (f) 9 kA welding currents at constant 4 cycles welding time (Kianersi et al., 2014)

Energy dispersive X-ray (EDS) analysis was carried out to investigate if there exist changes in the chemical composition of the welded samples. Figure 2.7 shows SEM micrographs taken from specimens which were welded by using 4 kA and 8 kA welding currents and Table 2.3 summarizes EDS elemental analysis results. As can be observed from Figure 2.7, the chemical composition in different area of weld nugget is approximately similar to the base metal composition and no significant variations detected. However, the weight percentage of molybdenum increased within higher welding current. The amount of ferrite promoting elements such as molybdenum (Mo) and silicon (Si) are higher at points number 5 to 8 which is sample welded by using 8 kA welding current. While, in case sample welded with low welding current (4 kA), weight percentage of the ferrite-promoting elements, specifically Mo and Si, is lower and it confirms that there is low amount of ferrite in the microstructure of the weld nugget.

Table 2.3: EDS elemental analysis of the welded samples with 4 kA and 8kA welding current (Kianersi et al., 2014)

Point number	Fe	Cr	Ni	Mo	Mn	Si	Ti
1	67.07	15.27	9.87	4.37	1.27	1.14	0.55
2	66.45	15.96	9.99	4.93	1.10	1.07	0.50
3	66.60	16.13	9.34	4.78	1.87	0.86	0.41
4	65.68	15.33	10.56	5.85	0.90	1.13	0.55
5	62.66	14.7	10.38	8.47	2.02	1.43	0.27
6	63.05	14.92	9.51	8.39	1.92	1.89	0.32
7	62.51	15.19	9.67	8.24	1.97	2.23	0.19
8	63.17	15.42	10.20	7.93	1.82	1.33	0.12

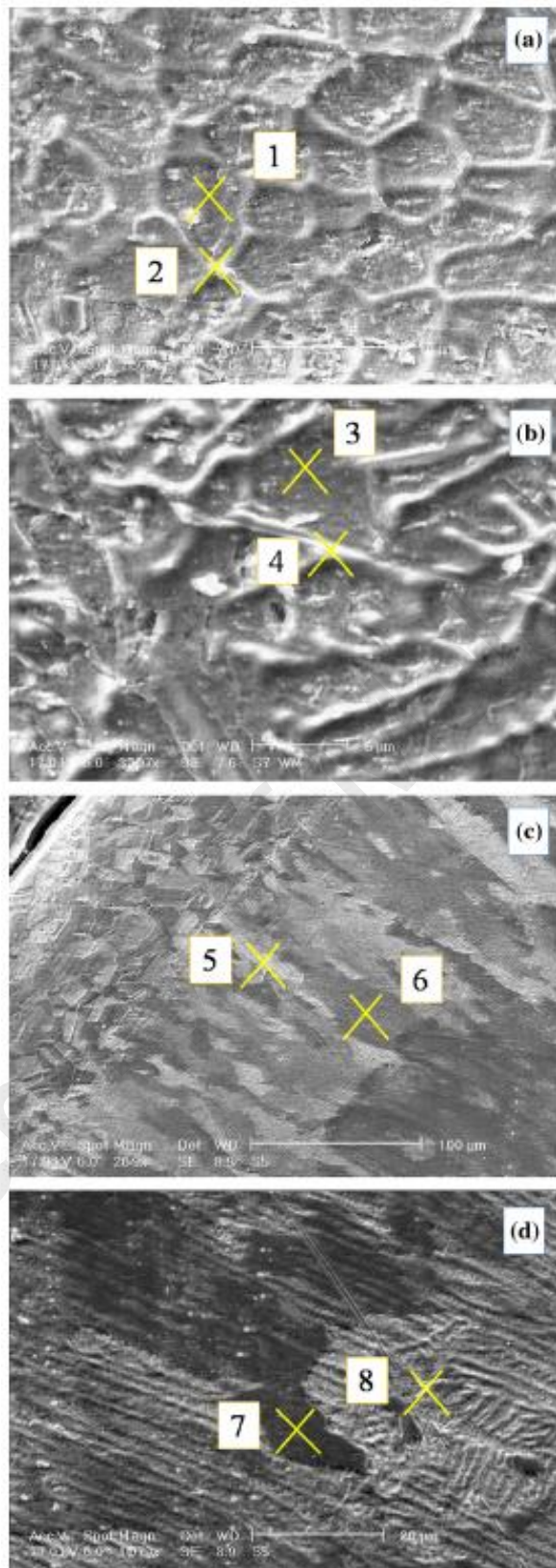


Figure 2.7: SEM images taken from weld nugget area (a and b) welded by using 4 kA welding current and (c and d) welded by using 8 kA welding current. EDS elemental analysis were carried out at the determined points (Kianersi et al., 2014)

Backscattered electron scanning microscopic images (BE-SEM) analysis revealed that skeletal and lathy delta ferrite morphology are the main microstructures in the weld nugget area of specimen which was welded under low heat input (4 kA welding current). Moreover, acicular delta ferrite as well as skeletal and lathy delta ferrite morphology was found in weld nugget of the sample which was welded under high heat input (8 kA welding current). In fact, increasing in generated heat input may lead to slightly coarsening of weld nugget microstructure by forming acicular delta ferrite morphology in this region. EDS results confirmed formation of ferrite in the welded sample made by 8 kA welding current due to presence higher weight percent of ferrite-promoting elements such as molybdenum (Mo) and silicon (Si) in chemical composition of weld metal. Moreover, the image analysis for quantitative microscopy employed with clemex software revealed that the ferrite composition which resides in the FZ is higher than HAZ and BM.

(Kahraman, 2007) found that the microstructural examination on the welded joint of commercially pure (CP) titanium sheets (ASTM grade 2) showed that the deformation during the welding process was in the form of twinning rather than shearing in the welding area. It was also observed that high pressure and welding time increased the twinning. The optical microscope images of the weld nugget of resistance spot welded joints are shown in Figure 2.8. When the images in Figure 2.8 (a) and (b) are examined, it is seen that twinning is not obvious for both atmosphere due to low electrode force. For Figure 2.8 (c) and (d) when compared to those obtained under 2000 N applied load, it can be observed that the amount and dimensions of the twinning increase. Furthermore, another significance difference is the formation of large grain sizes obtained under 4000 N although the weld time were the same for both applied loads thus results in the expansion of the weld nugget dimensions. When compared to the welds obtained using the same current time and under 2000 and 4000 N pressure, grain growth in Figure 2.8 (e) and (f)

increased due to applied high amount of welding current. Moreover, due to the applied deformation the size of twin lines increased more.

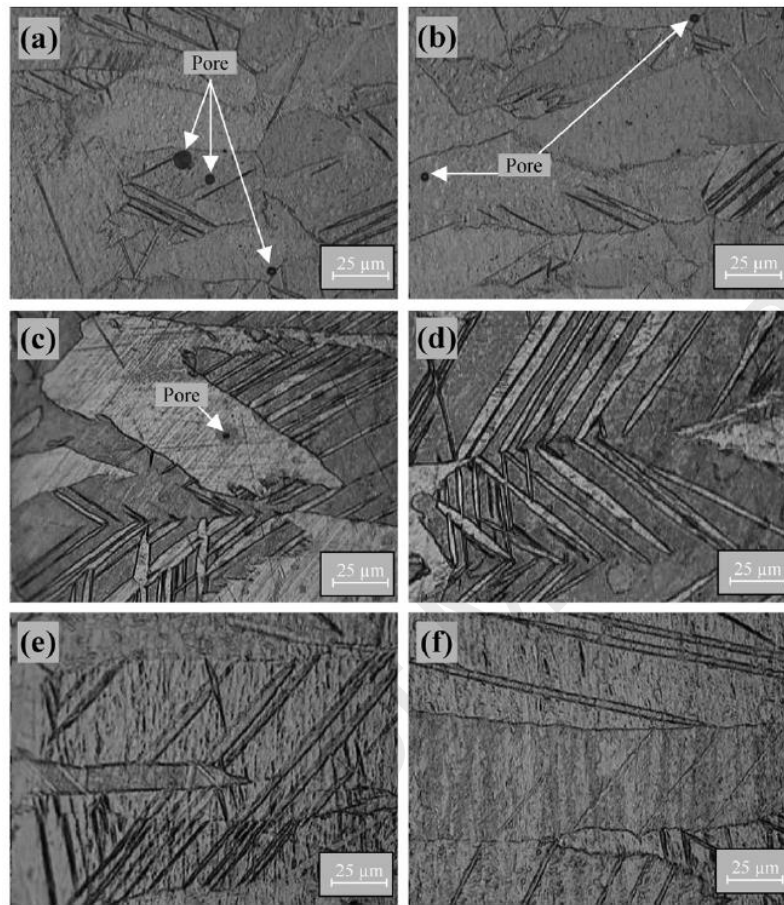


Figure 2.8: Optical microscope images of the weld nugget of resistance spot welded joints joined at: (a) 2000 N, 15 cycle, (b) 2000 N, 15 cycle-Argon, (c) 4000 N, 15 cycle, (d) 4000 N, 15 cycle-Argon, (e) 6000 N, 15 cycle and (f) 6000 N, 15 cycle-Argon. (Kahraman, 2007)

X-ray diffraction (XRD) provides most definitive structural information. Therefore, in order to detect whether the intermetallic compound (IMC) formed at the interface in the peripheral region of the welded joint, X-ray diffraction patterns from the fractured surfaces are analyzed by using XRD analysis, as shown in Figure 2.9. Figure 2.9 shows the micro X-ray diffraction profile of the interfacial region in the welded joint of RSW using dissimilar materials of 6008-T66 aluminum alloy and H220YD galvanized high strength steel (W. Zhang et al., 2015). The results identified the existence of intermetallic compound (IMC) of Fe_2Al_5 and $\text{Fe}_4\text{Al}_{13}$ at the interface in the welded joint.

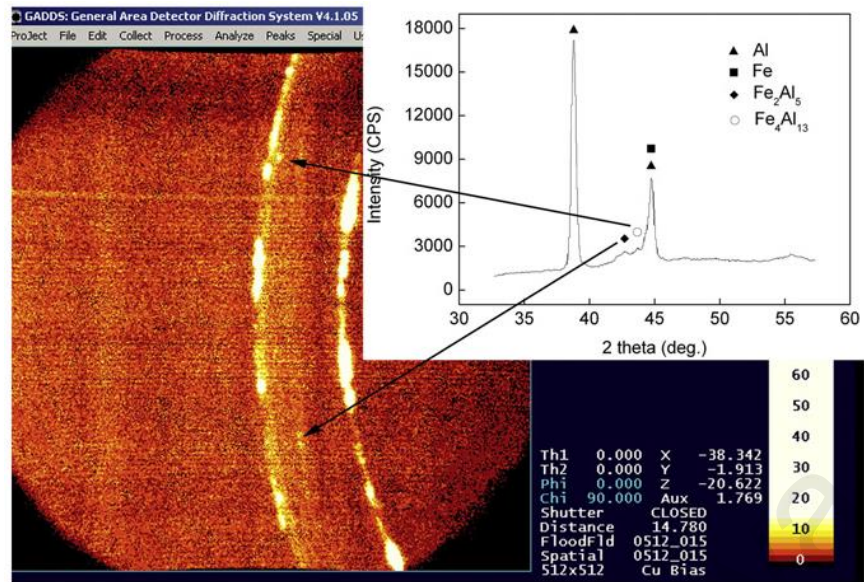


Figure 2.9: Micro X-ray diffraction profile of interfacial region in the welded joint (W. Zhang et al., 2015)

The formation of TiFe and TiFe₂ intermetallic compound (IMC) are not desired for μ RSW process. This is because the formation of this IMC at the interface of diffusion bonding between TC4/00Cr18Ni9Ti is proven to be hard and brittle which is the main cause that leads to poor bond strength. Therefore, it is an important aspect that should be investigated and utilized the formation and growth model of IMC for the control process of diffusion bonding (He & Liu, 2006). Other than that, by using laser metal deposition between SS 316 and Ti-6Al-4V will also formed a hard and brittle TiFe (IMC) which compromise the mechanical properties of diffusion bonds between each of the base metals (W. Li et al., 2017). Therefore, they employed filler metals as transition layers to eliminate the TiFe intermetallic effectively.

2.6.1 MICROHARDNESS TESTING

Microhardness testing is a method of determining a material's hardness or resistance to penetration when test samples are very small or thin, or when small regions in a composite sample or plating are to be measured. The microhardness test can measure surface to core hardness on carburized or case-hardened parts (case depths), as well as surface conditions such as grinding burns, carburization or decarburization.

Microhardness testing provides valuable information for the following purposes:

- Certify conformance to hardness requirements for carburizing, nitriding, plasma nitriding, induction, flame and many other surface hardening processes
- Measure the effective case depth in case hardening heat treatments
- Measure surface or core hardness of carburized parts, as well as surface conditions such as grinding burns or decarburization
- Provide precise and detailed information on surface features of materials that have a fine microstructure, are multi-phase, non-homogeneous or prone to cracking
- Determine hardness of different micro-constituents within a structure, or measure steep hardness gradients such as those encountered in casehardening

2.6.1.1 Vickers hardness test

The Vickers hardness test can be performed on both the micro and macro scales (some Vickers testers have a maximum test load of up to 50 kilograms). These tests are performed by applying controlled pressure for a standard length of time, but with a square-based diamond pyramid indenter. The diagonal of the resulting indentation is measured under a microscope, then this measurement and the test load are used in a specific formula to calculate the Vickers hardness value.

Kianersi et al. (2014) performed Vickers microhardness measurements on the weld nugget, HAZ and base metal on specimens which were welded by applying low (4 kA) and high (8 kA and 9 kA) welding current and/or heat input. Fig. 2.10 shows direction of the microhardness profile applied on specimens. Initial microhardness of the AISI 316L sample was around 275 HV. Effects of various welding currents on welds hardness were determined. Hardness profile of the resistance spot welded areas is shown in Fig. 2.11. According to the obtained results, microhardness studies showed that hardness of weld nugget was lower in comparison to HAZ and base metal. Also, hardness of weld nugget and HAZ areas was slightly higher in the specimen welded under low heat input (4 kA welding current) in comparison to the specimen welded under high heat input (8 kA welding current). It can be related to the grain growth phenomenon which may occur during RSW process of AISI 316L stainless steel.

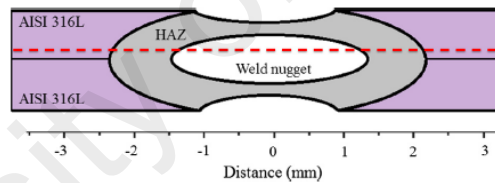


Figure 2.10: Schematic of the microhardness measurements taken from cross section of the samples (Kianersi et al., 2014)

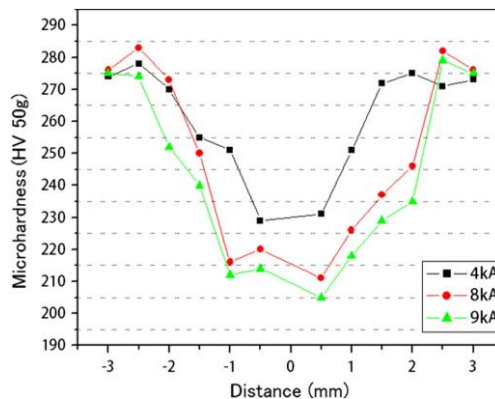


Figure 2.11: Microhardness profiles of welds manufacture by using various welding current (Kianersi et al., 2014)

Kaya & Kahraman (2012) carried out the hardness measurement on all the resistance-welded titanium specimens in order to determine the hardness variations in the welding zone (base material, heat affected zone and fusion zone). The hardness measurements were made into two different directions: one along the radius of the weld nugget while the other along the sheet thickness as shown in Figure 2.12. It can be observed that there is a decrease in the hardness value as the distance from the weld nugget to the base metal increases. Meanwhile the highest hardness value can be seen at the FZ and this is followed by the HAZ and the BM. Furthermore, the obtained results show that the highest hardness value of about 125 ± 10 HV belongs in the FZ. Based on the investigation made, it is considered that rapid melting and rapid cooling of the mixture at the weld nugget led to high hardness value. Based on these findings, it is important to find the optimal squeeze and hold time.

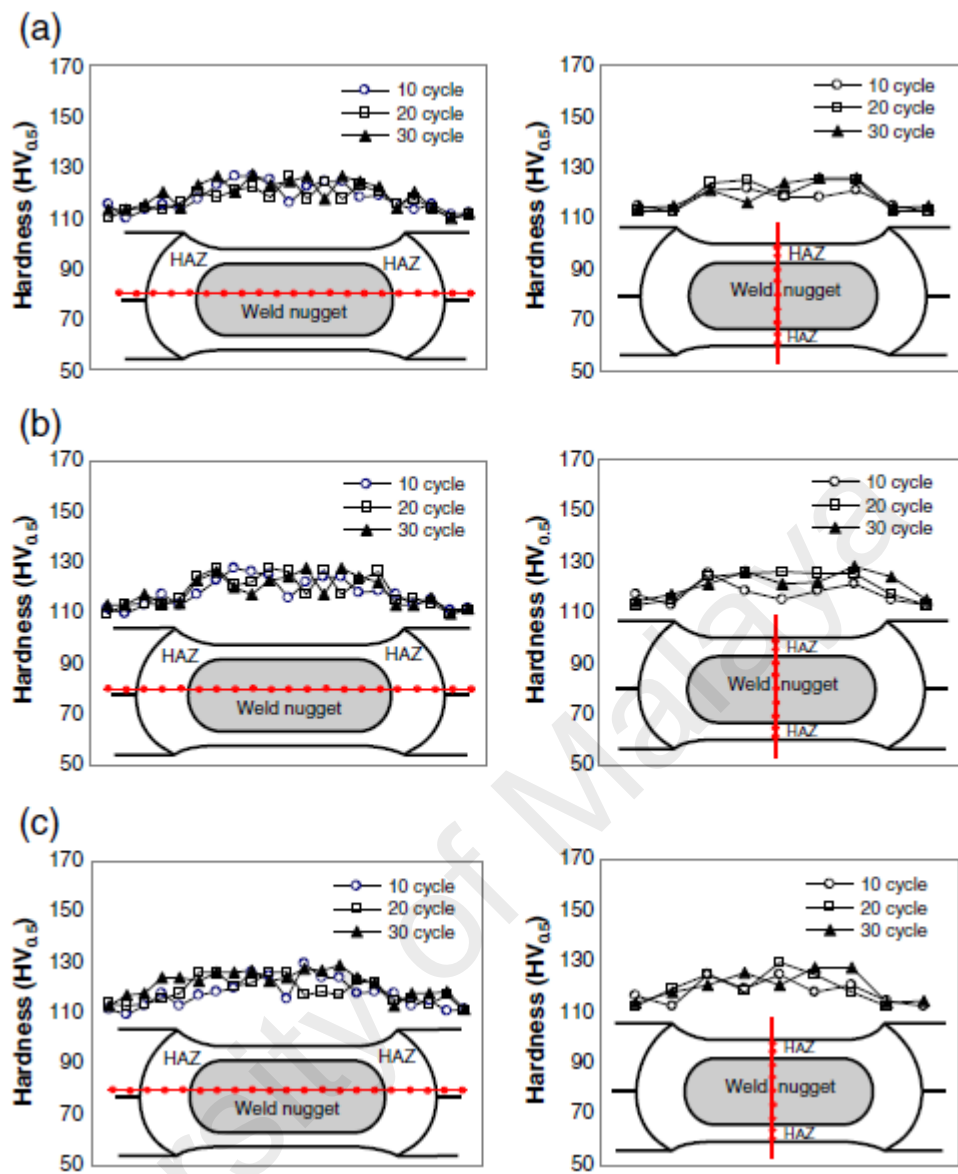


Figure 2.12: Hardness variation in the welded specimens obtained at 3 kN electrode force and at (a) 3 kA, (b) 5 kA and (c) 7 kA welding currents (Kaya & Kahraman, 2012)

2.7 EFFECT OF PROCESS PARAMETERS ON THE FAILURE MODES

Failure mode of resistance spot welds is a qualitative measure of mechanical properties. Figure 2.13 shows the schematic representation of fracture surfaces at the main failure modes during the mechanical testing of the spot welds. Basically, spot welds can fail in four distinct modes described as follows:

- (I) Interfacial failure (IF) mode, in which the fracture propagates through the FZ.
- (II) Pull-out failure (PF) mode, in which the failure occurs via withdrawal of the weld nugget from one sheet. In this mode, fracture may initiate in the BM, HAZ or HAZ/FZ depending on the metallurgical and geometrical characteristics of the weld zone and the loading conditions. Generally, the PF mode exhibits the most satisfactory mechanical properties.
- (III) Partial interfacial mode, in which the fracture first propagates in the FZ and then redirected through the thickness direction.
- (IV) Partial thickness–partial pull-out (PT–PP), in which slant crack propagates into the FZ and part of the mating sheet thickness are removed during separation.

Failure mode can significantly affect load bearing capacity and energy absorption capability of resistance spot welds. Generally, the pull-out mode is the preferred failure mode due to its higher associated plastic deformation and energy absorption.

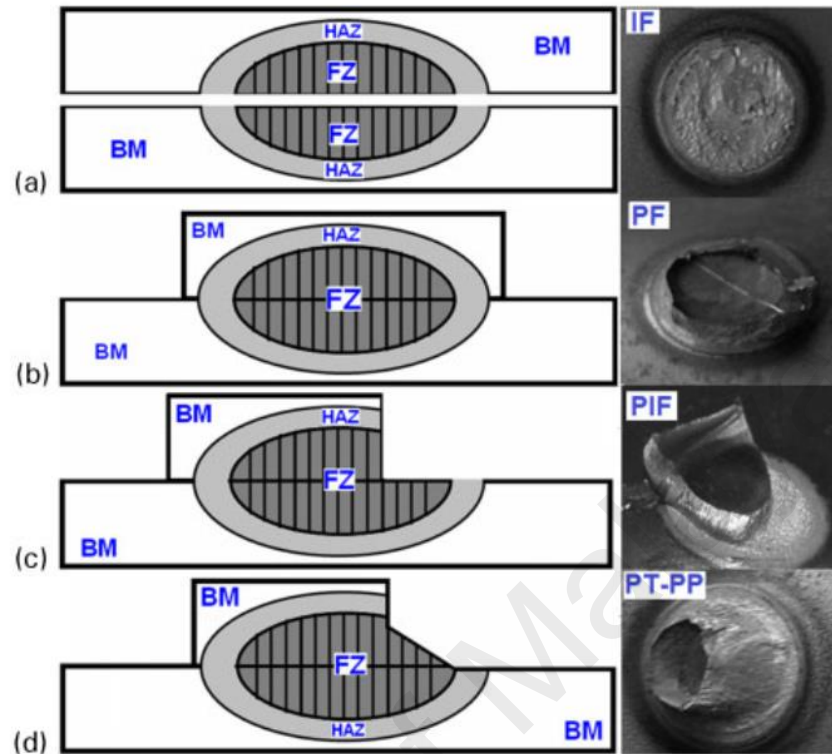


Figure 2.13: Schematic representation of various failure modes which can occur during mechanical testing of resistance spot welds, (a) IF; (b) PF; (c) partial interfacial failure (PIF); (d) PT-PP (Pouranvari & Marashi, 2013)

Failure mode, fracture characteristics and sheet separation of the welds are features which influenced quality of the resistance spot welded specimens. Fig. 2.14 presents macrographs of six different failure modes observed in tensile tests of ASS 316L specimen. As it is expected and seen from Fig. 2.14, within increasing the welding current, these modes can be characterized from solely interfacial failure mode (IF) to completely tearing around weld nugget and heat affected zone, HAZ (Kianersi et al., 2014). They concluded that by increasing welding current at constant welding time, various failure modes occurred from solely interfacial failure mode to completely tearing around weld nugget from HAZ. Specimens that have interfacial fractures were rejected and ones which tore from HAZ, base metal or compound modes were accepted. The best weld had button pullout with tearing from the base metal failure mode.

Also, calculated failure energy from load-displacement curves showed that welded specimen with 8 kA welding current has the highest plastic deformation with pullout failure mode.

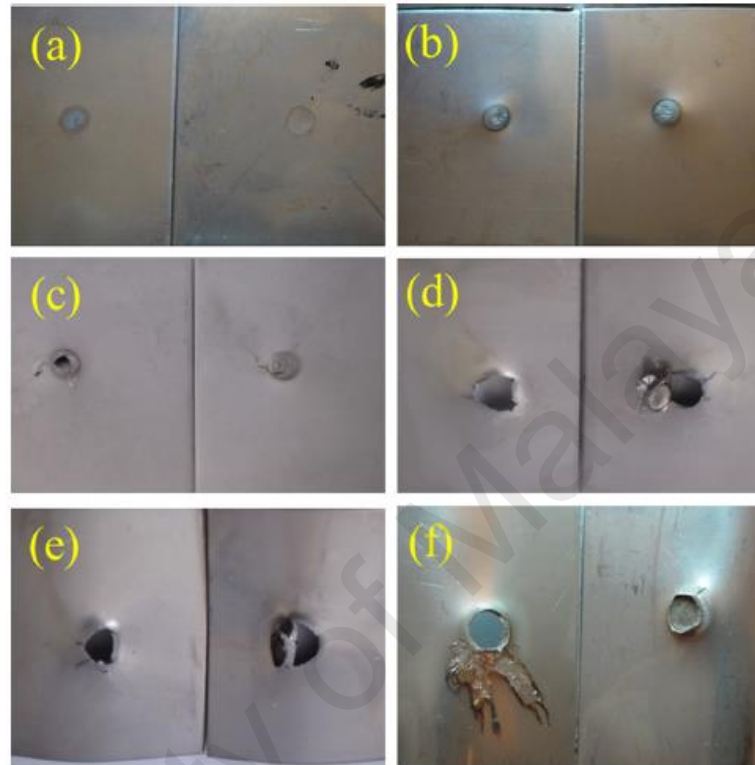


Figure 2.14: Various types of failure modes obtained from tensile shear test samples (Kianersi et al., 2014)

By performing metallography through fracture analysis, Ertek Emre & Kaçar (2016) found that zinc forms at the faying surface around the fusion zone during the spot welding of Zn-galvanized steel (Figure 2.15). Furthermore, the coating on the surface of the TRIP800 (Transformation Induced Plasticity) steel reduces the dimension of weld nugget and tensile shear strength of the welded joint thus affecting the specimen failure mode from pullout to interfacial or partial interfacial. This indicate that by coating TRIP800 steel RSW specimen, it will strongly affect the failure mode of the welded joint.

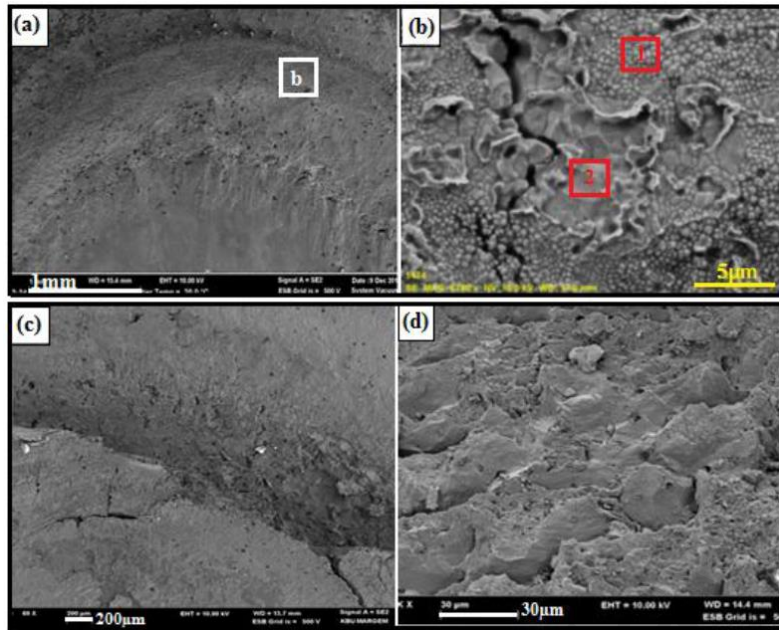


Figure 2.15: Failure modes: (a) IF mode. (b) Magnification view of IF mode (1 and 2 are point of EDS analysis). (c) PIF mode. (d) Magnification of PIF mode (Ertek Emre & Kaçar, 2016)

Results indicate that the coating strongly affects the failure mode of the spot weldment of TRIP steels. The failure mode of the test samples was examined. As seen in Figure 2.16, an interfacial failure (IF) mode was evaluated for galvanized samples that were joined at a 6 kA welding current for all welding times.

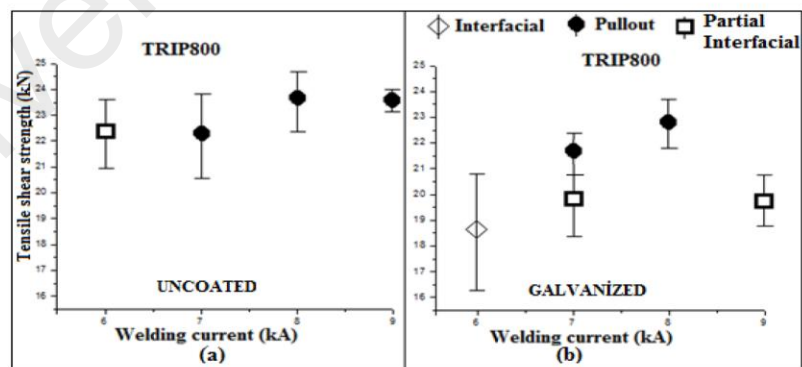


Figure 2.16: Effect of welding parameters on the tensile shear strength and failure types: (a) uncoated; (b) galvanized (Ertek Emre & Kaçar, 2016)

The interfacial fracture (IF) mode can be avoided by either reducing the fusion zone hardness or alternatively extending the nugget diameter for a given sheet thickness. Increasing the heat input enabled a joining at a larger area, which resulted in a desired pullout failure (PF) mode for both weldments. A partial interfacial failure (PIF) mode was observed in the uncoated sample joined at 6 kA for all welding times due to insufficient heat input. Meanwhile, a PIF mode due to excessive heat input was also observed in the galvanized sample joined at 9 kA for all welding times. These failure types indicate that the heat input related with the welding parameters passes through to a critical level that causes expulsion and results in a PIF type.

Ma et al. (2008) investigated the fracture characteristics of spot-welded DP600 steel. The maximum load carried by the specimens welded with a current range of 8.1–8.3 kA reached the highest value in the static tensile shear tests. The specimens with the occurrence of expulsion exhibited a lower fracture load. However, even though the interfacial fracture occurred in this case, the load bearing ability of the spot weld was still high enough. Fatigue tests showed a slightly lower fatigue limit for the specimens with the expulsion. Four typical fracture modes have been identified. At very high-load levels, the fracture can either be interfacial failure, or initiate in the HAZ near the nugget and fail with some plastic deformation. At very low load levels close to the fatigue limit, the cracks basically initiate at the nugget boundary, penetrate through the thickness and propagate along a straight line in the base metal in the direction normal to the loading axis. At intermediate load levels, the cracks initiate at the nugget boundary and propagate along about 10–50% of the circumference and finally into the base metal. Throughout the research Ma et al. (2008) have examined the interfacial fracture that occur. In the case of low electrode force, small welding current or short welding time, interfacial fracture would occur.

Figure 2.17 shows a typical interfacial failure mode at high fatigue load levels. Figure 2.17 (a) shows an overall view of the failed spot weld at low magnification. There exist macro-voids and cracks which lead to low welded joint strength. Such voids can be seen clearly in Figure 2.17 (b) at higher magnification for the area indicated in Figure 2.17 (a). further magnified Figure 2.17 (c) shows part of the fracture surface morphology exhibiting the characteristics of ductile fracture as shown in Figure 2.17 (e) and (f). From Figure 2.17 (e), the fractured weld spot exhibit dimple-like fracture characteristics meanwhile for Figure 2.17 (f) reveal dendrite and ductile shear combination area. In Figure 2.17 (d) reveal the weld spot exhibit dendrite structures which presents the existing of the welding defects resulting from the solidification shrinkage. In this research, they've discovered that by using low welding current, some white spots at the top of the dendrites were found to be enriched in Zn. This is an important discovery as investigating failure modes lead to the discoveries of the brittleness properties at the welded joint. Based on the results obtained, interfacial (IF) fracture does not necessarily represent low strength of welded joint. Moreover, the IF fracture was also found to be related to the carbon equivalence (CE). The higher carbon equivalence from elements of the base metals will make the weld hard and brittle, which congregated in the grain boundaries thus increasing the boundary energy which lead to solidification cracking. The weld will undergo IF fracture if CE is greater than 0.24%.

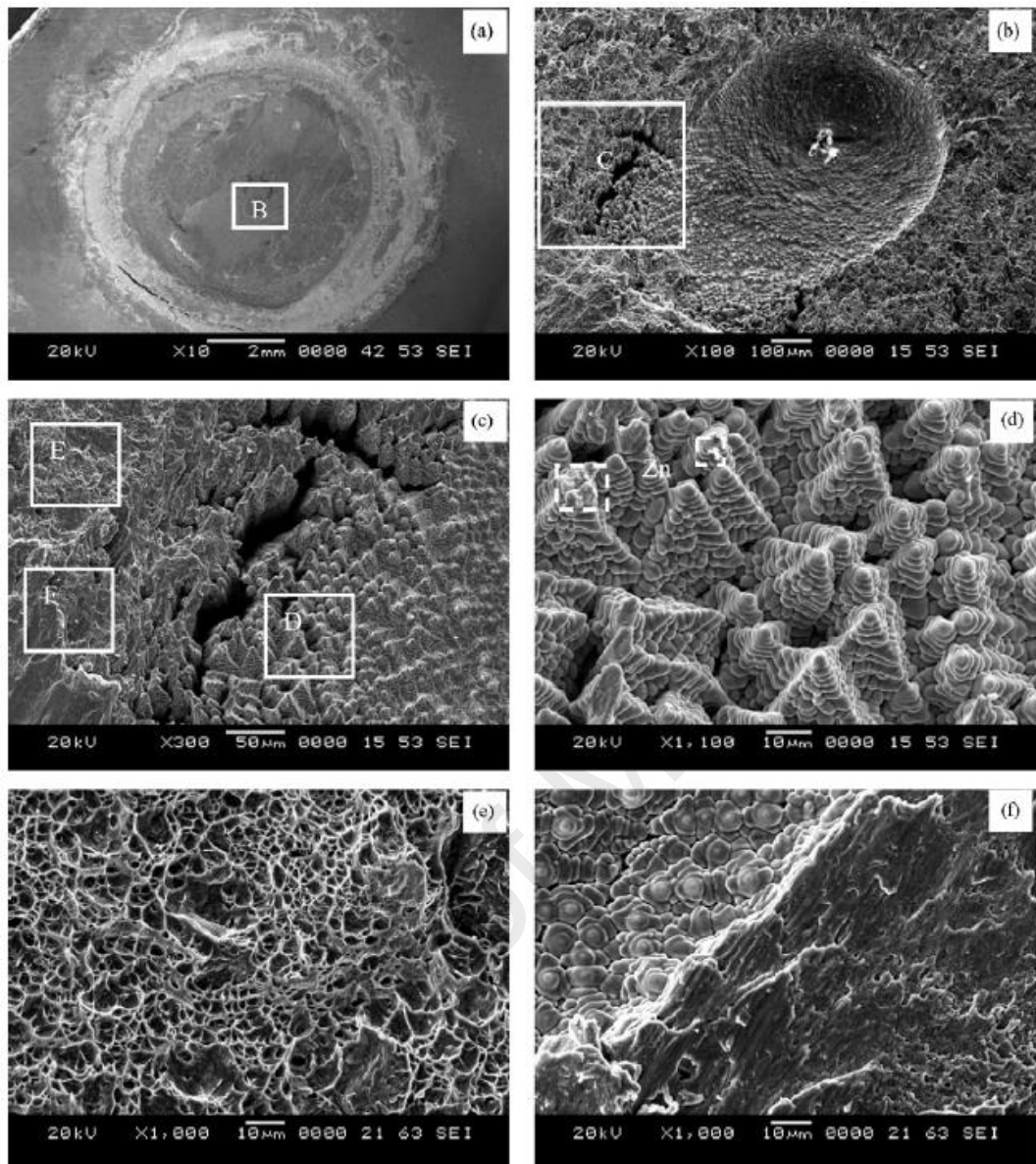


Figure 2.17: Interfacial fracture with dendrite and ductile characteristics. (a) A view of low magnification, (b and c) magnified views of the weld nugget with dendrite and ductile fracture characteristics, (d) characteristic dendrite, (e) dimple-like ductile fracture characteristics, (f) dendrite and ductile shear combination area, where the locations of micrographs (b-f) are indicated by B-F, respectively, for the sample welded with 8.35 kA (Ma et al., 2008)

2.8 RESEARCH GAP

Among the materials used for the RSW, there are no specification of materials on welding between dissimilar materials at micro-scale. To be precise, there are no research that have been done on μ RSW between titanium alloy grade 5 (Ti-6Al-4V) with austenitic stainless steel 316L. Furthermore, the use of RSW are commonly practice in automotive industry. The research on micro-resistance spot welding other than automotive industry are limited and lack of published work despite the increasing demand.

Currently there have been an increasing demand, in the fabrication of electronic and medical devices, for resistance spot welding of very thin metal sheets which is less than 0.5 mm and most being combinations of similar and dissimilar non-ferrous metals. This application of resistance spot welding (generally termed as micro-, fine, or small-scale resistance spot welding) requires much more precise electrical and mechanical control and uses lower electrode force and current/energy input.

The definition of micro-scale here represents the metal sheet thickness and the welding electrode geometry. Therefore, in this research, study and investigation will be done on micro-resistance spot welding between 0.5 mm thickness titanium alloy grade 5(Ti-6Al-4V) and 0.5 mm thickness austenitic stainless steel 316L. Based on the preliminary testing and experiment, truncated cone electrode shape are chosen. The diameter of the upper electrode is 1.5 mm and the diameter of the lower electrode used are 3mm.

2.9 SUMMARY

From the literature review, resistance spot welding (RSW) process is feasible for the specific joining between similar and dissimilar metals, such as Al-Steel, Mg-Al, Mg-Steel, Al-Ti, and galvanizes steel to stainless steel. The effects of process parameters such as the welding current, electrode force, and welding time on the joint strength and the nugget diameter were studied. As reviewed in section 2.3, the effect of the welding parameters, such as welding time, welding current, and electrode force on the microstructure and the mechanical properties of the welded joint, do provide a clear view and point of idea on the design of the experiment. Furthermore, the discussion on the microstructure analysis and the mechanical properties studies in section 2.6 introduces the methodology on using SEM, EDX, and XRD, as well as revealing some relevant results which can be compared with current research development.

Base on the literature review, the use of full factorial design of experiment (DoE) with analysis of variance (ANOVA) are confirmed to be the most feasible way to be utilized in this research to determine the optimal combination of welding parameters and study the effects of interaction between each welding parameters. The investigation on the strength of the welded joint by using the reviewed mechanical engineering test is a well-known technique which will reveal sufficient data and results in order to study the mechanical properties of the weld nugget formed. Methods used for microstructure analysis is essential and suffice to ensure good results and outcomes. Other than that, limitations and regulation upon each steps of investigation will provide a more accurate and precise results with scientific explanation.

CHAPTER 3: RESEARCH METHODOLOGY

3.1 OVERVIEW OF METHODOLOGY

This section describes the sequence of the research methodology. This algorithm function as a precaution guideline for both parts of the research study.

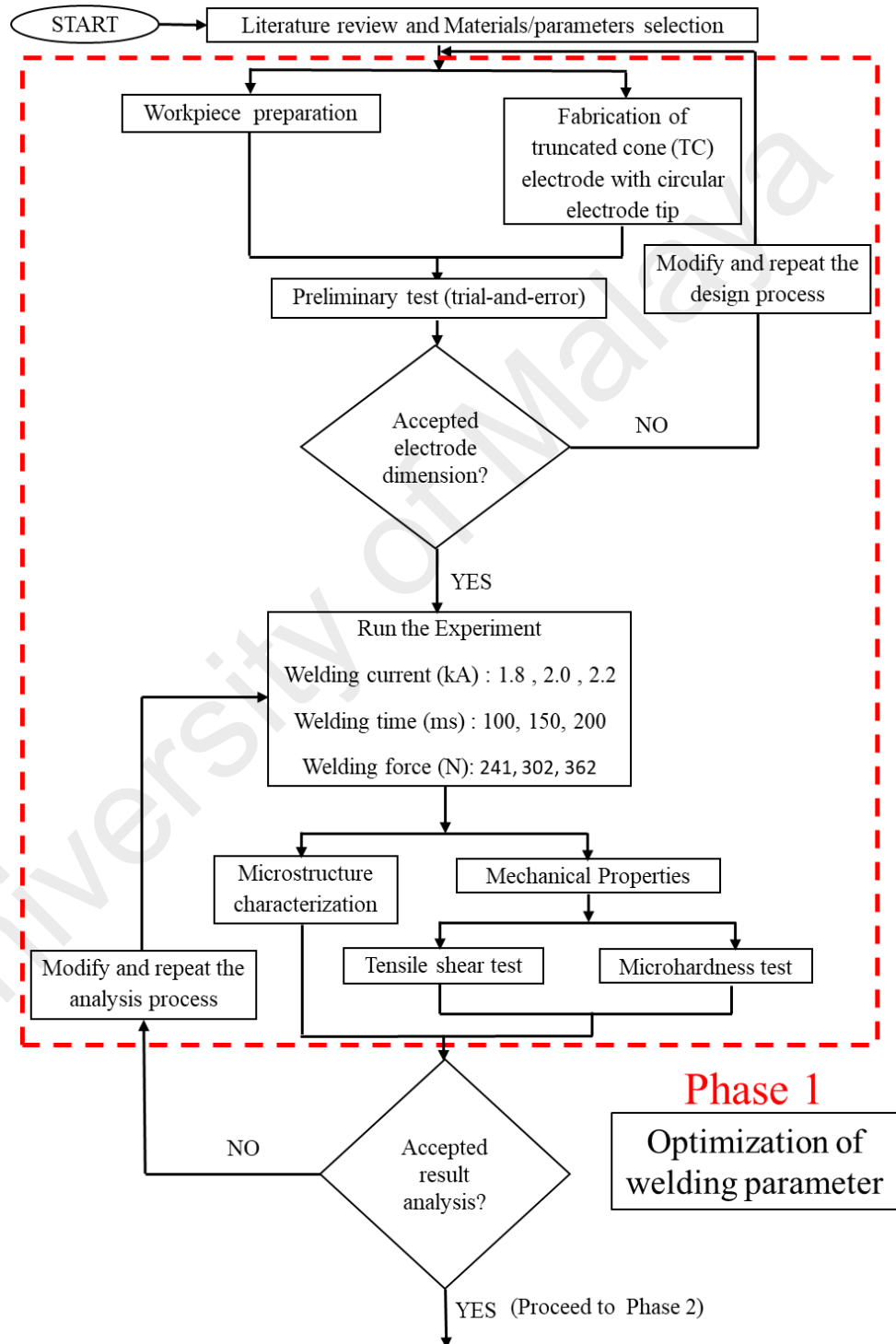


Figure 3.1 Flow chart of research methodology.

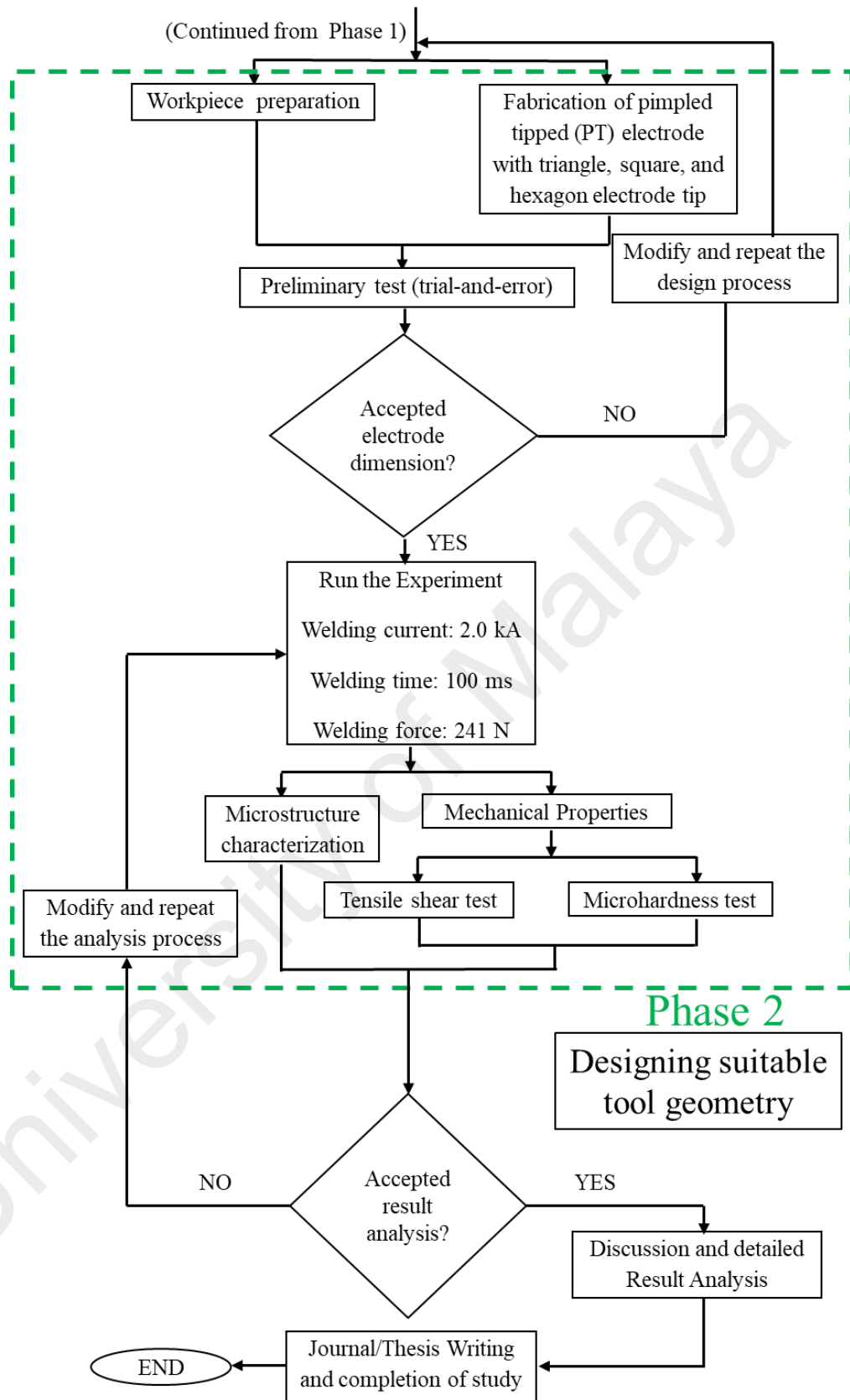


Figure 3.1 (continue): flow chart of research methodology

As illustrated in Figure 3.1, it begins by preparing the initial design of the experiment which were obtained from the literature review and past research work which have done in previous years. It is followed by materials and process parameters selection. Materials are properly selected by investigating the mechanical properties and the weldability to form a good joint between each base metal. Preliminary test in the form of try-and-error method have been incorporated into this study and peers review also have been considered to eliminate unnecessary factors that could attribute to the demeaning of the research work. Next stage, the sample specimen is prepared by following μ RSW standard procedure from previous researchers and required items are developed which involves designing and fabricating the electrode geometries. Then, full factorial design of experiment (DOE) with L_{27} orthogonal array and analysis of variance (ANOVA) are utilized to obtain the optimum combined welding process parameters that can yield the highest tensile shear load.

After that, the experiment is conducted which comprises of six different assigned values of welding current, welding time, and welding force as the variables, and the squeeze time, hold time, electrodes geometry as constants. The aim at this stage is to obtain the best condition of different welding parameters base on the welded joint strength and the formation of the weld nugget in term of shape and size. At this stage, the surface appearance and condition are thoroughly observed on both sides to prevent some of the possible welding defects such as excessive indentation, micro-cracks, and burn-thru. Finally, to evaluate the quality of the product via welded joint, microstructural and mechanical analysis was performed which included SEM, EDS, metallographic investigation, tensile shear stress load test, and Vickers microhardness evaluation test.

After the optimum parameters have successfully obtained, the research study is continued to Phase 2. At the start of this phase, the workpiece was prepared as usual and followed by designing and developing three different design of electrode geometries. The electrodes were fabricated by using the lathe machine and CNC milling machine. In the next stage, the experiment was performed by using the optimum welding process parameters obtained in Phase 1 on three different electrode tip shape which is triangle, hexagon and square. The squeeze and hold time were kept constant throughout the experiment run. At this stage also, the surface appearance and condition were thoroughly observed on both sides to prevent some of the possible welding defects such as excessive indentation, micro-cracks, and burn-thru. Finally, in order to evaluate the quality of the product via welded joint, the same technique that were used during phase 1 was employed where the microstructure and mechanical analysis was performed. It included SEM, EDS, metallographic investigation, tensile shear stress load test, and Vickers microhardness evaluation test.

3.2 PREPARATION OF MATERIALS AND ELECTRODE

The preparation of the experiment consists of the groundwork of materials and tools as well as dimensioning the workpiece and electrodes. For this particular work, dissimilar materials were used for the upper and lower part of the specimen. Lap joint configuration was employed during resistance spot welding. Austenitic stainless steel 316L sheets of 60 x 20 x 0.5 mm were used as the upper part of the specimen and titanium alloy (ASTM grade 5) sheets of 60 x 20 x 0.5 mm were used as the lower part of the specimen. These materials are selected due to the availability in the market, high temperature strength and exhibit excellent corrosion properties in the manufacturing of eyeglass frame. The chemical composition and physical properties of austenitic stainless steel 316L and titanium alloy (ASTM grade 5) are presented in Table 3.1 and Table 3.2.

Table 3.1: Chemical composition of ASS 316L and Ti6Al4V

Element	Stainless steel 316L	Titanium alloy grade 5
Cr	17.68	-
Ni	12.6	-
Si	0.663	-
Mn	1.53	-
Mo	2.38	-
Co	0.121	-
Cu	0.211	-
W	0.029	-
P	0.02	-
S	0.003	-
Al	0.018	5.5-6.75
Ti	0.021	Balance
V	0.663	3.5-4.5
Fe	Balance	0-0.4
C	0.016	0-0.08
O	-	0.02
N	-	0.05

Table 3.2: Physical properties of base material

Mechanical properties at room temperature	Material	ASS 316L	Ti-6Al-4V
	Yield Strength (MPa)	170	206
	Ultimate Tensile Strength (MPa)	485	897
	Modulus of Elasticity (GPa)	193	114
	Elongation at Yield (%)	-	-
	Elongation at Break (%)	40	10
Thermal Properties	Melting Point (°C)	1450	1670
	Thermal Conductivity (W/mK)	16.3	7.2
	Electrical Resistivity ($\mu\Omega$.cm)	74	170

Prior to resistance spot welding, all titanium alloy (ASTM grade 5) sheets were first mechanically polished using SiC abrasive paper (No.400 grit size) to remove the cutting-edge burr, surface contamination and the oxide layer formed on the surface. Then, the surface impurities were removed and the surface were cleaned by using ethanol. Meanwhile the stainless-steel specimen surface was only cleaned by using ethanol. Cleaning the specimen surface is an important step in μ RSW as surface contamination will cause random expulsion welds with random tensile-shear strength values (Fan et al., 2016). Austenitic stainless-steel type 316L was used instead of type 316 because of the extra low carbon content that minimizes harmful carbide precipitation due to welding process. This property will assure optimum corrosion resistance and the main reason why it is used extensively as the primary material in welding.

In order to improve the weldability between dissimilar materials and solve the inherent problems in micro resistance spot welding, the shape of the upper and lower part of the electrode was designed optimally and different electrode tip diameter were employed throughout the welding process in Phase 1. Electrodes made of CuCrZr alloy (RMWA class 2 Chromium Zirconium Copper 18150) were used. The schematic diagram of the electrodes used in Phase 1 are shown in Figure 3.2. A truncated cone with planar circular tip shaped electrode with 1.5 mm tip diameter on stainless steel side and truncated cone with planar circular tip shaped electrode with 3 mm tip diameter on titanium alloy side were employed throughout the welding process. Since design of the upper electrode have smaller diameter than the lower electrode, higher welding current density will form at the electrode tip/workpiece interface thus more heat input is being distributed at the upper part of the electrode. Therefore, it is better to have the ASS 316L on the upper part due to having higher thermal conductivity so that the heat will loss to the environment rapidly.

Furthermore, the different design of electrode tool tip morphology exists in order to avoid the formation of the crescent button shape for the weld nugget instead of round button shape. In addition, after performing various experimental procedure through trial-and-error method, the diameters for the upper and lower electrode tip were considered the optimal dimension as various imperfections and welding defects can be prevented. All electrodes had an alloy composition of 98.715Cu-1.175Cr-0.11Zr. The electrodes used during the experiment for Phase 1 is shown in Figure 3.3. The schematic illustration for the μ RSW used in this research study are shown in Figure 3.4. Originally all of the electrodes used for this μ RSW machine are cylindrical shape with flat nose electrode tip. Due to the usage of different electrode geometry. All of the electrodes are fabricated by using the lathe machine and the CNC milling machine available inside faculty of engineering, University of Malaya. The upper electrode is designed with such shape due to the electrode being inserted inside a keyhole with 5 mm diameter and to enable proper grip at the weld head.

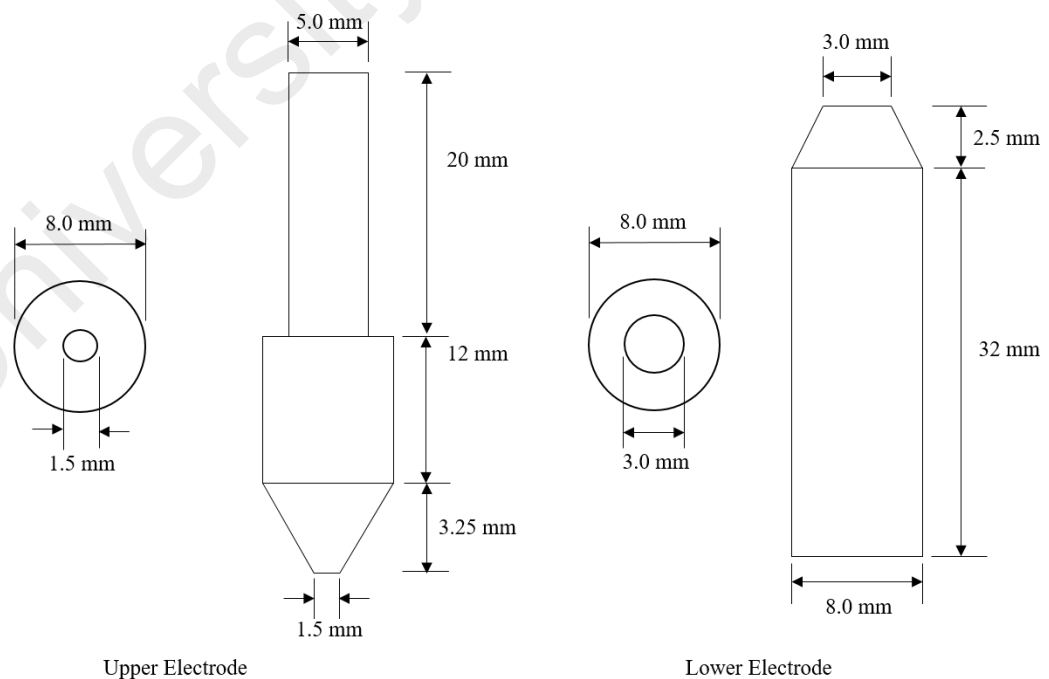


Figure 3.2 Schematic diagram of tool



Figure 3.3 Electrodes used during the experiment

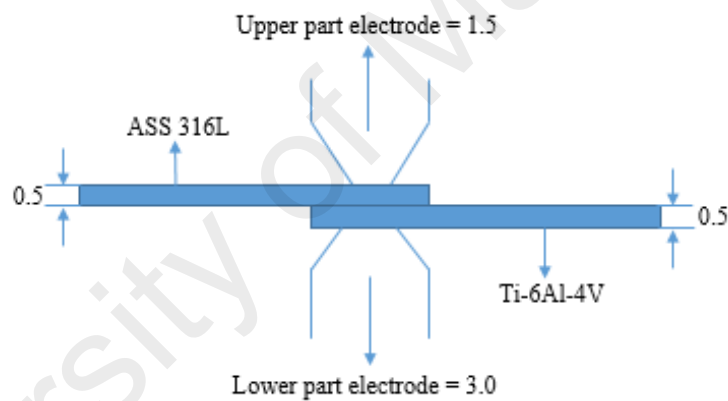


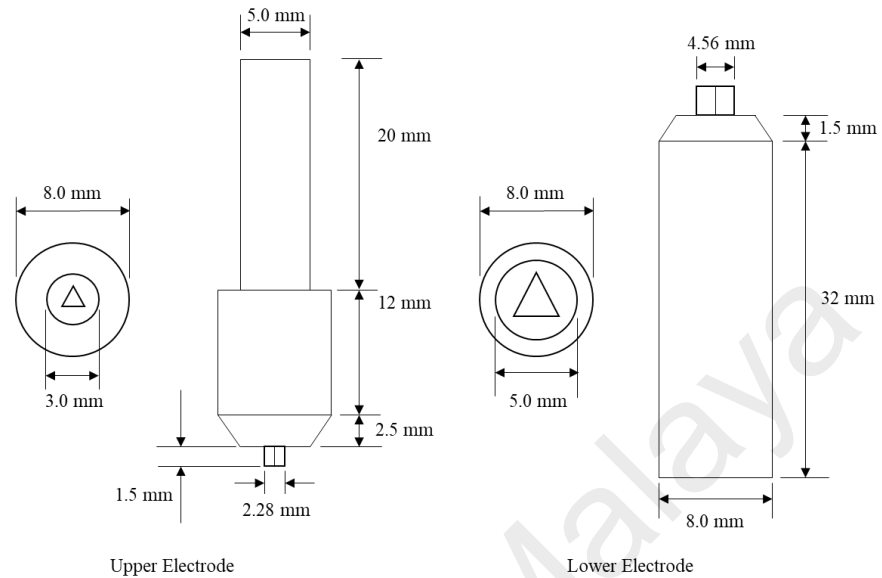
Figure 3.4 Schematic illustration of micro resistance spot welding

In Phase 2, there are three different designs of electrode used in order to determine the optimum tool design based on the optimum parameters obtained from Phase 1 that can be configured throughout the μ RSW of dissimilar metals. In μ RSW process, a small variance either internal or external factor could lead to a huge significant different outcome. The main reason why this research use such electrode design is to investigate the effects of having number of edges on the electrode tip towards the overall strength of the welded joint. Moreover, to determine the effects of pimple

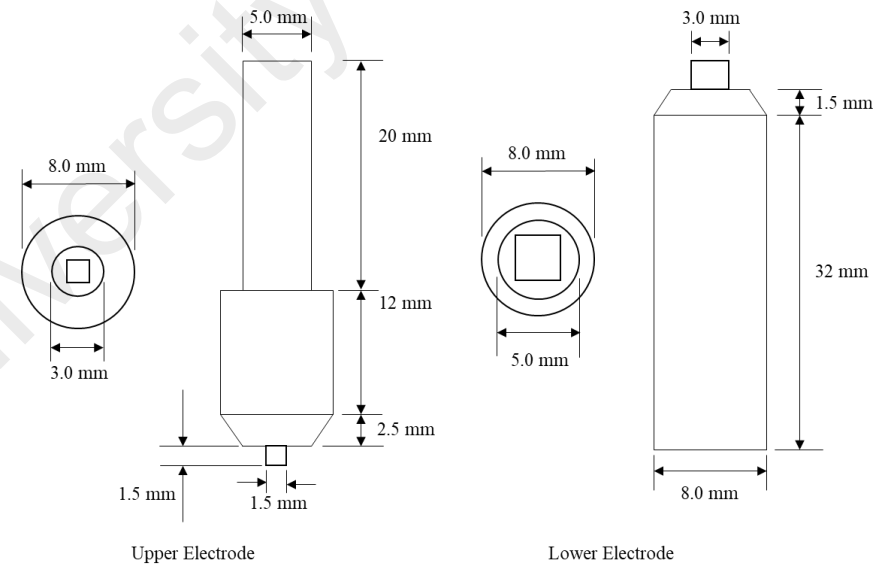
tipped (PT) electrode tip on the tensile shear load instead of using truncated cone (TC) design. Other than that, triangle shape is chosen because of the minimum edges it possesses and hexagon has maximum allowable edges. Shapes with more than 6 edges are not feasible to be used in μ RSW as problems occur during the fabrication process and welding defects could possibly occur to the welded joint such as electrode sticking. Furthermore, geometries with edges are employed throughout this study because to investigate the effects on the shape of the weld nugget formed either round weld or not. The overall dimension of the electrode tip or the contact surface area between the faying surface of the electrodes and the workpiece controls the size of the weld nugget formed (A. M. Saeed et al., 2014). If the dimension of the electrode tip is too small, a weak joint may be formed. Furthermore, in Phase 2 the effect of contact surface area was investigated. Questions arise: what happens to the formation of the weld nugget and the strength of the welded joint if the contact surface area increased. Therefore, in Phase 2 the contact surface area increased from 1.77 mm^2 to 2.25 mm^2 for the upper part and 7.07 mm^2 to 9 mm^2 .

Based on the study conducted by (R.J. Bowers et al., 1990), electrode sheet interface angles approaching 90° will provide more uniform current distribution throughout the electrodes' contact surface area as the design acts as a large heat sink. It was expected that the pimple-tipped (PT) geometry would exhibit greater current uniformity than the truncated cone (TC) geometry. Increased welding current nonuniformity was also predicted to adversely affect electrode tip life cycle. Therefore, by changing the welding current distribution density, it will affect the size of the weld nugget. The formation of the weld nugget is the most important factor contributing towards the strength of the welded joint.

The same type of material is used for the fabrication of electrode in Phase 2. The schematic diagram of the electrodes used in Phase 2 are shown in Figure 3.5.



(a)



(b)

Figure 3.5: Schematic diagram of the different design of electrodes used, (a) triangle shape, (b) square shape, and (c) hexagon shape electrode tip

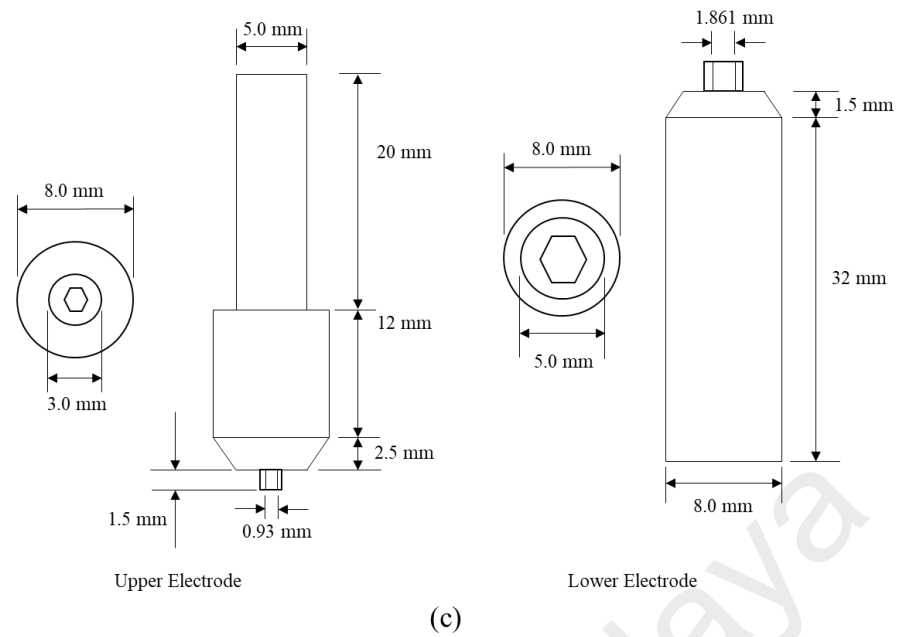


Figure 3.5 (continue): Schematic diagram of the different design of electrodes used, (a) triangle shape, (b) square shape, and (c) hexagon shape electrode tip

3.3 EXPERIMENTAL DESIGN AND PROCEDURE

Welding experiments were carried out by using micro resistance spot welding device (model SIW-608AD) equipped with HND-001 system controller and ZH-32 air driving unit as shown in Figure 3.6.

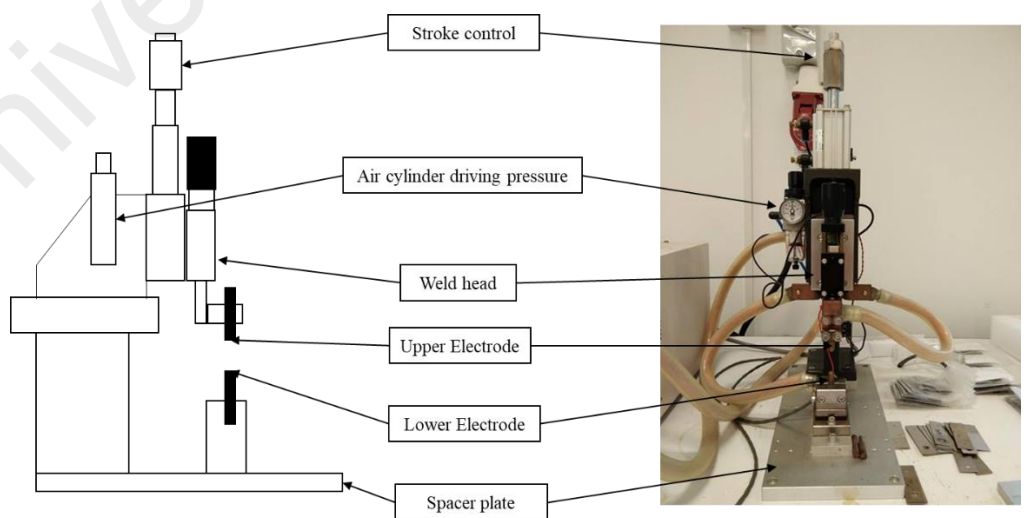


Figure 3.6: Micro-resistance spot welding machine.

This machine was equipped with a pneumatic pressure system. Welding, squeezing and holding time were selected manually on the system controller. Welding was performed under normal atmospheric conditions. The welding parameters used were shown as follows: welding current (1.8 kA-2.2 kA), welding time (100 ms-200 ms), electrode force (241 N-362 N), squeezing time (900 ms) and hold time (100 ms) respectively with no current ramp-up or ramp-down times. The chosen parameters are used after successful undergoes trial-and-error method. The parameters which are kept constant are the electrode tip diameter and electrode material. Before welding, an X was marked on the center of the upper face of the specimens in order to provide consistency to the accuracy of the alignment of the electrode tip on the center of the overlap area during welding process.

Experiments were conducted as shown in Table 3.3 according to the test conditions specified by the full factorial experimental design procedure with L27 Orthogonal Array (OA) which includes three factor and three level. Full factorial design is selected in order to fully investigate and study all the possible effects and interaction between each welding parameters that can possibly happen during the welding process. From the literature reviewed, welding current, welding time, and welding force is the most dominant and significant factor which influence the formation of weld nugget and strength of the welded joint. After the data successfully obtained from the experiment and tensile shear stress test, analysis of variance (ANOVA) was used to determine and acquire which parameter affects most of the quality of the weld nugget and provide significant effects on the strength of the welded joint during welding take place. The detailed welding parameters are listed in Table 3.4. The design of experiment and analysis was done by using the MINITAB 17 software. For Phase 2, the most optimal combination of welding parameters obtained from Phase 1 was used for the experiments.

Table 3.3: Welding parameters used in the study

Welding parameters	Level 1	Level 2	Level 3
Welding current (kA)	1.8	2.0	2.2
Welding time (ms)	100	150	200
Welding force (kN)	241	302	362
Squeeze time (ms)	900	900	900
Hold time (ms)	100	100	100

Table 3.4: Number of experiments during welding and joining process

EXPERIMENT	WELDING CURRENT (kA)	WELDING TIME (ms)	WELDING FORCE(N)
1	1.8	100	241
2	1.8	100	302
3	1.8	100	362
4	1.8	150	241
5	1.8	150	302
6	1.8	150	362
7	1.8	200	241
8	1.8	200	302
9	1.8	200	362
10	2	100	241
11	2	100	302
12	2	100	362
13	2	150	241
14	2	150	302
15	2	150	362
16	2	200	241
17	2	200	302
18	2	200	362
19	2.2	100	241
20	2.2	100	302

21	2.2	100	362
22	2.2	150	241
23	2.2	150	302
24	2.2	150	362
25	2.2	200	241
26	2.2	200	302
27	2.2	200	362

Several calculations are made for each main factor and interaction term:

1. Sum of Squares (SS): the sum of all the squared effects for each factor.
2. Degrees of Freedom (df): number of free units of information.
3. Mean Square (MS): (SS/df) for each factor.
4. Mean Square Error (MSE): pooled variance of samples within each level.
5. F-statistics: (MS for each factor/MSE).

First and foremost, to start an ANOVA work, the data are presented in a data table. There must be at least three groups of data although more are possible. The groups selected are not compulsory to be the same size. The Σx , Σx^2 and n are calculated for each group of data. ANOVA always assumes that the populations involved follow a normal distribution of data, thus, it's an analysis which is categorized as a hypothesis tests known as parametric tests. Other than that, the variance of data should be the same in all the groups. The basic principle of the analysis of variance is to summarize the divergence or division that exist in all the observations made and divide it into several separated sources.

From this point of view, there are 5 simple key step procedures:

- 1) State the null and alternative hypothesis. The null hypothesis for an ANOVA always assumes the population means are equal.

H_0 : All means are equal

H_a : Not all means are equal

- 2) Calculate the appropriate statistical test. The ANOVA test statistic is the variance ratio which define as the ratio between and within the groups mean square inside the data set. It follows an F distribution. A large value of F means to reject the null hypothesis. A small value means not to reject.

$$F = \frac{S^2}{S_p^2} \quad (3.1)$$

Where F = computed F-value,

S^2 = Pooled sample variance,

S_p^2 = Population variance.

- 3) All these equations are used in the ANOVA calculations. All except equation (a) appear in the ANOVA calculation table. Steps for ANOVA calculations:

- a) Calculate the correction factor:

$$CF = \frac{(\Sigma X)^2}{N} \quad (3.2)$$

- b) Calculate the Sum of Squares Total Value (SS Total):

$$SS \text{ Total} = \Sigma x^2 - CF \quad (3.3)$$

c) Calculate the SS Group value:

$$SS \text{ Group} = \sum \frac{(\sum x)^2}{n} - CF \quad (3.4)$$

d) Calculate the SS Error value:

$$SS \text{ Error} = SS \text{ Total} - SS \text{ Group} \quad (3.5)$$

e) Calculate MS Group value:

$$MS \text{ Group} = \frac{SS \text{ Group}}{df \text{ Group}} \quad (3.6)$$

f) Calculate MS Error value:

$$MS \text{ Error} = \frac{SS \text{ Error}}{df \text{ Error}} \quad (3.7)$$

g) Calculate F value (V.R.):

$$V. R. = \frac{MS \text{ Group}}{MS \text{ Error}} \quad (3.8)$$

4) Obtain the critical value from an F distribution, along with the significance level:

$$F_T = F_{K_1, K_2, 1-\alpha} \quad (3.9)$$

Where K_1 = Numerator degrees of freedom (df1) = $J - 1$

K_2 = Denominator degrees of freedom (df2) = $J(I - 1)$

J = Number of columns, I = Number of rows

α = significance level = 0.05

- 5) State the decision rule. The Decision rule is to reject the null hypothesis if F (computed) is greater than F_T (table) with numerator and denominator degrees of freedom. That is, reject H_0 if $F > F_{K_1, K_2, 1-\alpha}$
- 6) Translate the results and draw an appropriate conclusion.

3.4 TENSILE SHEAR TEST MEASUREMENT

Tensile shear test was used in this research to evaluate the welded joint quality and the maximum force needed to break the welded joints. For μ RSW, there are no particular or known standard that can be used or referred to for the tensile test measurement. Such geometry have been selected because of the viable information from the results obtained by previous researchers such as (Fukumoto et al., 2008), (Manladan et al., 2017) and (Saeed et al., 2014) which all specialized and focused on the μ RSW process.

To execute the tensile shear test, a hole is drilled at the end of each specimen so that a cylindrical L-shaped block can be inserted to clamp the specimen firmly at the clamp of the tensile shear test machine so that the specimen will not break upon inserting and removal process, as shown in Figure 3.7. The tensile shear test was then performed by using a universal testing machine (INSTRON, Model: 3369, Necomb Sdn. Bhd., Singapore) at room temperature with a crosshead speed of 0.5 mm/min and 10 kN load cell. The results were determined from the average value of three samples. The peak (maximum) load was extracted from the load-displacement curve. The fracture mode of the specimens was determined by examining the fracture surface. Micrographs of the cross-section of failed welded joint obtained from SEM imaging were examined in order to investigate the failure mechanism.

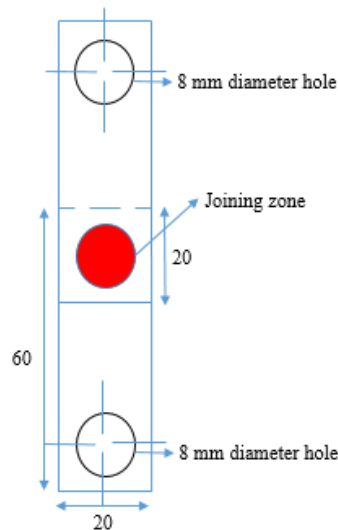


Figure 3.7: Schematic illustration of tensile shear test specimen

3.5 MICROSTRUCTURAL CHARACTERIZATION ANALYSIS

After welding, metallographic samples were obtained by cross sectioning the welded joint through center of the weld nugget perpendicular to the weld surface plane and mounted in an epoxy (a mixture of resin and hardener) followed by grinding and polishing in sequence. After grinding and polishing, the samples were etched using Kroll's reagent (92 mL distilled water, 6 mL nitric acid (HNO₃) and 2 mL hydrofluoric acid (HF)) for 15 s at room temperature. The microstructures were observed using an optical microscope (OM, Olympus, Tokyo, Japan) and SEM (Phenom Pro X, Crest System (M) Sdn. Bhd., Eindhoven, The Netherlands). The SEM employed was equipped with EDX.

3.6 MICROHARDNESS TEST

The Vickers micro-hardness profile, which include the base metal (BM), fusion zone (FZ), partially melted zone (PMZ), and heat affected zone (HAZ) was evaluated by using a pyramidal diamond indenter (HMV-1 series, SHIMADZU, Kyoto, Japan) micro-hardness tester with a load of 100 g and a dwell time of 15 s. All indentations were spaced adequately to avoid any possible effects of strain fields produced by adjacent indentations. Nineteen indentations at an indentation interval of 50 μm were performed across the weldment. All profile lines began with Ti-6Al-4V base metal zone, went through the fusion zone and ended within the ASS 316L.

3.7 SUMMARY

The methodology used are sufficient to investigate the mechanical properties and performed a thorough microstructure analysis. The methods indicate in chapter 3 are conducted with concise guidelines to ensure the results and data obtained can be replicate by other researchers. Most of the parameters or conditions used in the research are obtain through trial-and-error method to obtain an acceptable value with less negative impact on the results. Other than that, human error also is taken into account for each test or experiment run to reduce results with error and the creditability of data.

CHAPTER 4: RESULTS AND DISCUSSION

PHASE 1: THE INVESTIGATION OF OPTIMIZATION PROCESS

PARAMETERS OF μ RSW

4.1 INTRODUCTION

This chapter discusses the results in detail obtained in phase 1 of this study. The results are comprised of tensile shear strength test, ANOVA, failure modes analysis, characterization of microstructure which includes SEM and EDX analysis, microhardness test, and experimental investigation of the design of electrode geometry on the welded joint during the μ RSW process.

4.2 MECHANICAL PROPERTY ANALYSIS

This section presents the results that correspond to the tensile shear strength test and Vickers microhardness test of the welded joint interface.

4.2.1 Tensile Shear Strength Analysis

The tensile shear strength test is the most commonly used test for evaluating the resistance spot welding welded joint mechanical behaviours in static condition. Maximum load (N) which can be acquired from the tensile shear load displacement curve describes the mechanical behaviours of the welded joint. A total of 3^3 which is 27 combinations of the input parameters were considered, according to the full factorial design of experiments (DOE). Table 4.1 shows the experimental results of tensile shear strength collected by using the DOE mentioned.

Table 4.1: Experimental data collected as per full-factorial design of experiments

Experiment Run	Welding Current(kA)	Welding Time(ms)	Welding Force(N)	Maximum Load (N)
1	1.8	100	241	356.36
2	1.8	100	302	344.72
3	1.8	100	362	356.42
4	1.8	150	241	367.59
5	1.8	150	302	335.55
6	1.8	150	362	350.52
7	1.8	200	241	339.78
8	1.8	200	302	311.95
9	1.8	200	362	331.64
10	2	100	241	378.25
11	2	100	302	334.83
12	2	100	362	358.49
13	2	150	241	369.64
14	2	150	302	350.30
15	2	150	362	369.11
16	2	200	241	340.21
17	2	200	302	320.82
18	2	200	362	339.49
19	2.2	100	241	338.61
20	2.2	100	302	307.25
21	2.2	100	362	336.167
22	2.2	150	241	340.48
23	2.2	150	302	291.66
24	2.2	150	362	316.22
25	2.2	200	241	313.20
26	2.2	200	302	276.45
27	2.2	200	362	283.12

The statistical significance of the full linear models predicted was evaluated by a statistical analysis technique called the analysis of variance (ANOVA). Throughout the entire analysis, the confidence interval used is set to 95%. The model developed was used to determine the highest level for each factor, which results in gaining the most optimal combination of welding parameters for micro resistance spot welding between austenitic stainless steel 316L and ASTM titanium alloy grade 5 (Ti-6Al-4V).

ANOVA with all the process parameters and their respective values were analyzed using the statistical software Minitab 17. ANOVA is a unique decision support tool which is important for regression coefficients significance management, where partition of sums of squares. It is a statistical concept where partitioning of the sum of squared deviations into different components which permits the overall variability in a group of data to be assign to various types with the relative importance of each being quantified by the size of each component of the overall sum of squares.

ANOVA can be computed with two distinct variables in the course of analyzing the model. First, the F-test can be used to verify and test that whether the model developed is enough to present the data obtained. Second, the significance of contribution for each coefficient is represented by the F-value and P-value, which define the variance decomposition in a multilevel regression model. In general, a bigger F-value and smaller P-value is desired for a developed model as it's indicated the significance contribution and same goes for its coefficients. If the P-value is smaller than 0.05, it is considered as a significant variable to the model developed. Whereas P-value greater than 0.1 indicate that the variable is insignificant (Zhao et al., 2014).

As seen in Table 4.2, the full linear model was significant as its F-value (Fisher's ratio) was 49.03 and its P-value was smaller than 0.05. The F-value is used to test the hypothesis and can be used to test that whether the model developed is enough to explain the data. In general, larger F-value and smaller P-value are desirable as they indicate the model is significant or not. Besides, all the terms welding current (kA), welding time (ms) and welding force (N) were significant since the P-values of them were less than 0.05. The coefficient of determination R^2 is the measure for examining the fitting degree of the regression equation. Its value is desirable to be as high as possible as, greater than 0.8 and close to 1.0 in order for the developed linear model established by ANOVA is acceptable (Jeang, 2015). The value of adjusted R^2 was 0.9172 confirming that less than 8% of the total variations in the variables could not be explained by the developed analytical expression. Meanwhile, it also indicated that there was a satisfactory and high degree of correlation between the experimental results and predicted data. The predicted R^2 was 0.8840 and it was close to the value of adjusted R^2 (Paventhana et al., 2011).

Table 4.2: Analysis of variance (ANOVA), $S=0.0752264$, $R^2=0.9363$, adj. $R^2=0.9172$, pred. $R^2=0.8840$

Source	Df	Sum of squares	Mean square	F-value	P-value
Model	6	16647	2774.52	49.03	0.001
Welding current	2	8054	4027.16	71.16	0.001
Welding time	2	4448	2223.88	39.30	0.001
Welding force	2	4145	2072.51	36.62	0.001
Error	20	1132	56.59		
Total	26	17779			

Figure 4.1 shows the percentage contribution of each welding process parameter to the total variation, indicating their degree of influence on the maximum load achievable. The value of percentage contribution was obtained by dividing sum of squares of each respective welding parameters towards sum of squares of total.

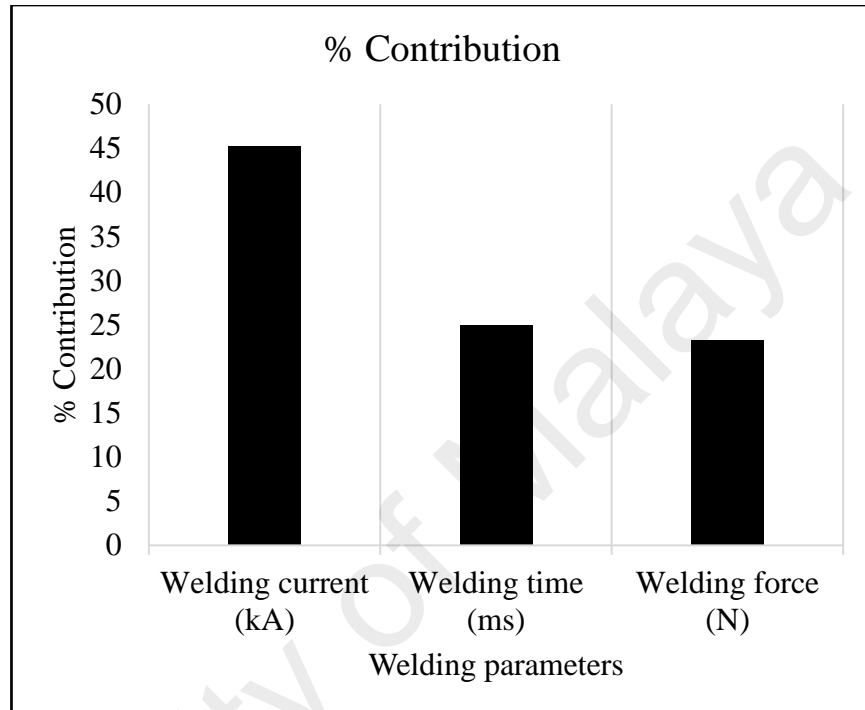


Figure 4.1: Effects of different control factors on Load (N)

The optimum conditions from full-factorial design of experiment analysis for micro-resistance spot welding of dissimilar material are found to be experiment run no. 10 with welding current at level 2 (2 kA), welding time at level 1 (100 ms) and welding force at level 1 (241 N). From Figure 4.1, the percentage contribution of various welding parameters which significantly influence the tensile shear strength is clearly indicated. For the micro-resistance spot welding of dissimilar sheets of metal (austenitic stainless steel 316L to ASTM titanium alloy grade 5), welding current(kA) is the most influenced/significant welding parameters by having the highest percentage contribution of 45.30%, followed by welding time(ms) and welding force(N) by having the percentage contributions of 25.02% and 23.31% respectively.

This is because more heat is required to form a sufficient solid-molten pool of weld at the interface of faying surfaces between ASS 316L and Ti-6Al-4V and the electrical resistivity of Ti-6Al-4V is comparatively higher than ASS 316L. Therefore, large amount of heat needs to be generated, which is achievable by allowing more current to flow through for a short period of time. This results into an enormous amount of heat generated at the interface which will decrease the surface contact resistance with the increase of temperature. It is also observed that for a factor with the highest percentage contribution, a small variation may greatly influence the output characteristics.

The influence of the welding parameters on the maximum tensile shear load (the forces needed to fracture the samples) are summarized in the interval plots shown in Figure 4.2. It can be seen that by increasing the welding current from 1.8 kA to 2.0 kA will increase the maximum tensile shear load of the spot welds from 343.84 to 351.24 N. However, when the welding current used is increased from 2.0 to 2.2 kA, the maximum tensile shear load decreases drastically from 351.24 to 311.46 N. This may be caused from the expulsion of molten metal from the fusion zone due to the increase of welding current thus limit the growth of the weld nugget size which lead to the significant decrease in the maximum tensile shear load values (Kazdal Zeytin et al., 2017). The effect of welding time on the maximum tensile shear load shows a slight decrement from 100 ms to 150 ms, whereas it significantly reduces the maximum tensile shear load at 200 ms. This is due to the overheating of the weldment at the joint causing micro-cracks, holes and weld metal expulsion (WME) during the formation of the weld nugget thus producing a weak welded joint. The effect of welding force on the maximum load reduce significantly from 241 to 302 N, whereas it shows a slight increase at 362 N.

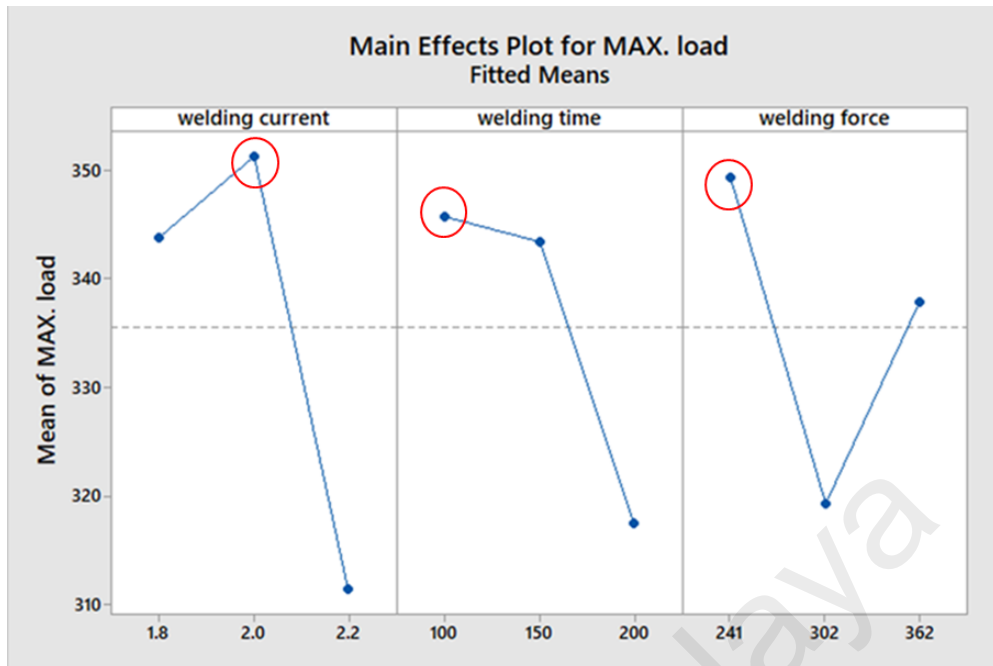


Figure 4.2: Mean of maximum load for each level of the welding parameters: (a) welding current [kA]; (b) welding time [ms]; (c) welding force [N]

The interaction plots are presented in Figure 4.3. These plots represent the interaction effect of the inputs on the responses. The following observations can be derived from Figure 4.3. Based on the interaction plot of mean maximum load against (welding current * welding time), the highest value of mean maximum load 363.017 N, obtained at current 2 kA and time 150 ms meanwhile the lowest value 290.92 N, obtained at current 2.2 kA and time 200 ms. Based on the interaction plot of mean maximum load against (welding current * welding force), the highest value of mean maximum load 362.7 N, obtained at current 2 kA and force 241 N meanwhile the lowest value 291.79 N, obtained at current 2.2 kA and force 302 N. Based on the interaction plot of mean maximum load against (welding time * welding force), the highest value of mean maximum load 359.23 N, obtained at time 150 ms and force 241 N meanwhile the lowest value 303.07, obtained at time 200 ms and force 302 N.

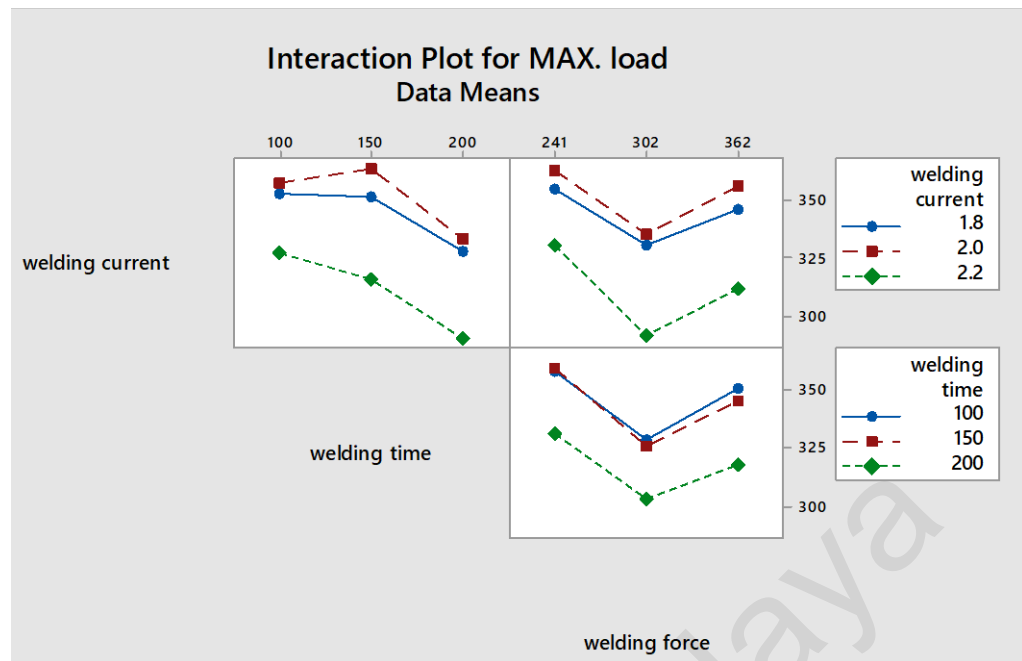


Figure 4.3: Interaction plot for maximum load

From the observations obtained, the value of mean maximum load decrease when welding current increased at lower welding time but the value of mean maximum load increase when welding force increased at lower welding current and welding time. This is due to the welding defects formed at the welded joint cause by excess of welding current and time. When excess in welding force and time, electrode wear is developed. If these electrodes are used, the efficiency of the welded joint formation will reduce throughout the welding process. In order to prevent this problem, the electrode should undergo proper electrode tip dressing process after used for several spot welding. When excess in welding force and current, a weak welded joint is formed. A weak welded joint usually refers to formation of brittle welds. A brittle weld is a resistance spot weld that fractures with little or no plastic deformation in either the weld or the surrounding metal. This explain the decrease in the value of mean maximum load.

When excess in welding current and time, weld metal expulsion will develop during the spot weld process (Fan et al., 2016). Weld metal expulsion is the forceful ejection of molten metal from the weld nugget. Severe expulsion may eject enough material to create a through-hole in the workpiece, commonly termed "burn through" or burn-thru. With the excess of welding current, the probability of the cracks and holes formation inside the weld nugget are likely high (Ma et al., 2008). These should be avoided as it will give weak joint formation thus causing low value of tensile shear strength obtained. This explain the decrease of mean maximum load when the welding current increase. The surface of the sheet metal interface could also contain cracks and holes formation due to high usage of welding current and time. Excessive indentation is also caused from excess used of welding current thus contribute to a small formation of weld nugget (Khodabakhshi et al., 2015).

4.2.2 Regression analysis

Further analysis using the regression analysis method was carried out to ensure the response values fits the model data produced by the ANOVA. The regression analysis used in this research study involved using mathematical models to observe the relationship between the control parameters and the performance of the welded joint in achieving maximum allowable load before fracture, based on the full-factorial design of L₂₇ orthogonal array (OA). The previous analysis developed the response equation by considering the effects of each welding process parameters which is the welding current (kA), welding time (ms), and welding force (N).

The mathematical model developed which relates towards the maximum achievable load by the welded joint and the welding process parameters is shown in equation (4.1):

$$\begin{aligned} \text{Max. Load [N]} = & 335.51 + 15.72 \text{ welding current} + \\ & 10.17 \text{ welding time} + 13.83 \text{ welding force} \quad [R^2 = 93.63\%] \end{aligned} \quad (4.1)$$

Based on the equation 4.1 obtained by the regression analysis, the predicted value for the maximum achievable load by the welded joint obtained from the optimum parameters which is 2.0 kA for welding current, 100 ms for welding time, and 241 N for welding force is 375.23 N simply by adding each welding parameter coefficients value with 335.51.

The optimum data for the maximum achievable load by the welded joint obtained from ANOVA were tabulated in Table 4.3 including the predicted value by regression analysis method and compared with the experimental values obtained for the confirmation test.

Table 4.3: Predicted and experimental values

Testing	Optimum parameters			Predicted value	Experimental value
	Welding current (kA)	Welding time (ms)	Welding force (N)		
Maximum load (N)	2.0	100	241	375.23 N	379.48 N

4.2.3 Failure modes

In this research, the failure mode of the test samples was investigated. Irrespective of the welding parameters used, only one type of failure mode is observed during the TS tests, the interfacial failure (IF) mode. Therefore, only one test sample (experiment no. 10) were analyzed and the metallographic characteristics of the fracture surface are investigated. Test sample experiment no. 10 is chosen among others as the specimen exhibit the highest load value.

In cases with low electrode force, small welding current or short welding time, interfacial failure (IF) mode would occur (Ma et al., 2008). Figure 4.4 shows the SEM micrographs of a typical interfacial failure mode surface of ASS 316L side for sample no. 10. Figure 4.4(a) shows an overall view of the failed nugget at a low magnification. From the microstructure observed, it is seen that there are macro-voids and multiple cracks exist throughout the structure of the weld nugget which constitute to the cause of interfacial failure (IF) mode and the main reason in the reduction of weld joint strength. A river-like pattern can be seen in Figure 4.4(b) which explain that the cracking start from the grain boundary. This structure is called trans-granular brittle fracture. The crack propagates across the grain boundary. It is also classified as a cleavage fracture which is a typical brittle overload fracture.

In Figure 4.4(c) shows a further magnified of weld metal expulsion fractured surface which also reveals some of the magnified part of the cracks indicating relatively poor joining. Even though, sample specimen no. 10 obtained the highest strength it still exhibits weld metal expulsion. This is because formation of weld nugget is affected by the properties of each base metals used for μ RSW. Since this research focused on dissimilar joining, WME are still expected to happen cause the difference in mechanical properties and elements composition. A part of the weld nugget also exhibit elongated dimple structure shown in Figure 4.4(d), which represent a characteristics of a brittle fracture (M Pouranvari & Marashi, 2012). This structure is called inter-granular brittle fracture. As shown in the figure, the crack propagates along the grain boundary.

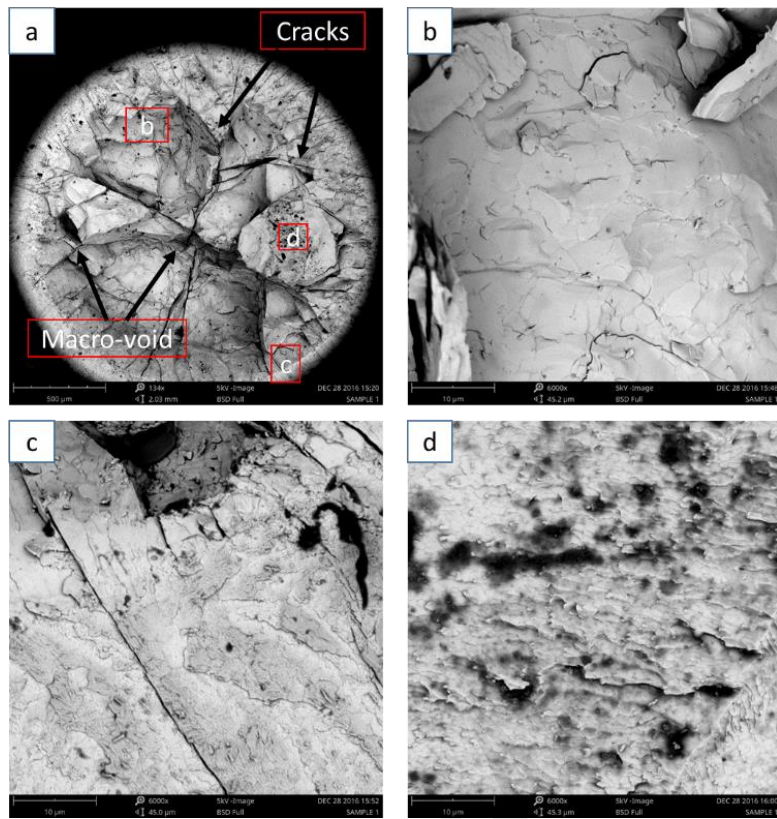


Figure 4.4: Fracture surface of ASS 316L side of the μ RSW joint

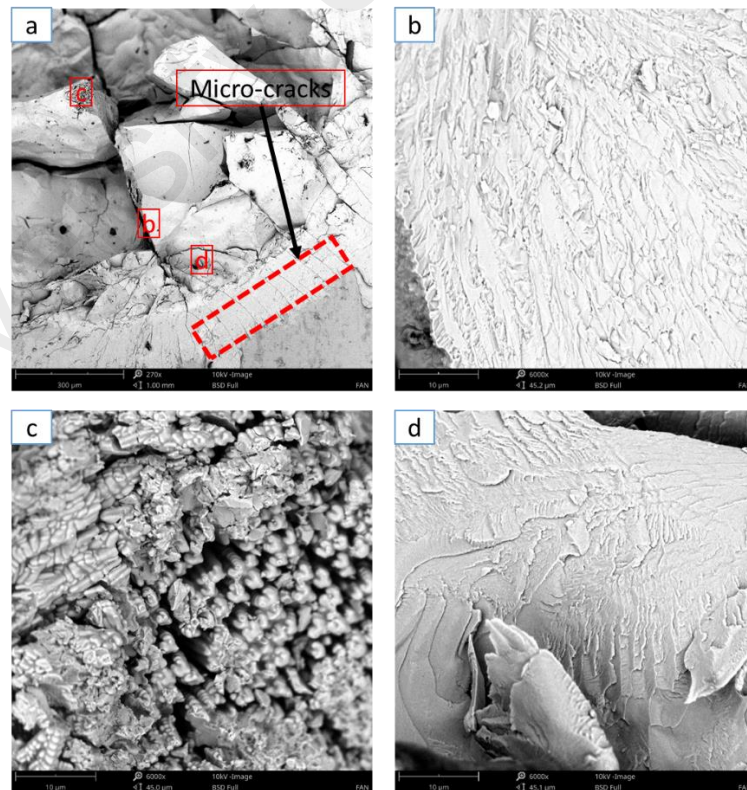


Figure 4.5: Fracture surface of Ti-6Al-4V side of the μ RSW joint

Figure 4.5 shows the SEM micrographs of the tensile shear load fracture surface of the μ RSW joint on the Ti-6Al-4V side. Figure 4.5(a) shows the lower right view of the failed nugget at a low magnification. It is seen that there are many micro-cracks which propagate from the weld metal expulsion area towards the center of the weld nugget. This weld imperfections would lead to the occurrence of interfacial failure and eventually reducing the weld strength. A similar phenomenon was observed by (Ma et al., 2008) while investigating the fracture characteristics of spot welded DP600 steel. The further magnified Figure 4.5(a) reveals part of the fracture surface exhibiting the characteristics of brittle fracture as shown in Figure 4.5(b,c, and d).

Figure 4.5(b) and (d) shows a characteristic of a river-like pattern which are formed due to the propagation of the cracks during the tensile shear load test. Because each grains in the FZ have different orientations with respect to each other, the crack generally divides into a terrace-like steps. These fracture mechanism are called cleavage fracture which is a form of transgranular brittle fracture. The occurrence of these fracture are also caused from the carbide precipitation take place during welding where the carbon is drawn out from the mixture and react with the atmosphere thus explaining the origin of the crack initiation area. This explain the brittle behaviour of the welded joint. Figure 4.5(c) shows that the fracture surface exhibit severals dendritic structures which presents direct evidence of welding imperfections are caused from solidification shrinkage.

4.2.4 Vickers Micro Hardness Test

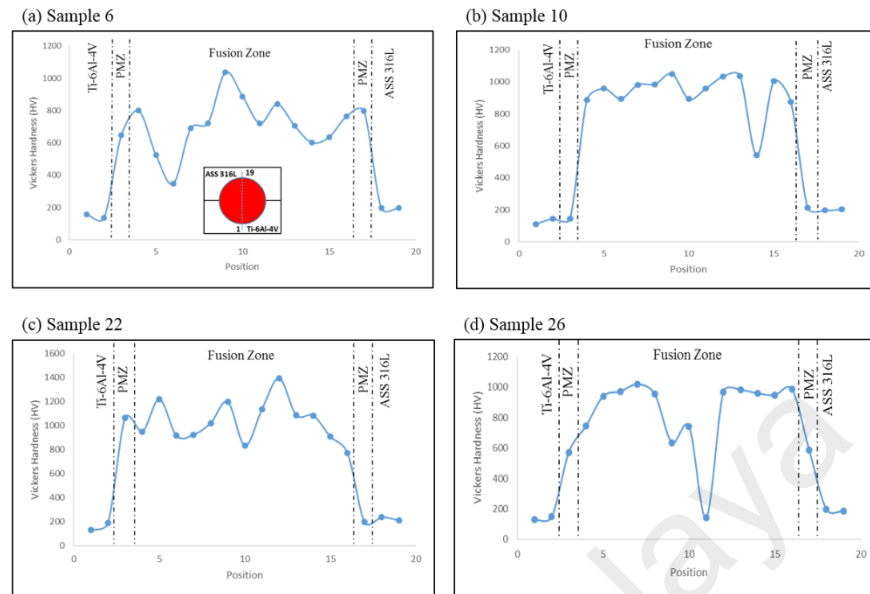


Figure 4.6: Vickers micro-hardness profile of μ RSW joint

FIGURE 4.6 shows the Vickers micro-hardness profile of μ RSW of sample specimen 6, 10, 22, and 26 at different welding parameters measured along the cross section of the welded joint, which exhibited a significant hardness increase from the base metal. Sample specimen 6 and 22 is chosen due to less formation of macro-cracks, void and porosities. Meanwhile sample specimen 10 exhibit the highest load value and sample specimen 26 exhibit the lowest load value. The micro-hardness measurements were taken across these welding regions: fusion zone (FZ), partially melted zone (PMZ), and base metal (BM). Micro-hardness at FZ and PMZ region show considerably higher values than that at BMs region.

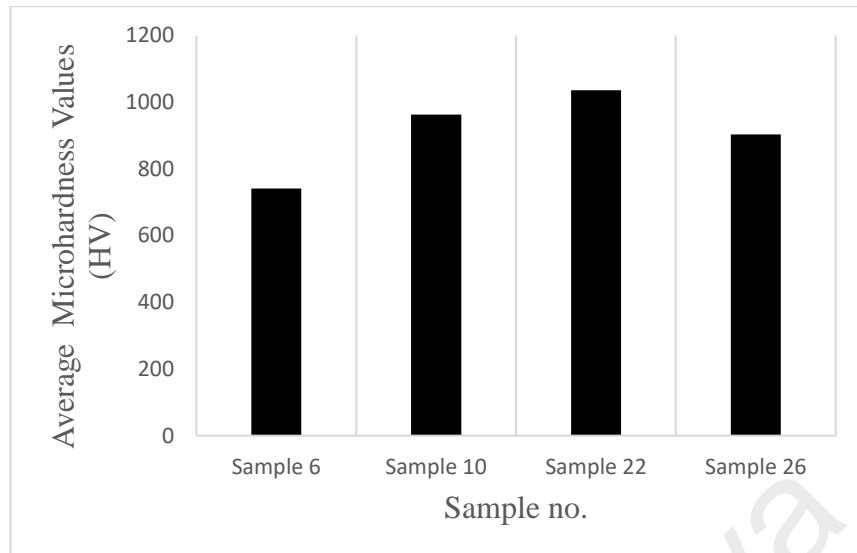


Figure 4.7: Effects of welding parameters on the average microhardness values at the FZ

The average microhardness values in the FZ obtained by implying different welding process parameters for each sample specimen are displayed in FIGURE 4.7. The average microhardness values of the weld nugget were found to be higher (in range of 741-1036.5 HV) than both base metals (ASS 316L=202 and Ti6Al4V=149). This is due to the formation of the intermetallic compound (IMC), TiFe and TiFe₂ at the FZ. With the abundance presence of the IMC at the FZ, it indicates the hard and brittle behavior of the welded joint. Another reason was that the FZ contain higher carbon percentage than the BM due to the carburization process where carbon is absorbed while the metals is heated during welding. A similar phenomenon was observed by (MI et al., 2008) while investigating the RSW of advanced high strength steel. It was reported that the FZ hardness is proportional to the carbon content (wt %) of the welded materials. Materials undergoes elevated carbon equivalence will experience an increase of hardness values around the FZ area.

The average microhardness of the FZ increased from 741 to 1036.5 HV with increase in the welding current supplied from 1.8 to 2.2 kA then gradually decreased to 904 HV when the welding time and welding force increased to 200 ms and 302 N respectively. The average microhardness corresponds to 1.8 kA, 2.0 kA, and 2.2 kA are 741 HV, 963 HV, and 1036.5 HV respectively. These trends which are observed from the results of Vickers microhardness test are different from the tensile properties obtained from the tensile shear load test. It was noted that the tensile shear load obtained increase by increasing the welding current. But when increasing the welding current further, it will reduce the tensile shear load as seen in sample 22. When increasing the weld current, welding imperfections such as micro-cracks are more likely to form inside the welded joint after the welding process.

The increase in the welding current supplied would increase the heat input per unit weld length at a constant squeeze and hold time but at different welding time and welding force with the same design of electrode geometry. High heat input supplied will increase the solute concentration in the weld nugget at the FZ due to the reversion process which is the dissolution of second phase particles.

Different phenomenon is observed from sample 26. At the same welding current with sample 22 but longer welding time and higher welding force, the microhardness value obtained is lower than sample 22. This is probably due to the damage formed at the electrode tip caused from longer welding time used which prolong the welding current supplied causing irregularities on the solute concentration at the FZ. The longer the duration of the welding time, the higher welding current concentration throughout the entire welding process. When the electrode tip is damaged, the welding current supplied from the electrode towards the welding nugget are disturbed causing ununiformed heat distribution at the FZ during welding process.

The microhardness value at the FZ between dissimilar metals in μ RSW process which involve ASS normally depends on the chemical composition of the BMs and the percentage of the weld metal dilution which define as the ratio of the carbon composition in the ASS to the weld nugget volume (Verma et al., 2014). Universally weld metal dilution is controlled by various combination of welding parameters. Subsequent rapid cooling rate also contribute to the fact that the microhardness values of FZ and PMZ is higher than the BMs. A similar phenomenon is observed by (Huin et al., 2016) during RSW of DP600 ferritic-martensitic steel. According to (Marashi et al., 2008) research, the hardness of the FZ are governed by the dilution between two BMs.

Some of the micro-hardness profiles that can be seen from Figure 4.6 shows some points are fluctuating to a lower hardness value. This is because these points are taken near the micro-cracks which determine that the area surrounds the micro-cracks are much softer than the other areas. These includes point no. 6 from sample 6, point no. 14 from sample 10, and point no. 11 from sample 26. On top of that, these points are not included in the calculation of the average micro-hardness of the FZ of each sample as its values diverge far from the mean values.

The observation on the evolution or grain structure in the intermetallic compound (IMC) phases have been performed in the microstructural analysis. The grain structure of the IMC inside the FZ is columnar dendritic zone (CDZ) structure. But the investigation on the grain size have not been performed. However, in dissimilar μ RSW process, there exist possibilities where increase in hardness value (HV) may be affected by the growth of the grain size and lattice diffusion of the grain boundary.

4.3 CHARACTERIZATION OF MICROSTRUCTURE

Figure 4.8 shows the typical macrostructure and microstructure image of the joint produced by the micro-resistance spot welding process. The welding joint produced show that an excellent weldability between ASS 316L and Ti-6Al-4V is possible, in which the elements in ASS 316L melted and fuse together completely with the elements in Ti-6Al-4V. Thus, upon solidification, a weld nugget is formed between ASS 316L and Ti-6Al-4V. This is because the maximum temperature achieved during welding was higher than the melting point of ASS 316L and Ti-6Al-4V. A similar phenomenon was observed by Russo Spena et al. (2016), during RSW of advanced Quenching and Partitioning (Q&P) steel/Transformation Induced Plasticity (TRIP) steel.

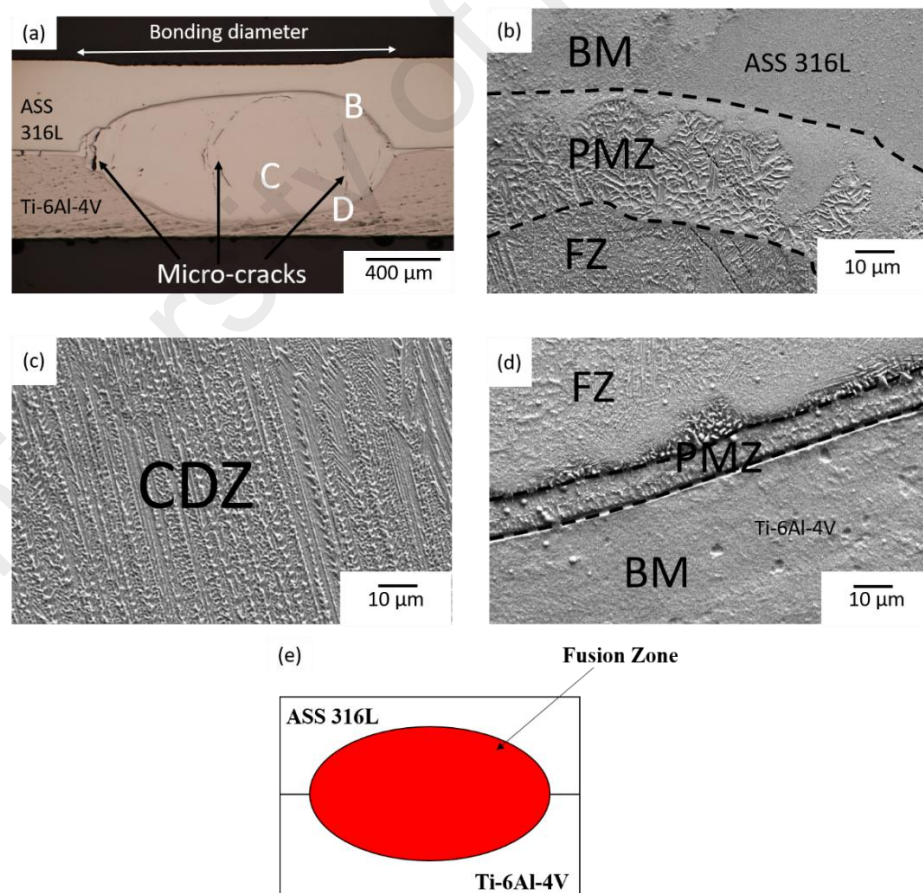


Figure 4.8: Typical macrostructure and microstructures of RSW joint: (a) Macrostructure; and microstructure of (b) region B in (a); (c) region C in (a); (d) region D in (a); (e) Schematic diagram for the Fusion Zone (FZ)

As can be seen in Figure 4.8 (a), micro-cracks are formed throughout the weld nugget, which started from the partially melted zone/base metal interface on each side and propagate into the fusion zone. This is due to the severe liquation cracking which occur in the partially melted zone (PMZ) during welding (Kou, 2003). Since the PMZ is weakened by the grain boundary liquation, micro-cracks formed when the solidifying weld metal contracts and pulls it. This also caused from the difference of the cooling rate between both material during welding which lead to non-equilibrium solidification (Manladan et al., 2017).

These micro-cracks were also identified by (Saeed et al., 2014) while studying the micro-spot brazing of commercially pure titanium and nickel sheets. The cracks formed during welding occurred when low electrode force is applied, higher usage of welding current, or any other conditions or combinations of parameters which can produce excessive heat input. They also found out that high thermal expansion and high welding shrinkage strain will lead to micro-cracks in the fusion zone. The higher carbon equivalents from each materials also contribute to the fact that it cause the welded joint hard and brittle behaviour, which congregated in the grain boundaries and increase the boundary energy which will easily cause the solidification cracks inside the welded joint (Ma et al., 2008).

Referring to Figure 4.8 (b) and (d), the microstructure of the joint can be divided into three zones, namely the base metal (BM), partially melted zone (PMZ), and the fusion zone (FZ). The size of the FZ often defined by some researchers as the width of the weld nugget at the sheet/sheet interface in the longitudinal direction. The FZ is the most important factor in investigating the quality of the spot welds (Pouranvari & Marashi, 2012). Prior to various etching time, there are no heat affected zone (HAZ) that can be seen clearly between the BM and PMZ.

One of the main reason is that there are no phase transformation or grain size enlargement in the BM of both material. This is due to the used of controlled heat inputs which prevents from the grain structure to undergoes grain coarsening process (Saha et al., 2012). The PMZ, which surrounds the FZ, is formed when the material is heated up to between the eutectic temperature and the liquidus temperature during welding. Therefore the material becomes a solid-plus-liquid mixture. Grain boundary liquation was observed at the PMZ as equiaxed dendritic grain structure are formed due to recrystallization after the welding process. This phenomenon is also observed on other cross sectional micrograph for all other specimen as well.

The microstructure at the edges (Figure 4.8 b and d) and center (Figure 4.8 c) of the FZ consisted of columnar dendritic zone structure (CDZ) only. Usually the structure will end up as equiaxed dendritic zone structure (EDZ) or combination of both CDZ and EDZ upon solidification. This is different from what was identified by Kou (2003). He described the changes of the solidification mode from planar to cellular, cellular to columnar dendrite, and finally equiaxed dendrite by using the theory of constitutional supercooling; with higher degree of constitutional supercooling and enhanced columnar-to-equiaxed transition (CET), the solidification mode will change from planar to equiaxed dendritic structure. Therefore, the formation of only CDZ in the FZ are possible because Ti-6Al-4V (which have lower thermal conductivity and higher electrical resistivity than ASS 316L) restrained heat dissipation and decreasing the rate of cooling time.

Figure 4.9 shows the microstructure image of the FZ at the weld nugget at different combination of welding parameters used. It could be seen clearly, for all the combination of welding parameters used during welding process, the FZ invariably showed the formation of columnar dendritic zone (CDZ) in the form of widmanstatten structure due to the difference of cooling rates between ASS 316L and Ti-6Al-4V.

These structure could also formed from a higher welding current used at a shorter welding time which will induce a high heat input and formed irregularities of heat distribution during the solidification period. Other than the structure of the surface on the FZ, micro-cracks can be seen in Figure 4.9 (b) which is sample specimen no. 6. This is due to the utilisation combination of low welding current and high welding force. Based on the welding issue and cause matrix design by G. E. Schmidt corporation which can be obtained through their official webpage, when high welding current or low welding force is used in the resistance spot welding process regardless of metal sheet thickness, welding defects such as micro-cracks are likely to form inside the welding nugget. This contradicts with the results obtained. This is probably due to the difference in material properties when dissimilar metals are used and the scale of the RSW process. To further investigate the morphology and the composition of the FZ, EDX analysis was performed.

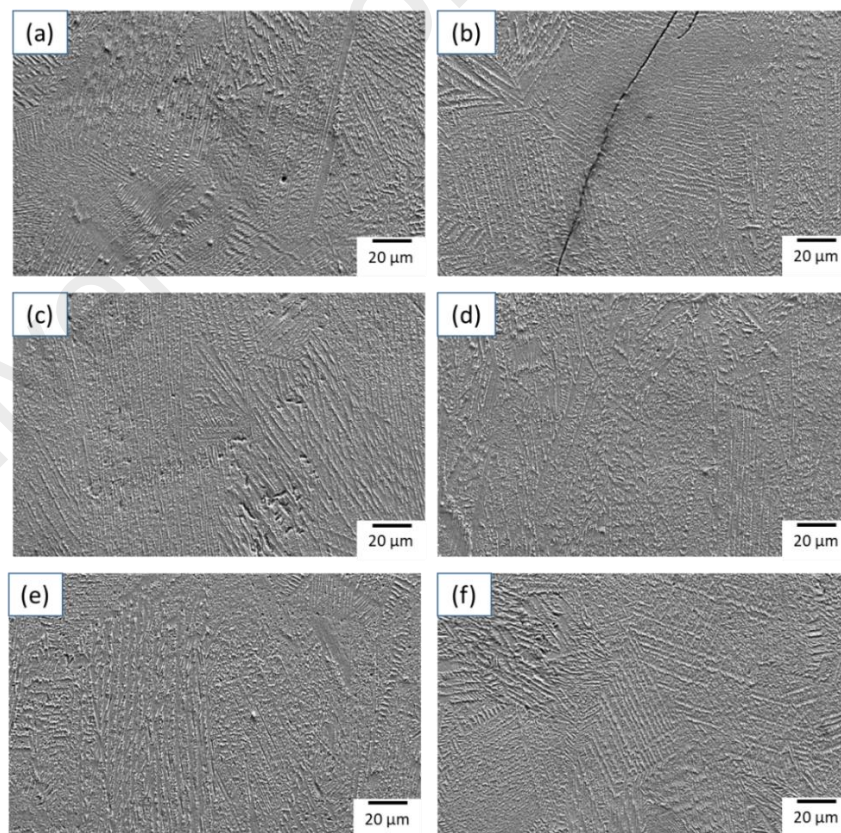


Figure 4.9: Microstructure image of the FZ of various samples: (a) FZ for sample 2; (b) FZ for sample 6; (c) FZ for sample 16; (d) FZ for sample 17; (e) FZ for sample 20; (f) FZ for sample 25

4.4 CHARACTERIZATION ANALYSIS OF INTERMETALLIC COMPOUNDS (IMC) OF THE WELDED JOINT

The morphology of intermetallic compound formation at the FZ in the welded joint were investigated and analysed by using EDX point analysis. By incorporating this method of analysis, the element atomic percentage presented in the composition at the FZ can be used to proof the existence of the intermetallic compound (IMC). The CDZ structure in figure 4.10 are predicted to be TiFe microstructures. Prediction made from reviewing and observing the chemical composition of the base metals where element atomic weight iron, Fe and titanium, Ti are significantly higher than others. This prediction is further confirmed by the EDS analysis displayed in Table 4.4, where the element atomic percentage of Fe, Ti and Ni was determined.

At the FZ, points A, B, and C had nearly the same percentage of Fe and Ti, indicating the presence and formation of TiFe intermetallic compound (IMC) between Fe base alloy and Ti base alloy during μ RSW. The points are referred to a specific microstructure which is the CDZ structure. The formation of TiFe IMC inside the whole matrix of FZ is not a good implication as these IMC is hard and brittle. Due to these characteristics, there exist possibility that it'll compromise the overall strength of the welded joint. The most obvious imperfection exhibit by this compound is the existence of voids, porosities and micro-cracks. At the PMZ on ASS 316L side, the percentage of Fe is higher than Ti. This shows that during welding, the BM is partially melted which caused some alloying element and impurities to mix together with the elements of the BM. The same mechanism applied on Ti-6Al-4V side where the percentage of Ti is higher than Fe.

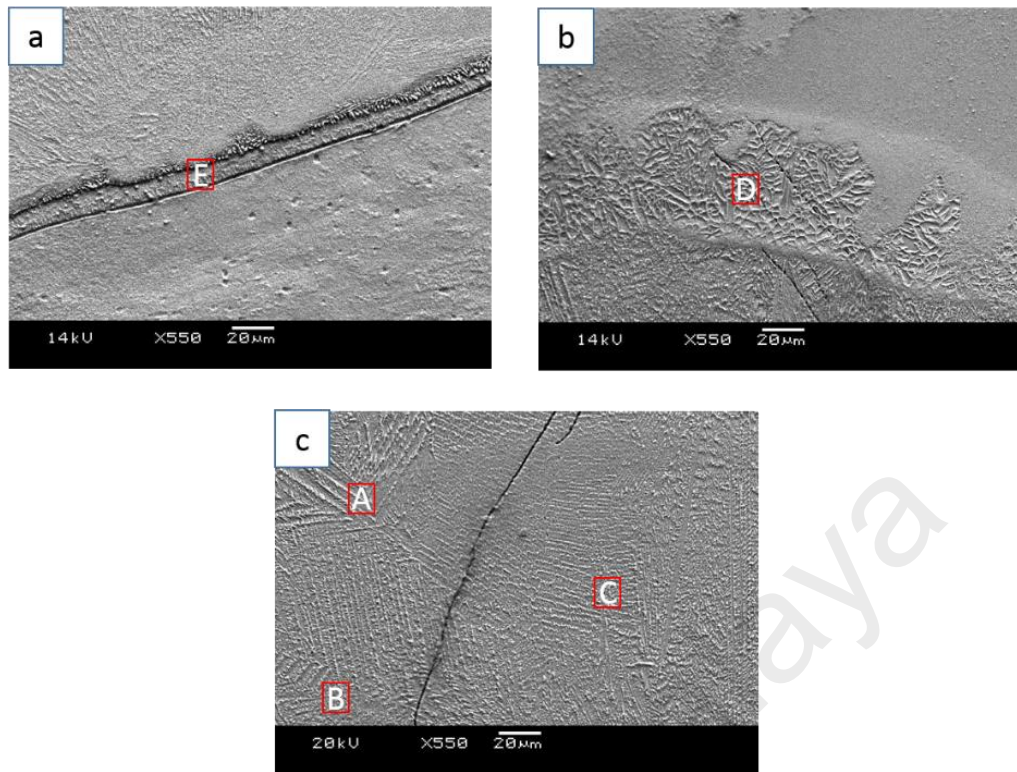


Figure 4.10: SEM micrographs of TiFe intermetallic compound formed (a) at the PMZ on Ti-6Al-4V side, (b) at the PMZ on ASS 316L side, and (c) at the FZ

Table 4.4: The element atomic percentage in sample specimen with 1.8 kA welding current, 150 ms welding time, 362 N welding force

Point	Mg(at.%)	Ti(at.%)	Fe(at.%)	Ni(at.%)	Total(%)	Phase
A	0.80	44.82	48.76	5.62	100	TiFe
B	0.08	42.61	51.14	6.17	100	TiFe
C	0.65	43.16	51.94	4.25	100	TiFe
D	0.61	39.07	56.35	3.96	100	-
E	0.16	66.96	28.82	4.06	100	-

PHASE 2: THE OPTIMAL DESIGN OF ELECTRODE GEOMETRY

4.5 INTRODUCTION

This chapter discusses the results in detail obtained in Phase 2 of this study. The results are comprised of tensile shear strength test, characterization of microstructure which includes SEM and EDX analysis, microhardness test, and experimental investigation regarding the design of electrode geometry on the welded joint during the μ RSW process.

4.6 MECHANICAL PROPERTY ANALYSIS

This section presents the results that correspond to the tensile shear strength test and Vickers microhardness test of the welded joint interface.

4.6.1 Tensile Shear Strength Analysis

Tensile shear strength test was performed by using the optimal process parameters, 2.0 kA welding current, 100 ms welding time, and 241 N welding force which is obtained in Phase 1. Three tests were carried out which represent each design of electrode geometry respectively. For each test, three readings were determined from three different samples in order to get an average value. Table 4.5 shows the experimental results of tensile shear strength test collected. It depicts the effect of different design of electrode tip shape on the maximum load of the welded joint.

Table 4.5: Experimental results of tensile shear strength test obtained in Phase 1 and Phase 2

Design of Electrode tip shape	Number of edges	Surface area of upper (mm ²)	Surface area of lower (mm ²)	First reading (N)	Second reading (N)	Third reading (N)	Average value (N)
Circle	0	1.77	7.07	429.04	363.53	342.18	378.25
Triangle	3	2.25	9.00	673.18	650.12	668.98	664.09
Square	4	2.25	9.00	585.80	636.80	613.65	612.08
hexagon	6	2.25	9.00	573.45	538.91	653.88	588.74

It is well noted from Table 4.5 that the maximum load achievable by the welded joint is highly influence by the design of the electrode tip shape (Saeed et al., 2014). Base on the data tabulated, electrode tip with triangle shape (three edges) have the highest maximum load achievable (664.09 N) whereas the electrode tip with hexagon shape (six edges) exhibit the lowest load value (588.74 N). It can be concluded that, as the design of pimple-tipped (PT) electrode tip shape increase in the number of edges, the maximum load achievable by the welded joint decrease gradually.

The electrode tip is in charge of the welding current flow pattern to pass through from the electrodes to the faying surfaces of the workpiece during the experiment take place. In order to obtain higher load value achievable in tensile shear strength test, the welded joint between two dissimilar metals must be strong enough to be able to withstand the stress distribution inside the welding nugget when heat is generated during μ RSW process. These stress distributions are affected by the sturdiness of the joint formed by the uniformity of the current distribution during welding. To maintain the current uniformity, an efficient design of electrode tip shape must be able to provide proper balance between thermal and mechanical properties (Bowers et al., 1990).

A good electrode tip design involves an acceptable trade-off between welding current uniformity and thermo-mechanical stiffness. For example, if employed an electrode tip design with the loss of current uniformity and the loss of mechanical stiffness will lead to electrode wear. However, the electrode tip geometry that only promotes one loss tends to minimize the other loss. Therefore, by using electrode tip that undergoes wear will affect the load value in tensile shear strength test in long term.

A thorough examination on the fracture surface of the joints produced with higher number of edges exhibit quite enormous amount of weld metal expulsion (WME) in μ RSW scale. This welding defect eventually lead to the formation of weak welded joint. Similar research done by Marashi et al. (2008) shows that a weak welded joint strength is associated with the formation of the weld metal expulsion (WME). The mechanical properties of a successful welded joint of an RSW process spot weld can be determined through performing various test on the welding nugget size which explain that the mechanical properties of a spot weld depend solemnly on the formation of the nugget in terms of size and strength coherently (Manladan et al., 2017).

Figure 4.11 compares the maximum load achievable by the welded joint obtained by four different shape of electrode tip in this research study. It can be observed here that electrode design with edges tip and large contact surface area yield higher maximum load (N) values than circular tip. Therefore, this suggest that pimped tipped (PT) design of electrode geometry in μ RSW process is optimal compared to truncated cone (TC) electrodes. This is because by increasing the contact surface area between the electrode and the faying surface of the workpiece from 1.77 mm^2 to 2.25 mm^2 for the upper part and 7.07 mm^2 to 9 mm^2 for the lower part allows higher density of welding current to pass through.

Furthermore, the design of pimple tipped (PT) electrode equipped with triangle, square and hexagon electrode tip function as a good heat sink where excess of heat distribution through the electrode are being dissipated allowing proper amount of heat to be retained in the workpiece yielding formation of stronger welding nuggets (Chan et al., 2006). According to Saeed et al. (2014) the dimension of the electrode tip or contact surface area of the electrode geometry control the size and strength of the weld nugget formed.

Overall, for this μ RSW study by using pimple tipped (PT) electrode with triangle shape electrode tip showed superior tensile shear performance when compared to truncated cone (TC) electrode with circular electrode tip due to the maximum load obtained by electrode tip with triangle shape was 664.09 N, which is approximately 43% higher than that obtained by using electrode tip with circular shape.

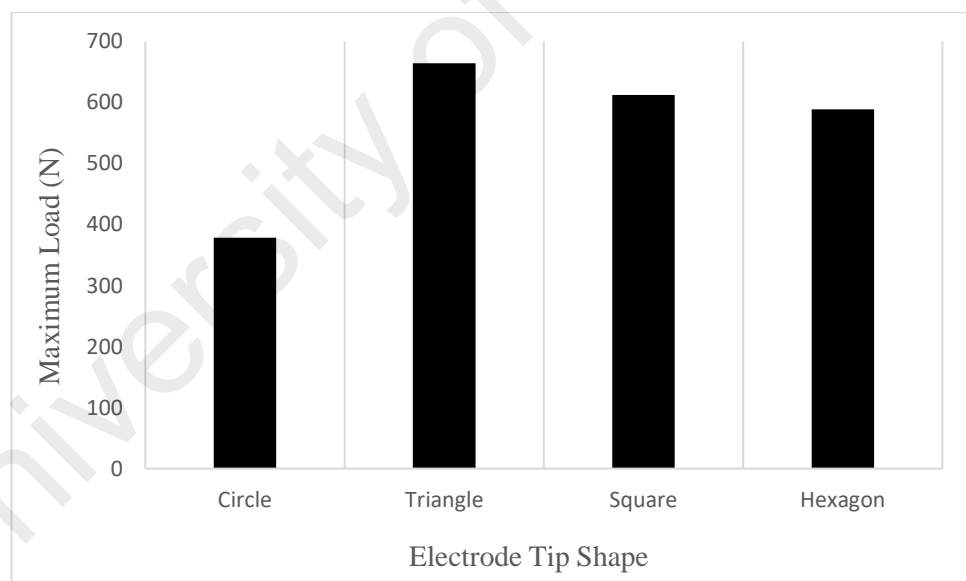


Figure 4.11: Maximum load achievable obtained from four different shape of electrode tip

4.6.2 Vickers Micro Hardness Test

According to Saeed et al. (2014), the hardness of the welded joint is an important factor that affect the spot weld of a μ RSW qualitatively. Figure 4.12 presents the Vickers micro-hardness profile of μ RSW process on the welded joint by using four different design of electrode geometry with different electrode tip shape measured along the cross section of the welded joint, which showed a significant hardness increase from the base metal. The micro-hardness measurements were taken across these welding regions: fusion zone (FZ), partially melted zone (PMZ), and base metal (BM).

From the observations made, the profiles are the same as the profiles obtained in Phase 1 where the micro-hardness at FZ and PMZ region present higher values than that at BMs region. Due to the existence of welding defects such as micro-cracks inside the weld nugget, some of the hardness values (HV) exhibit significantly lower than the others. This can be seen in the micro-hardness profile at point 14 in Figure 4.12 (a) for weld nugget using truncated cone (TC) electrode with circular tip. This reveal that the area surrounding the micro-cracks inside weld nugget is softer about 44% compared to the average hardness value calculated. Meanwhile for profiles obtained using pimped tipped (PT) electrode with square tip exhibit two anomaly values, point 7 and 13. This reveal that the area surrounding the micro-cracks inside weld nugget is softer about 18% and 21% respectively. Therefore, micro-cracks obtained from using TC electrode with circular tip are proven to be one of the reasons for low tensile shear load.

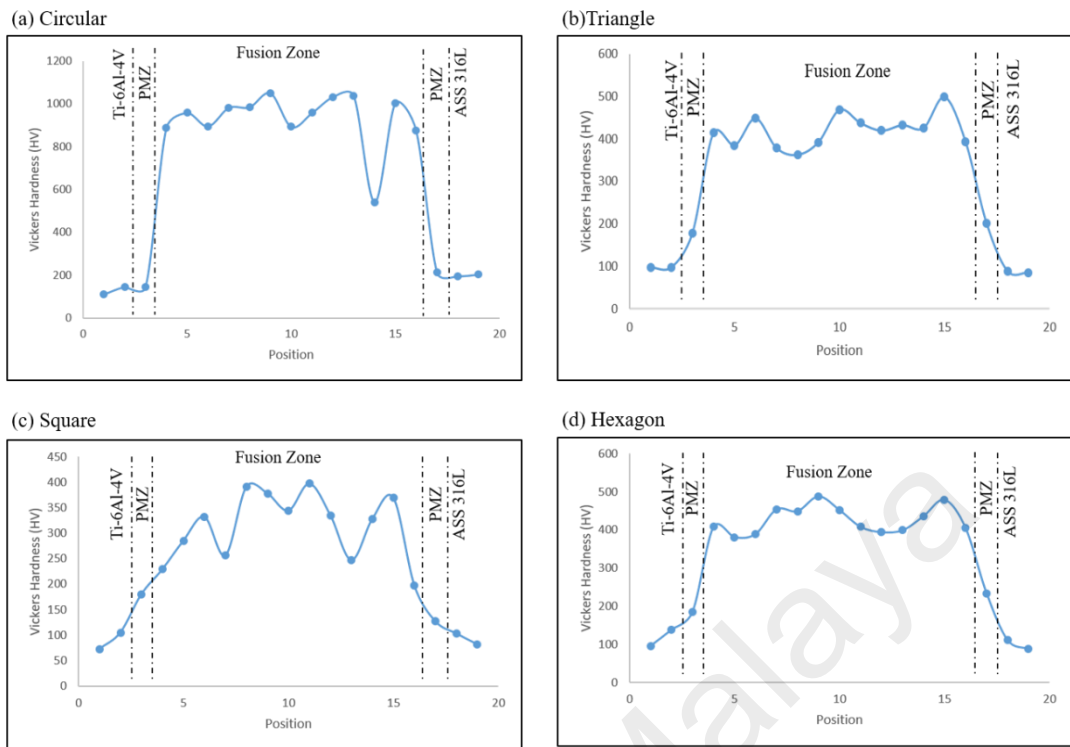


Figure 4.12: Vickers micro-hardness profile of μ RSW joint

Figure 4.13 shows the average microhardness values in the FZ obtained by using four different design of electrode geometry with different shape of electrode tip and the μ RSW process were conducted by using the same welding parameters. Furthermore, the average microhardness values of the weld nugget from each sample specimen was found to be higher than both base metals. This phenomenon occurs as a result from the formation of the intermetallic compound (IMC) such as TiFe and TiFe₂ in the FZ. This finding is similar to the analysis made in Phase 1.

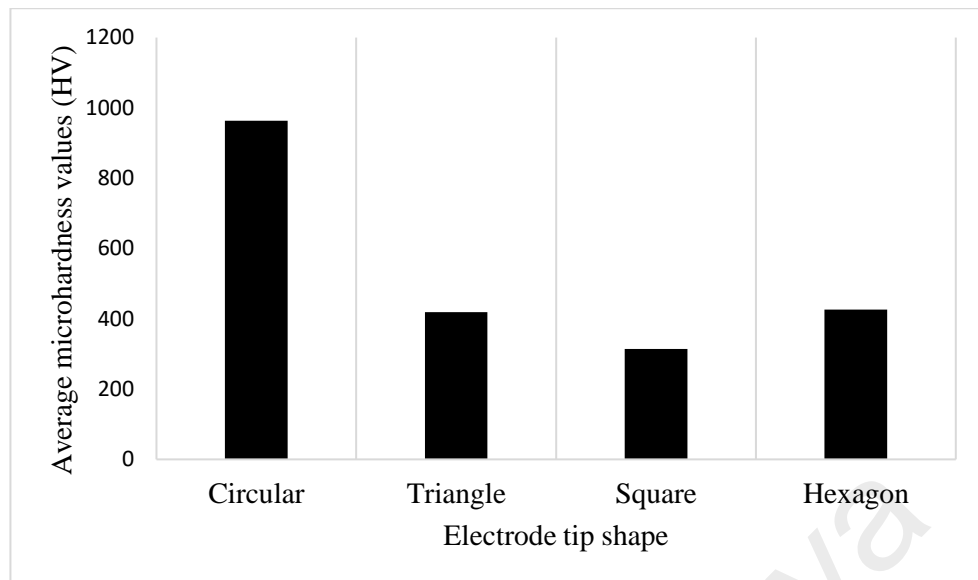


Figure 4.13: Effects of different design of electrodes on the average microhardness values at the FZ

According to Marashi et al. (2008), higher microhardness values are achievable at the FZ of the welded joint due to the martensite formation process during welding. Rapid cooling rates encourages the martensite formation at this region. Martensite is formed in metals that contain iron, Fe and carbon, C by the subsequent rapid cooling of the austenite inside ASS 316L at such a high rate that the carbon atoms do not have the time to diffuse out of the crystal structure in large enough quantities which eventually form cementite, Fe_3C thus exhibit hard and brittle behaviour for the weld nugget at the FZ (Safanama et al., 2012). Martensite is a supersaturated solution of carbon formed inside the weld nugget. Due to the high lattice distortion during welding, martensite retains high residual stresses inside the FZ. The high lattice distortion induces high hardness and strength inside the weld nugget. Due to this phenomenon, ductility is loss hence making the martensite to be brittle in nature.

The average microhardness of the FZ decrease significantly from 963 to 314 HV with an increase in the contact surface area of the electrode from 1.77 to 2.25 mm² for upper electrode and 7.07 to 9 mm² for lower electrode with the addition of the edges at the electrode tip. This is because the design of electrode with edges electrode tip such as triangle, square and hexagon exhibit higher welding current density due to the pimpled tipped (PT) design. When the current density is high, the temperature supplied at the FZ will increase during welding process. Due to the high temperature, FZ with concentrated mixture of IMC are formed causing the FZ to exhibit higher hardness value. Other than that, this reveal that larger contact surface area will supply higher amount of heat input.

In case of electrode tip with edges, hexagon shape yields the highest hardness value but decrease gradually when change to square shape electrode tip. When triangle shape is used, the average microhardness value increase from 314 to 419 HV. This suggest that the 90° edges pose a problem to the welding current uniform distribution which subsequently affecting the current concentration at the outer edge of the electrode face. Due to this problem, less heat is retained in the composition of the FZ during welding which results into formation of weak IMC. Furthermore, it's also predicted to cause welding defects such as micro-cracks inside the FZ and the weld metal expulsion (WME).

Furthermore, the square shape also shows some problems related to the wear and tear of the electrode tip life. Directly after the experiment ended (when the hold time is finished), the electrode tip was found to be stuck towards the surface of the sample specimen. These phenomena are called electrode sticking. It is a common problem in μ RSW caused by inadequate and not suitable design of the electrode tip shape. Therefore, it can be deducted here that the design of electrode with square shape electrode tape are not suitable to be used in μ RSW process between ASS 316L and Ti-6Al-4V.

Moreover, excessive indentation by the square shape electrode tip also occur which leads to burn-thru problems at the surface of the welding area. These leads to imperfect size of weld nugget at the FZ caused by the micro-cracks form from burn-thru as can be seen from Figure 4.16 (a). Overall, these problems will affect the performance of the electrode tip life cycle in μ RSW process.

The average microhardness value obtained through this study which corresponds to electrode tip with circular, triangle, square and hexagon shape are 963 HV, 419 HV, 314 HV and 426 HV respectively. These trends which are observed from the results of Vickers microhardness test are the opposite findings from the tensile properties obtained from the tensile shear strength test. It was noted that the tensile shear load obtained increased significantly by using pimple-tipped (PT) electrodes with the addition of edges. But when the number of edges increased further, it will reduce the tensile shear load. When increasing the number of edges, welding imperfections such as micro-cracks are predicted to form inside the FZ area after welding process due to subsequent rapid cooling process thus weakened the welded joint which yield low tensile shear load. A large number of edges causes the electrode to act as a small heat sink which causing the heat to dissipate into the environment at a fairly quick pace thus leading to rapid cooling process. In other word, the excessive heat does not get stored in the electrodes during μ RSW.

The change in electrode tip design will affect the welding current supplied thus affecting the heat input per unit weld length. When pimple-tipped (PT) electrodes are used, welding current distribution is uniform causing a good amount of heat being retain inside the weld nugget during welding and reducing the current concentration at the edges of the electrode tip. When a good amount of heat supplied to form the weld nugget, it will decrease the solute concentration thus reducing further the dissolution of second phase

particles which is the IMC. Therefore, causing the PT electrodes to yield lower hardness value than TC electrode.

Figure 4.14 shows the effect of different electrode tip shape with the same welding parameters on the microhardness values (HV) at the PMZ. The hardness values in this zone are not significantly different from each of the electrode design. Furthermore, the hardness values obtained inside this region range from 127 to 234 HV for ASS 316L side and 145 to 185 for Ti-6Al-4V which is 50% to 80% more than the BMs hardness values. Based on the observations made, the PT electrodes yields higher hardness values at the Ti-6Al-4V side than the TC electrodes. On the other hand, for the ASS 316L side, only hexagon electrode tip yields higher hardness values than the TC electrodes which have the circular electrode tip shape. This is because the difference in chemical composition and the mechanical properties exhibited by each of the BMs.

This can be explained further in the liquation mechanism (Kou, 2003). Based on this mechanism, during μ RSW process the BMs are heated up to between the eutectic temperature and the liquidus temperature. Therefore, the material becomes a solid-plus-liquid mixture, that is, it is partially melted. Overall, the hardness value is lower on the Ti-6Al-4V side when compared to ASS 316L side at the PMZ because Ti-6Al-4V has higher electrical resistivity and lower thermal conductivity. These combined properties cause higher heat being generated at the Ti-6Al-4V side during welding (Saeed et al., 2014). This high heat generated led to a significant reduction in the hardness values at the PMZ on the Ti-6Al-4V side.

Different phenomenon can be observed when square electrode tip shape is used. Lower hardness values are obtained at the PMZ on the ASS 316L side. This maybe caused from the design of the electrode tip geometry itself which affects the generation of heat in terms of electrical current uniformity and the welding current density at the electrode tip

respectively. For example, larger contact surface area will provide more access for the supplied welding current and vice versa. Thus, contributing to a significant change in the liquation mechanism during welding. From Bowers et al. (1990), it was reported that the PT electrode tip geometry would exhibit greater welding current uniformity than the TC electrode geometry due to its 90° contact angle design. Greater welding current uniformity lead to a proper supplied of heat distribution during welding.

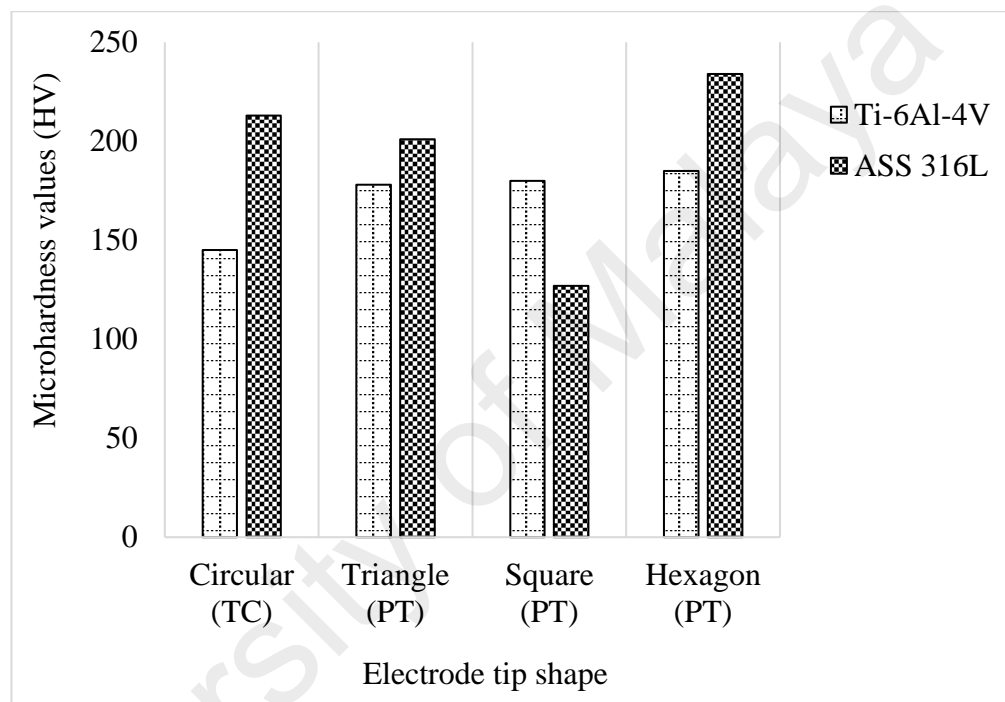


Figure 4.14: Effects of different design of electrodes on the micro-hardness values (HV) at the PMZ

In conclusion, due to the difference design of electrode tip shape, the heat supplied are varied according to the shapes and dimension used during welding thus affecting the liquation mechanics and solidification rate for each sample specimen and consequently affecting the hardness values at the PMZ and FZ.

4.7 CHARACTERIZATION OF MICROSTRUCTURE

Figure 4.15 shows the macrostructure and microstructure image of the welded joint produced by μ RSW process using the triangle shape electrode tip. The welded joint obtained show that a good weldability can be achieved by using pimple-tipped (PT) electrode with triangle shape electrode tip.

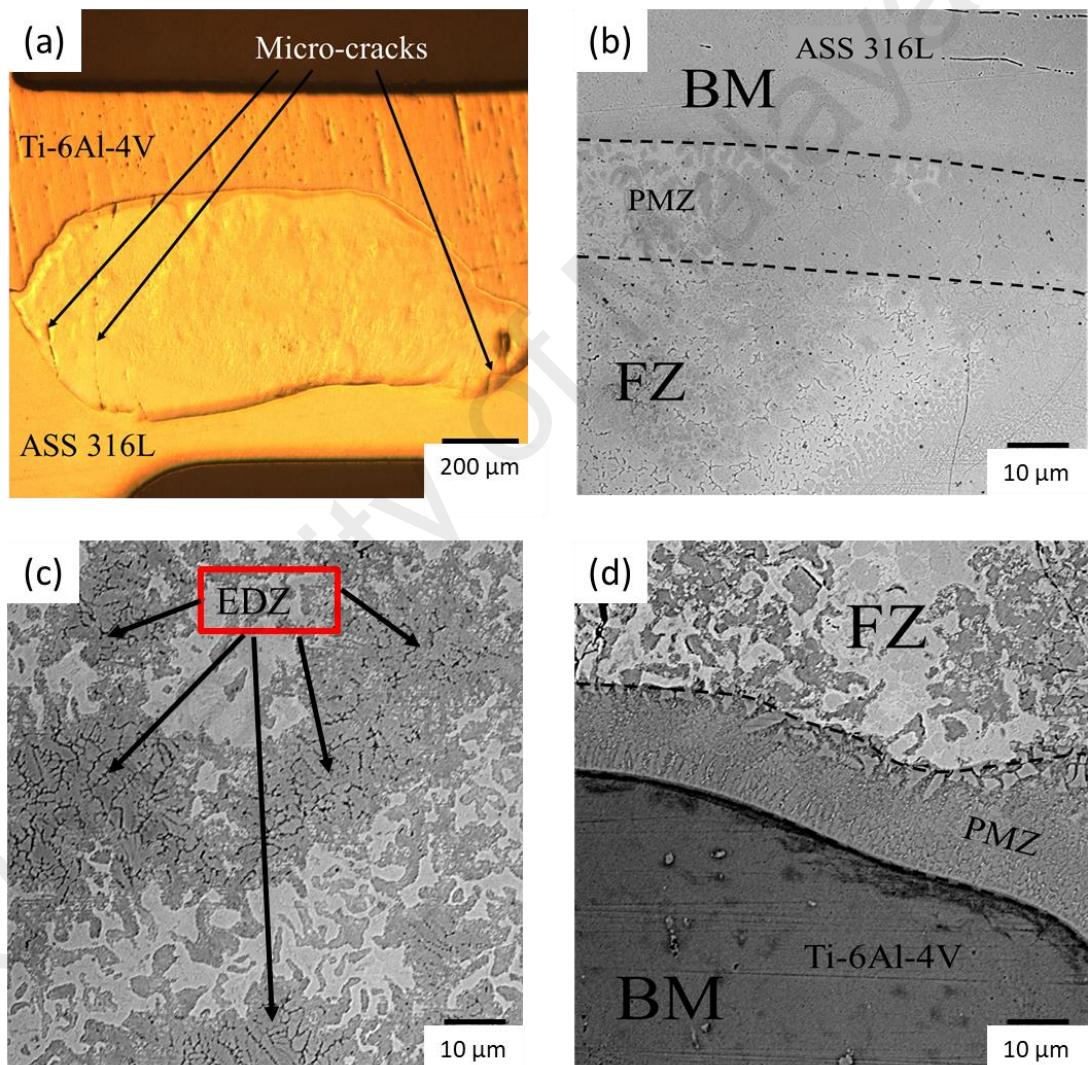


Figure 4.15: Macrostructure and microstructure of welded joint by using triangle shape electrode tip: (a) Macrostructure; and microstructure of (b) PMZ on the ASS 316L side; (c) the FZ; (d) PMZ on the Ti-6Al-4V

As can be seen in Figure 4.15 (b), the microstructure of the welded joint at ASS 316L side can be divided into three zones, namely the base metal (BM), partially melted zone (PMZ), and the fusion zone (FZ). Similar to the results obtained in Phase 1, when using triangle electrode tip shape and various etching time, there are no heat affected zone (HAZ) that can be seen clearly between the BM and PMZ due to the fact that there is no phase transformation and the grain structure does not receive any residual heat from the FZ to undergoes grain size enlargement. There are two different type of grain structure that can be seen clearly inside the PMZ which is cellular-like structure and columnar dendritic zone (CDZ) structure.

In the PMZ, the equiaxed austenite grain structure undergoes liquation mechanism where the ASS 316L are heated above the eutectic temperature, T_E . During this phase, the grain structure starts to liquified and becomes a solid-plus-liquid mixture. Since the grain structure does not heated above the liquidus temperature, T_L , the element compositions present inside the BMs does not dissolves completely with each other to form a mixture at the FZ. Thus, the size of the grain structure in the PMZ are bigger compared to the grain structure in the BM. Furthermore, the grain structure at the PMZ on the ASS 316L side become larger because of solid-state diffusion where some of impurities or element compositions from Ti-6Al-4V diffuses slowly into the grain structure of ASS 316L. The welding time also plays an important role during μ RSW process as it controls the rate of the solid-state diffusion. In the FZ, the equiaxed austenite grain structure of ASS 316L can be seen to disappear slowly as it propagates from the edge of the PMZ towards the middle of the FZ as it dissolves completely with the element composition of Ti-6Al-4V after the solidification process.

By referring to Figure 4.15 (c), the microstructure of the FZ consisted of equiaxed dendritic zone (EDZ) structure only. This finding is different from the results obtained when using TC electrodes with circular electrode tip shape in Phase 1 where the microstructure of the FZ consisted of columnar dendritic zone (CDZ) structure only. These observations of the FZ microstructure shows that the solidification mode of the grain structure of the welded joint creates the columnar-to-equiaxed transition (CET). This is because the usage of the PT electrode with triangle electrode tip shape function as a well-established heat sink during μ RSW process where the heat supplied does not restrained inside the welded joint thus affecting the cooling rate of the welded joint (Bowers et al., 1990).

Figure 4.15 (d) shows the microstructure of the welded joint at Ti-6Al-4V side which also can be divided into three different zones similar to the microstructure of the welded joint at ASS 316L side. Moreover, there is also no phase transformation or grain size enlargement that could form the HAZ. At the PMZ, due to the liquation mechanism of lamellar $\alpha+\beta$ structure inside Ti-6Al-4V, cellular structure can be seen clearly which eventually transform into a small columnar dendrite structure upon entering the FZ. This finding conforms towards what was identified by Kou (2003) using the basis of the constitutional supercooling theory where the solidification mode will change from planar to equiaxed dendritic structure.

Figure 4.16 shows the macrostructure and microstructure image of the welded joint by using the square shape electrode tip design. The welded joint obtained show that a fairly good weldability can be achieved by using pimple-tipped (PT) electrode with square shape electrode tip.

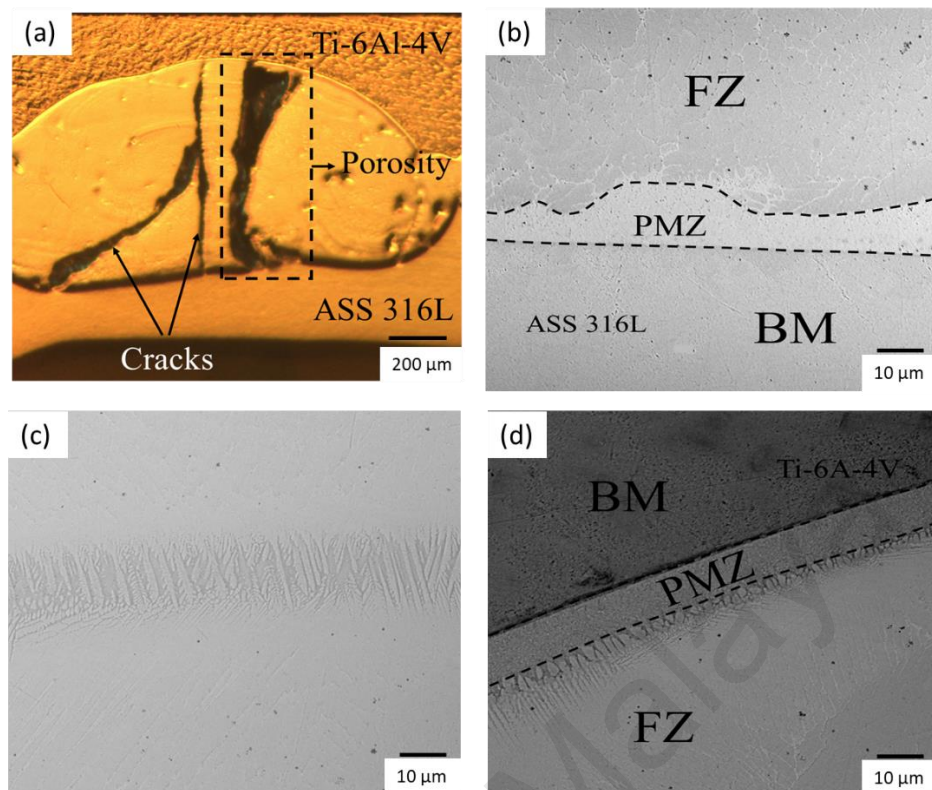


Figure 4.16: Macrostructure and microstructure of welded joint by using square shape electrode tip: (a) Macrostructure; and microstructure of (b) PMZ on the ASS 316L side; (c) the FZ; (d) PMZ on the Ti-6Al-4V

In Figure 4.16 (b) and (d), it can be seen clearly that the microstructure image obtained also show similar results as circular and triangle shape electrode tip with a clear delineation between each zone. It can be divided into three aforementioned zones, the base metal (BM), the partially melted zone (PMZ), and the fusion zone (FZ) respectively. There's also no HAZ that can be seen between the BMs and the PMZ. The microstructure obtained at the PMZ and the edges of the FZ showed a similar observation as previous test sample specimen. The only difference is the microstructure image obtained at the middle area of the FZ as shown in Figure 4.16 (c). It can be seen that the FZ consisted a mixture of columnar dendritic zone (CDZ) and cellular structure. This observation shows similarities as the microstructure image of the FZ obtained when using circular electrode tip shape.

Figure 4.17 shows the macrostructure and microstructure image of the welded joint by using the hexagon shape as the electrode tip design. The welded joint obtained show that a good weldability can be achieved by using pimple-tipped (PT) electrode with hexagon shape electrode tip.

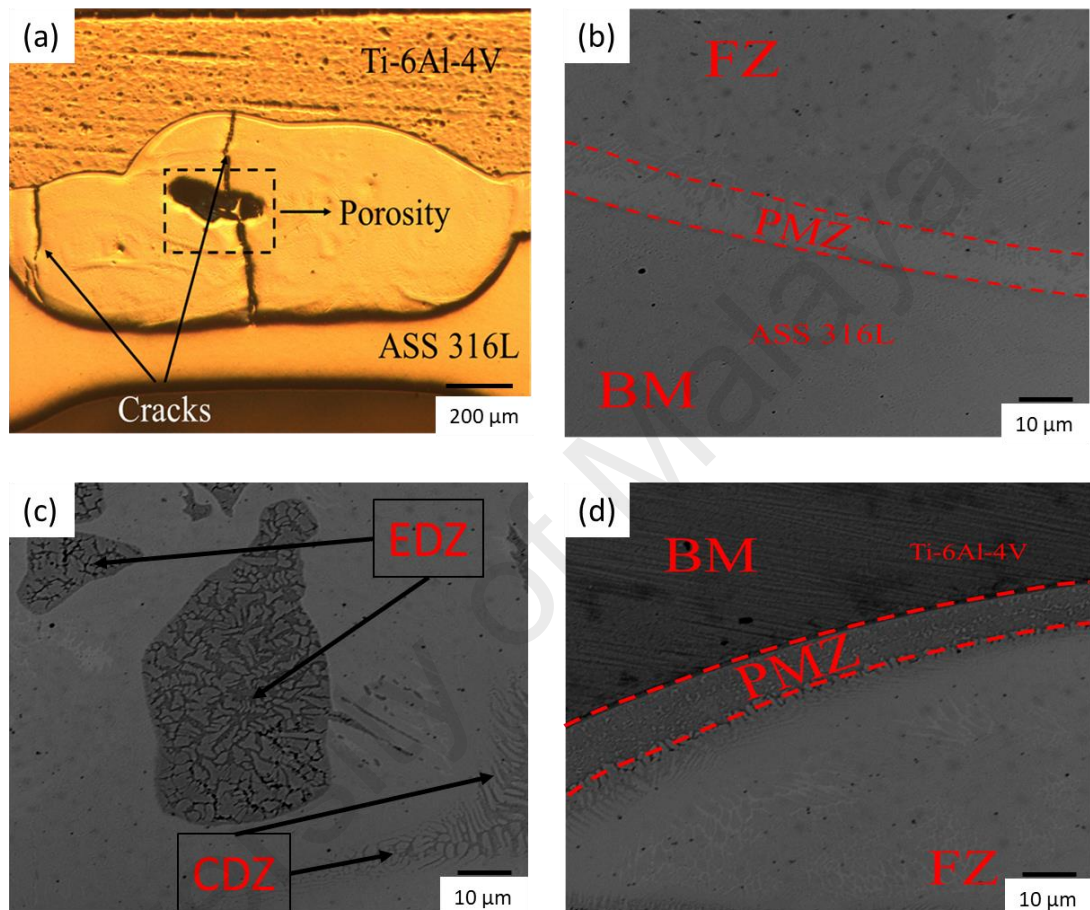


Figure 4.17: Macrostructure and microstructure of welded joint by using hexagon shape electrode tip: (a) Macrostructure; and microstructure of (b) PMZ on the ASS 316L side; (c) the FZ; (d) PMZ on the Ti-6Al-4V

In Figure 4.17 (b) and (d), it can be seen clearly that the microstructure image obtained at the PMZ and the edges of the FZ show similar results as previous shape of electrode tip design with a clear delineation between each zone. The microstructure image obtained at the middle area of the FZ in Figure 4.17 (c) shows similar results as triangle shape of electrode tip design. The FZ consisted of equiaxed dendritic zone (EDZ) structure. Other

than that, there are some area in the FZ also consisted small quantities of columnar dendritic zone (CDZ) structure. This phenomenon occurs maybe by the fact that the interruption in the columnar-to-equiaxed transition. This transition could be related to the constitutional supercooling theory by Kou (2003).

The design of hexagon shape electrode tip decreasing the heat supplied to the weld nugget because exhibit lower welding current concentration thus lowering the temperature gradient and increasing the growth rate. Therefore, this caused the planar structure to become unstable which continue to change until it stabilises at the columnar dendritic zone (CDZ) structure. But some of the planar structure stabilise at equiaxed dendritic zone (EDZ) structure. These variations could also happen as a result from utilizing pimple tipped (PT) electrode design with more than four edges at the electrode tip.

As can be seen from all of the macrostructure image of the weld nugget obtained in Phase 2, several cracks and micro-cracks are formed throughout the joining area, which started from the PMZ/BM interface on each side and propagate towards the FZ. These findings are similar results obtained in Phase 1. The existence of porosity inside the weld nugget obtained by using square and hexagon shape electrode tip may have been formed due to the difference in the rate of solidification and the weld metal dilution level caused by the usage of electrode tip with edges higher than four. Furthermore, due to the irregularities in the heat distribution supplied from the PT electrode design across the weld nugget during μ RSW process also contributes towards these welding defects at the joining area thus affecting the microstructure formed. These porosities also contribute to the propagation of the micro-cracks inside the weld nugget. Therefore, affecting the mechanical properties of the welded joint.

From this investigation, it can be concluded that the design of electrode tip shape plays an important role in supplying the heat input either by restraining the heat or releasing the heat from residing inside the weld nugget and subsequently affecting the solidification and the cooling rate of the weld nugget during and after μ RSW process.

4.8 CHARACTERIZATION ANALYSIS OF INTERMETALLIC COMPOUNDS (IMC) OF THE WELDED JOINT

Similar in Phase 1, the morphology of the intermetallic compound (IMC) formation at the PMZ and FZ in the welded joint were thoroughly analysed by using EDX point analysis. By performing this analysis, all of the element atomic percentage resides within the area of the PMZ and FZ can be determined to investigate the existence of the intermetallic compound (IMC). Figure 4.18 shows the EDX analyses for the sample specimen welded by using electrode tip with triangle shape. Table 4.6 shows the elemental distributions at the designated points inside the welding area.

By referring to Figure 4.18 (a), at point A, the percentage of atomic for Ti is higher than Fe approximately about 44%. This shows that during welding, the BM of Ti-6Al-4V is partially melted which caused some alloying element and impurities to fuse together with the elements from the BM of ASS 316L. The same mechanism applied at point B in Figure 4.18 (b) on ASS 316L side where the percentage of atomic for Fe is higher than Ti approximately about 73%. This proves that the rate of liquation mechanics slows down by a small amount of percentage at the PMZ when a design of electrode tip with triangle shape are used throughout the μ RSW process. Figure 4.18(c) shows the area of the FZ that have been selected for EDX point analysis. In the FZ, points C, D, and E had nearly the same percentage of Fe and Ti, indicating the existence of TiFe compound.

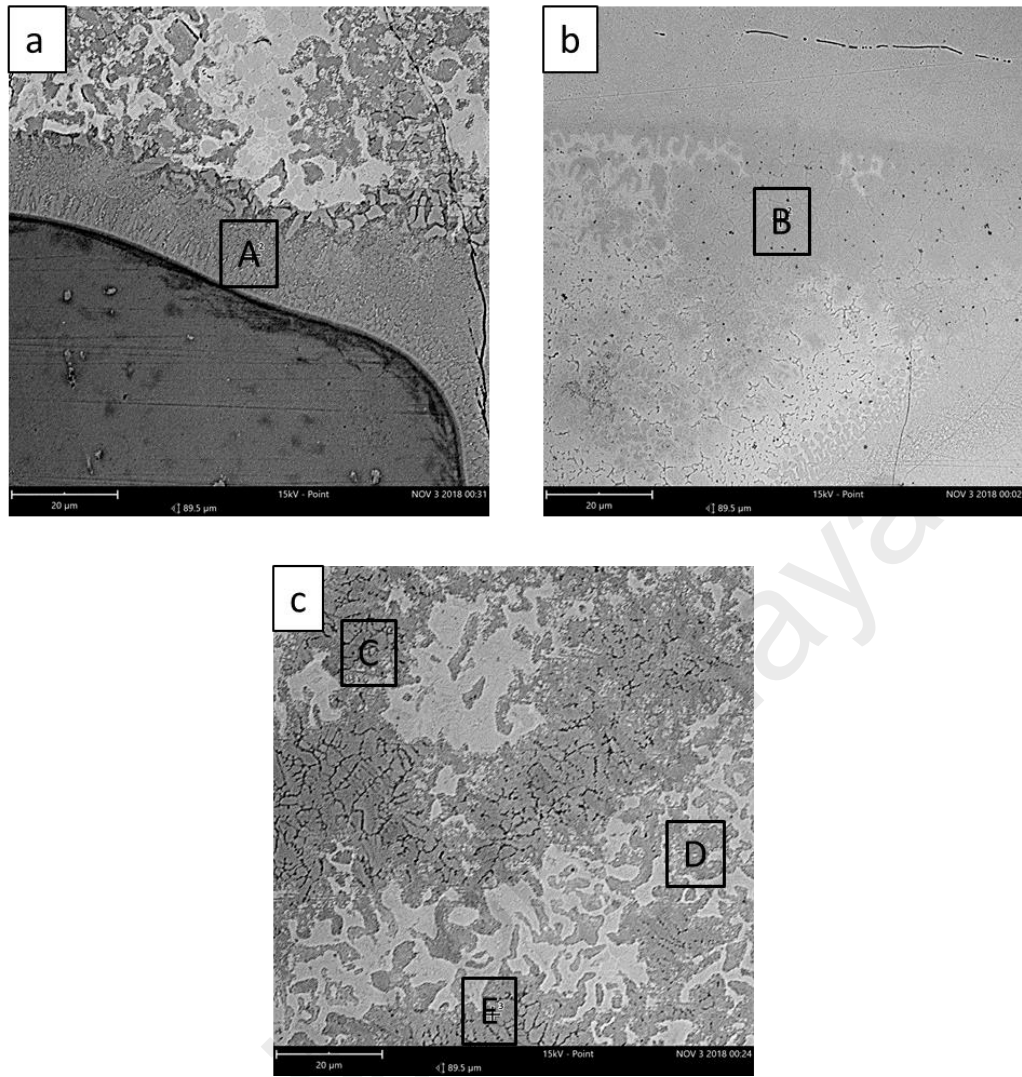


Figure 4.18: SEM micrographs of (a) the PMZ on Ti-6Al-4V side, (b) the PMZ on ASS 316L side, and (c) TiFe intermetallic compound formed at the FZ for specimen using triangle shape electrode tip

Table 4.6: The element atomic percentage in sample specimen using triangle shape electrode tip

Point	Ti(at.%)	Fe(at.%)	Ni(at.%)	Total(%)	Phase
A	70.27	26.34	3.39	100	-
B	8.93	81.89	9.18	100	-
C	59.72	35.27	5.01	100	TiFe
D	42.99	52.78	4.23	100	TiFe
E	56.20	36.82	6.98	100	TiFe

Figure 4.20 shows the EDX analyses for the sample specimen welded by using electrode tip with square shape. Table 4.7 shows the elemental distributions at the designated points inside the welding area. By referring to Figure 4.20 (a), at point A, the percentage of atomic for Ti is higher than Fe approximately about 40%. This is similar observation made from previous experiments where the BM of Ti-6Al-4V is partially melted allowing elements from the BM of ASS 316L to fuse and formed a non-homogeneous mixture. The same mechanism applied at point B in Figure 4.20 (b) on ASS 316L side where the percentage of atomic for Fe is higher than Ti approximately about 58%. Based on the numbers obtained, the rate of liquation mechanics also slows down by a small amount of percentage at the PMZ when a design of electrode tip with square shape are used throughout the μ RSW process.

Figure 4.20 (c) shows the area of the FZ that have been selected for EDX point analysis. In the FZ, points C and D had nearly the same percentage of Fe and Ti, indicating the existence of TiFe compound. Meanwhile different results were obtained at point E. The atomic percentage of Fe is twice as atomic percentage of Ti, indicating the existence of TiFe₂ compound. This finding shows that by using the square shape electrode tip allows higher welding current concentration to access into the welded joint causing higher heat distribution throughout the weld nugget. Based on the Ti-Fe binary phase diagram in Figure 4.19, the heat supplied during μ RSW process is within 1317 °C and 1427 °C which allows the TiFe₂ intermetallic compound to form caused by the segregation of alloying elements.

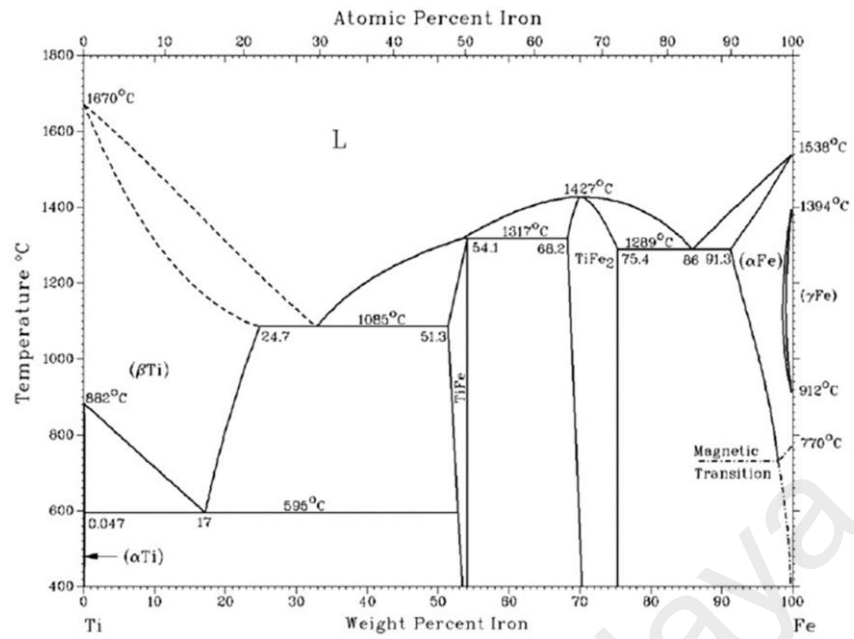


Figure 4.19: Ti-Fe binary phase diagram

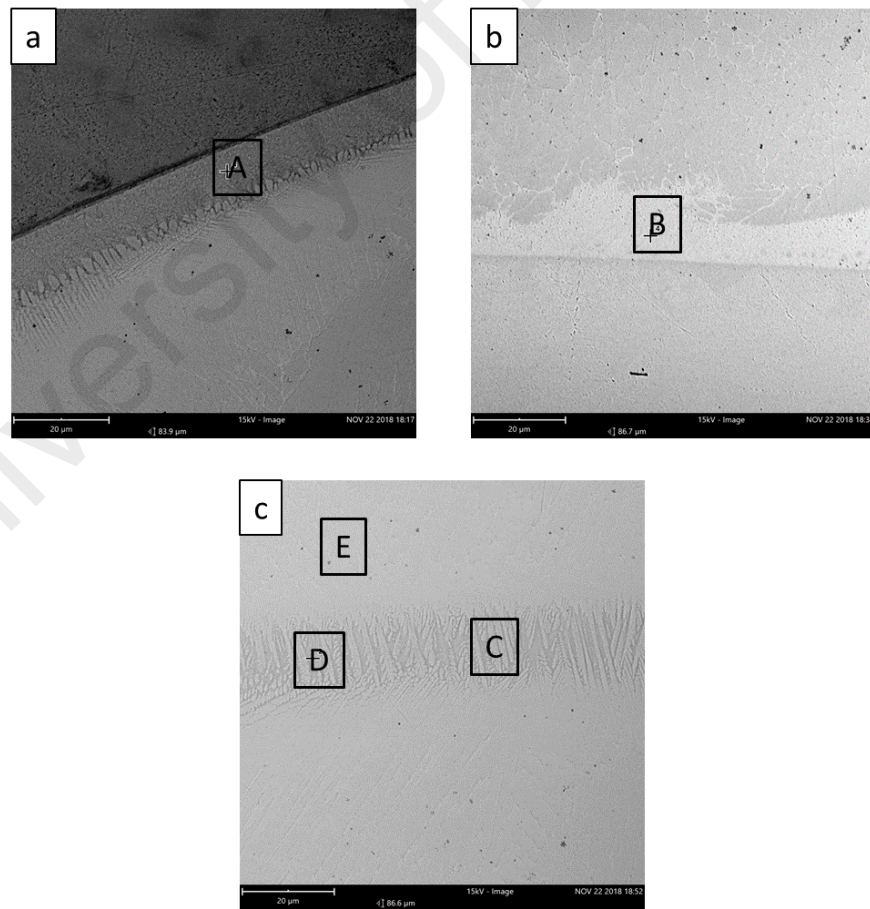


Figure 4.20: SEM micrographs of (a) the PMZ on Ti-6Al-4V side, (b) the PMZ on ASS 316L side, and (c) TiFe and TiFe₂ intermetallic compound formed at the FZ for specimen using square shape electrode tip

Table 4.7: The element atomic percentage in sample specimen using square shape electrode tip

Point	Ti(at.%)	Fe(at.%)	Ni(at.%)	Total(%)	Phase
A	67.40	27.08	5.52	100	-
B	16.41	74.10	9.49	100	-
C	44.69	51.18	4.73	100	TiFe
D	48.44	43.83	7.73	100	TiFe
E	29.76	60.4	9.84	100	TiFe ₂

Figure 4.21 shows the EDX analyses for the sample specimen welded by using electrode tip with hexagon shape. Table 4.8 shows the elemental distributions at the designated points inside the welding area. By referring to Figure 4.21 (a), at point A, the percentage of atomic for Ti is higher than Fe approximately about 43%. This shows that during welding, the BM of Ti-6Al-4V is partially melted which caused some alloying element and impurities to fuse together with the elements from the BM of ASS 316L. The same mechanism applied at point B in Figure 4.21 (b) on ASS 316L side where the percentage of atomic for Fe is higher than Ti approximately about 56%. This proves that the rate of liquation mechanics also slows down by a small amount of percentage at the PMZ when a design of electrode tip with hexagon shape are used throughout the μ RSW process.

Figure 4.21 (c) shows the area of the FZ that have been selected for EDX point analysis. In the FZ, point D has nearly the same percentage of Fe and Ti, indicating the existence of TiFe compound. At point C, the atomic percentage of Ti is higher than the atomic percentage of Fe. This indicates a non-homogeneous mixture have been formed inside the FZ caused by the segregation of the elements. Due to this phenomenon, the compound formed is neither an intermetallic nor homogeneous compound. It is classified as a eutectic mixture. The grain boundary liquid solidifies first as a solute-depleted α but

finally as eutectic when the liquid composition reaches eutectic solute concentration. Meanwhile different results were obtained at point E. The atomic percentage of Fe is twice as atomic percentage of Ti, indicating the existence of TiFe_2 compound. Similar to the finding obtained by using the square shape electrode tip, hexagon shape electrode tip also allows higher welding current concentration to access into the welded joint causing higher heat distribution throughout the weld nugget.

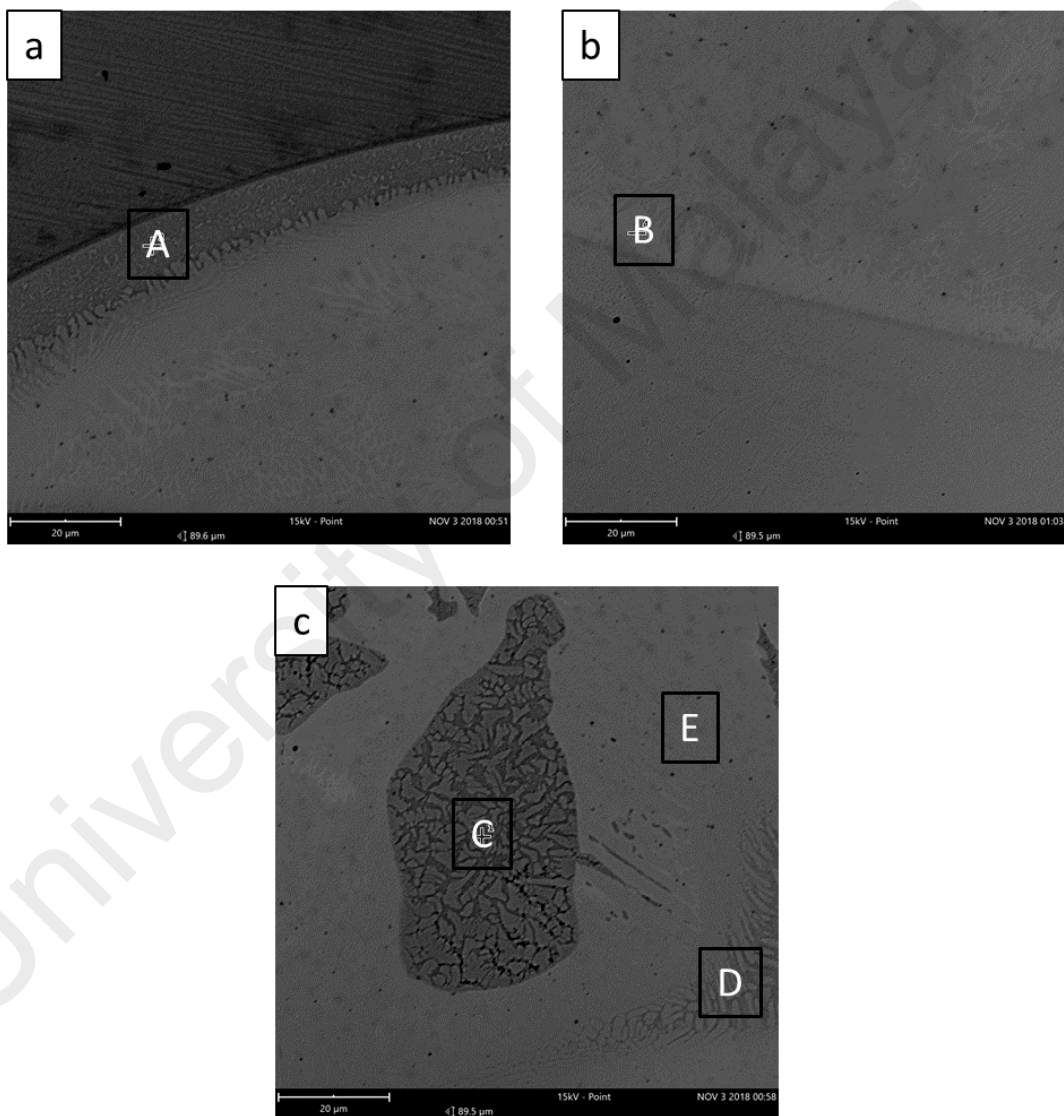


Figure 4.21: SEM micrographs of (a) the PMZ on Ti-6Al-4V side, (b) the PMZ on ASS 316L side, and (c) TiFe and TiFe_2 intermetallic compound formed at the FZ for specimen using hexagon shape electrode tip

Table 4.8: The element atomic percentage in sample specimen using hexagon shape electrode tip

Point	Ti(at.%)	Fe(at.%)	Ni(at.%)	Total(%)	Phase
A	68.6	25.71	5.69	100	-
B	17.44	73.10	9.46	100	-
C	65.81	29.67	4.52	100	-
D	45.25	48.5	6.25	100	TiFe
E	27.81	65.33	6.86	100	TiFe ₂

4.9 SUMMARY

In conclusion, by utilizing the pimped tipped (PT) electrode design, a slower rate of liquation mechanics can be achieved at the PMZ area. This is important to the formation of the weld nugget as the strength at the PMZ may also constitute towards the overall strength of the welded joint. Furthermore, this may prevent from severe liquation cracking. Several points can be deduced from the investigation on the mechanical properties and microstructure analysis of μ RSW between ASS 316L and Ti-6Al-4V:

1. The optimal combination of welding parameters has successfully determined through the use of full factorial design of experiment (DoE) with L₂₇ orthogonal array and welding current is selected as the most significant welding parameters among the rest through analysis of variance (ANOVA).
2. The investigation of microstructure revealed columnar dendritic zone (CDZ) and equiaxed dendritic structure (EDZ) at the fusion zone (FZ). Furthermore, TiFe and TiFe₂ intermetallic compound (IMC) were formed which exhibit hard and brittle characteristics thus affecting the strength of the welded joint. The microhardness test show that the hardness of the FZ area is higher than the PMZ and BM. With this information, a well-planned μ RSW process can be performed and a strong joint can be obtained.

3. An effective and efficient design of electrode geometries which includes the electrode tip should be implemented to enhance the strength of the welded joint in terms of thermal and mechanical properties due to welding current uniformity supplied through the electrode tip towards the workpiece metal sheet interface.

Furthermore, the results obtained show that the alloy elements resided inside the FZ was non-homogeneous due to the nature of μ RSW process between two dissimilar metals. Similar analysis and results were obtained in research done by (Saeed et al., 2014). The main caused of this phenomenon where the non-homogeneous elemental distributions inside the FZ occurred is caused by the segregation of the elements within the area of welding. Based on the principal of metallurgies, segregation is defined as the solid solubility. This result may occur because of the short welding time (welding cycle), which may have been insufficient amount of time for the elements to diffuse uniformly during the μ RSW process. Meanwhile at the PMZ, grain boundary segregation that develops during the solidification of the grain boundary liquid causing the alloying elements to become non-homogeneous mixture (Kou, 2003).

Other than that, the intermetallic compound formed at the joining area between ASS 316L and Ti-6Al-4V in μ RSW process was mainly composed of TiFe and TiFe₂ phases, and the surface morphology of the IMC varied with the locations across the weld nugget. Similar findings have been observed by (W. Zhang et al., 2011) where the morphology and thickness of the intermetallic compound layer varied with the locations along the interface of the welded joint of H220 Zn-coated high strength steel and 6008 aluminum alloy. In addition, one of the characteristics of the TiFe₂ intermetallic compound (IMC) surface morphology can be seen clearly in Figure 4.20 (c) and Figure 4.21 (c). It is neither equiaxed nor columnar dendritic structure. It reveals a cellular-like structure.

Moreover, when incorporating pimple-tipped (PT) electrode design with four or more edges, TiFe_2 , an intermetallic compound with hard and brittle in nature may formed due to high welding concentration through the electrode interface causing high heat input supplied throughout μRSW process between dissimilar metals thus compromising the overall joining strength of the welded joint.

University of Malaya

CHAPTER 5: CONCLUSION

5.1 Conclusion

In Phase 1, the dissimilar micro resistance spot welding (μ RSW) between 0.5-mm-thick austenitic stainless steel 316L and 0.5-mm-thick ASTM titanium alloy grade 5 (Ti-6Al-4V) was successfully assessed. From the statistical analysis which consisted of full-factorial design of experiment (DoE) and analysis of variance (ANOVA), the welding current (kA) with 45.30% of percentage contribution was found to have the most significant effect on the strength and quality of the welded joint produced by using μ RSW technique. Furthermore, base on the full-factorial design of experiment results, experiment run no.10 produce the highest achievable maximum peak load with combination of welding parameters : welding current 2 kA, welding time 100 ms, and welding force 241 N. In addition, interfacial failure (IF) mode was observed on every sample specimen during tensile shear load test. From the observation made, it was found that the surface morphology of the fracture interface exhibit hard and brittle behaviour.

For the microstructure analysis, the partially melted zone (PMZ) and the fusion zone (FZ) is observed at the weld nugget area. Since there are no phase transformation or grain size enlargement that could be identified between the BM's and the PMZ, no heat affected zone (HAZ) can be observed in every sample specimen. For the Vickers micro-hardness analysis, the average microhardness value (HV) of the FZ for sample specimen 10 is 963 HV which is significantly higher than both of the base material hardness.

In Phase 2, the dissimilar micro resistance spot welding (μ RSW) between 0.5-mm-thick austenitic stainless steel 316L and 0.5-mm-thick ASTM titanium alloy grade 5 (Ti-6Al-4V) by using three different design of electrode tip shape was successfully assessed. The welding process parameters chosen are based from the most optimized results obtained during Phase 1. It was found that the shape of the electrode tip contribute a

significant amount of influence on the development and final shape of the weld nugget in dissimilar μ RSW process. For the tensile shear strength test, the μ RSW process by using electrode tip with triangle shape showed superior tensile shear performance. The maximum load achievable obtained by electrode tip with triangle shape was 664.09 N, which is approximately 43% higher than that obtained by using electrode tip with circular shape.

For the microstructure analysis, the partially melted zone (PMZ) and the fusion zone (FZ) is thoroughly investigated at the weld nugget area. The intermetallic compound (IMC) TiFe found present in all of the sample specimen while TiFe₂ can only be found in sample specimen using square and hexagon shape electrode tip. For the Vickers microhardness analysis, the highest average microhardness value (HV) of the FZ obtained among the pimple-tipped (PT) electrode design is hexagon shape electrode design with 426 HV which also shows significantly higher than both of the base material hardness. The main reason to the apparent difference in hardness value of circular shape and hexagon shape electrode tip is because of the existence of α Ti and β Ti solute particle inside the FZ area. The elements reside within this area are non-homogeneous mixture due to the segregation of the elements present.

In conclusion, for dissimilar μ RSW process, pimple-tipped (PT) electrode design with triangle shape electrode tip yields highest achievable maximum load and joining strength among other designs.

5.2 Recommendation for Future Work

The investigation on the feasibility study of micro-resistance spot welding (μ RSW) between dissimilar metals such as ASS 316L and Ti-6Al-4V should be continue towards simulation works where comparison can be made between predicted data with experimental values. On top of that, a lot of research work and studies could be carried out which is required to justify and verify its behaviour in terms of mechanical properties because joining strength is an important aspect that should be properly explored by researchers for optimization purposes. In current research, only three independent variables (welding current, welding time, and welding force) with three different levels, more factors should be taken into proper consideration and thoroughly studied. The experiments, tests and data analysis need to be executed efficiently in order to improve the reliability of the joint so that this research met with current industrial application and requirements.

Throughout this study, the following recommendations for future works are:

1. The optimization of other welding parameters such as the squeeze and hold time.
2. Mechanical tests such as cross-tension are required to investigate and improve the reliability of the welded joint.
3. Other method to improve the strength of the welded joint should be explored such as adding fillers material which could be used to support and enhance the properties of the welded joint.
4. Devise a study plan to reduce the formation of intermetallic compound (IMC) and to mitigate failures properly.
5. An XRD test should be carried out for better phase identification of any particular crystalline structure/elements present in the welded joint.

REFERENCES

- Arghavani, M., Movahedi, M., & Kokabi, A. (2016). Role of zinc layer in resistance spot welding of aluminium to steel. *Materials & Design*, 102, 106-114.
- Aslanlar, S. (2006). The effect of nucleus size on mechanical properties in electrical resistance spot welding of sheets used in automotive industry. *Materials & Design*, 27(2), 125-131.
- Bowers, R., Sorensen, C., & Eagar, T. (1990). Electrode geometry in resistance spot welding. *Welding Journal*, 69(2), 45S.
- Chan, K. R., Scotchmer, N., Bohr, J. C., Khan, I., Kuntz, M. L., & Zhou, Y. (2006). Effect of electrode geometry on resistance spot welding of AHSS. *SMWC XII Session*, 7-4.
- Chino, S., Tsukahara, Y., Nishida, T., Imabayashi, I., Mizunaga, M., & Irie, N. (1994). Application of titanium to eyeglass frames, vacuum bottles and other consumer goods. *Nippon Steel Tech. Rep.(Japan)*, 62, 29-33.
- Ely, K., & Zhou, Y. (2001). Microresistance spot welding of Kovar, steel, and nickel. *Science and Technology of Welding and Joining*, 6(2), 63-72.
- Ertek Emre, H., & Kaçar, R. (2016). Resistance spot weldability of galvanize coated and uncoated TRIP steels. *Metals*, 6(12), 299.
- Fan, Q., Xu, G., & Gu, X. (2016). Expulsion characterization of stainless steel resistance spot welding based on dynamic resistance signal. *Journal of Materials Processing Technology*, 236, 235-240.

- Fukumoto, S., Fujiwara, K., Toji, S., & Yamamoto, A. (2008). Small-scale resistance spot welding of austenitic stainless steels. *Materials science and engineering: A*, 492(1-2), 243-249.
- He, P., & Liu, D. (2006). Mechanism of forming interfacial intermetallic compounds at interface for solid state diffusion bonding of dissimilar materials. *Materials science and engineering: A*, 437(2), 430-435.
- Huin, T., Dancette, S., Fabrègue, D., & Dupuy, T. (2016). Investigation of the failure of advanced high strength steels heterogeneous spot welds. *Metals*, 6(5), 111.
- Ignasiak, A., Korzeniowski, M., & Ambroziak, A. (2012). Investigations of Microstructure of Resistance Spot-Welded Joints Made of HSLA340 and DP600 Steels/Badanie Mikrostruktury Złączy Zgrzewanych Punktowo Ze Stali HSLA340 I DP600. *Archives of Metallurgy and Materials*, 57(4), 1081-1086.
- Ilman, M., & Soekrisno, R. (2011). Corrosion Fatigue Behavior of Resistance Spot Welded Dissimilar Metal Welds between Carbon Steel and Austenitic Stainless Steel with Different Thickness. *Procedia Engineering*, 10, 649-654.
- Kahraman, N. (2007). The influence of welding parameters on the joint strength of resistance spot-welded titanium sheets. *Materials & Design*, 28(2), 420-427. doi:10.1016/j.matdes.2005.09.010
- Kaya, Y., & Kahraman, N. (2012). The effects of electrode force, welding current and welding time on the resistance spot weldability of pure titanium. *The International Journal of Advanced Manufacturing Technology*, 60(1-4), 127-134.
- Kazdal Zeytin, H., Ertek Emre, H., & Kaçar, R. (2017). Properties of resistance spot-welded TWIP steels. *Metals*, 7(1), 14.

- Khodabakhshi, F., Kazeminezhad, M., & Kokabi, A. (2015). Metallurgical characteristics and failure mode transition for dissimilar resistance spot welds between ultra-fine grained and coarse-grained low carbon steel sheets. *Materials science and engineering: A*, 637, 12-22.
- Kianersi, D., Mostafaei, A., & Amadeh, A. A. (2014). Resistance spot welding joints of AISI 316L austenitic stainless steel sheets: Phase transformations, mechanical properties and microstructure characterizations. *Materials & Design*, 61, 251-263.
- Kou, S. (2003). *Welding metallurgy*. New Jersey, USA, 431-446.
- Li, W., Yan, L., Karnati, S., Liou, F., Newkirk, J., Taminger, K. M. B., & Seufzer, W. J. (2017). Ti-Fe intermetallics analysis and control in joining titanium alloy and stainless steel by Laser Metal Deposition. *Journal of Materials Processing Technology*, 242, 39-48.
- Li, Y., Wei, Z., Li, Y., Shen, Q., & Lin, Z. (2013). Effects of cone angle of truncated electrode on heat and mass transfer in resistance spot welding. *International Journal of Heat and Mass Transfer*, 65, 400-408.
- Liu, L., Xiao, L., Feng, J., Tian, Y., Zhou, S., & Zhou, Y. (2010). The mechanisms of resistance spot welding of magnesium to steel. *Metallurgical and Materials Transactions A*, 41(10), 2651-2661.
- Ma, C., Chen, D., Bhole, S., Boudreau, G., Lee, A., & Biro, E. (2008). Microstructure and fracture characteristics of spot-welded DP600 steel. *Materials science and engineering: A*, 485(1-2), 334-346.
- Manladan, S., Yusof, F., Ramesh, S., Zhang, Y., Luo, Z., & Ling, Z. (2017). Microstructure and mechanical properties of resistance spot welded in welding-

brazing mode and resistance element welded magnesium alloy/austenitic stainless steel joints. *Journal of Materials Processing Technology*, 250, 45-54.

Marashi, P., Pouranvari, M., Amirabdollahian, S., Abedi, A., & Goodarzi, M. (2008). Microstructure and failure behavior of dissimilar resistance spot welds between low carbon galvanized and austenitic stainless steels. *Materials science and engineering: A*, 480(1-2), 175-180.

MI, K., ML, K., Biro, E., & Zhou, Y. (2008). Microstructure and mechanical properties of resistance spot welded advanced high strength steels. *Materials Transactions*, 0805260435-0805260435.

Navidi, W. C. (2008). *Statistics for engineers and scientists*: McGraw-Hill Higher Education New York, NY, USA.

Pashazadeh, H., Gheisari, Y., & Hamed, M. (2016). Statistical modeling and optimization of resistance spot welding process parameters using neural networks and multi-objective genetic algorithm. *Journal of Intelligent Manufacturing*, 27(3), 549-559.

Patel, P. S. S., Patel, P. M. G., & Momin, P. A. G. (2013). Parametric Optimization for Weld Strength of Resistance Spot Welding Using Full Factorial Method.pdf.

Paventhana, R., Lakshminarayanan, P., & Balasubramanian, V. (2011). Prediction and optimization of friction welding parameters for joining aluminium alloy and stainless steel. *Transactions of Nonferrous Metals Society of China*, 21(7), 1480-1485.

Phadke, M. S. (1995). *Quality engineering using robust design*: Prentice Hall PTR.

- Pouranvari, M., & Marashi, S. (2012). Failure of resistance spot welds: tensile shear versus coach peel loading conditions. *Ironmaking & Steelmaking*, 39(2), 104-111.
- Pouranvari, M., & Marashi, S. (2013). Critical review of automotive steels spot welding: process, structure and properties. *Science and Technology of Welding and Joining*, 18(5), 361-403.
- Russo Spena, P., De Maddis, M., D'Antonio, G., & Lombardi, F. (2016). Weldability and monitoring of resistance spot welding of Q&P and TRIP steels. *Metals*, 6(11), 270.
- Saeed, A., Zuhailawati, H., Ismail, A., Samad, Z., & Ariga, T. (2014). Weldability of titanium and nickel with alloy filler addition and different electrodes tip shapes by using micro spot brazing method. *The International Journal of Advanced Manufacturing Technology*, 73(5-8), 591-599.
- Safanama, D., Marashi, S., & Pouranvari, M. (2012). Similar and dissimilar resistance spot welding of martensitic advanced high strength steel and low carbon steel: metallurgical characteristics and failure mode transition. *Science and Technology of Welding and Joining*, 17(4), 288-294.
- Saha, D. C., Han, S., Chin, K. G., Choi, I., & Park, Y. D. (2012). Weldability Evaluation and Microstructure Analysis of Resistance-Spot-Welded High-Mn Steel in Automotive Application. *Steel research international*, 83(4), 352-357.
- Verma, A., Ghunage, S., & Ahuja, B. (2014). *Resistance Welding of Austenitic Stainless Steels (AISI 304 with AISI 316)*. Paper presented at the 5th International & 26th All India Manufacturing Technology, Design and Research Conference (AIMTDR 2014) IIT Guwahati, Assam, India.

- Vural, M., Akkuş, A., & Eryürek, B. (2006). Effect of welding nugget diameter on the fatigue strength of the resistance spot welded joints of different steel sheets. *Journal of Materials Processing Technology*, 176(1-3), 127-132.
- Wang, J., Wang, H.-P., Lu, F., Carlson, B. E., & Sigler, D. R. (2015). Analysis of Al-steel resistance spot welding process by developing a fully coupled multi-physics simulation model. *International Journal of Heat and Mass Transfer*, 89, 1061-1072.
- Xu, J., Jiang, X., Zeng, Q., Zhai, T., Leonhardt, T., Farrell, J., . . . Effgen, M. P. (2007). Optimization of resistance spot welding on the assembly of refractory alloy 50Mo–50Re thin sheet. *Journal of Nuclear Materials*, 366(3), 417-425.
- Zhang, H., & Senkara, J. (2011). *Resistance welding: fundamentals and applications*: CRC press.
- Zhang, W., Sun, D., Han, L., Gao, W., & Qiu, X. (2011). Characterization of intermetallic compounds in dissimilar material resistance spot welded joint of high strength steel and aluminum alloy. *Isij International*, 51(11), 1870-1877.
- Zhang, W., Sun, D., Han, L., & Li, Y. (2015). Optimised design of electrode morphology for novel dissimilar resistance spot welding of aluminium alloy and galvanised high strength steel. *Materials & Design*, 85, 461-470.
- Zhao, D., Wang, Y., Sheng, S., & Lin, Z. (2013). Real time monitoring weld quality of small scale resistance spot welding for titanium alloy. *Measurement*, 46(6), 1957-1963.

Zhao, D., Wang, Y., Wang, X., Wang, X., Chen, F., & Liang, D. (2014). Process analysis and optimization for failure energy of spot welded titanium alloy. *Materials & Design*, 60, 479-489.

Zhou, Y., Gorman, P., Tan, W., & Ely, K. (2000). Weldability of thin sheet metals during small-scale resistance spot welding using an alternating-current power supply. *Journal of electronic materials*, 29(9), 1090-1099.

University of Malaya

LIST OF PUBLICATIONS

1. Muhammad Safwan Mohd Mansor, Farazila Yusof, Tadashi Ariga, Yukio Miyashita (2018), “Microstructure and Mechanical Properties of Micro-Resistance Spot Welding between Stainless Steel 316L and Ti-6Al-4V”, The International Journal of Advanced Manufacturing Technology - Published

University of Malaya